MECHANISMS OF HIGH INSULIN AND HIGH GLUCOSE-INDUCED SKELETAL MUSCLE INSULIN RESISTANCE: FOCUS ON REGULATION BY ADIPONECTIN

Penny Felicia Ulrika Ahlstrom

A THESIS SUBMITTED TO

THE FACULTY OF GRADUATE STUDIES

IN PARTIAL FULFILLMENT OF THE REQUIREMENTS

FOR THE DEGREE OF

MASTER OF SCIENCE

Graduate Program in Biology

York University

Toronto, Ontario

September 2015

Abstract

Skeletal muscle insulin resistance is known to play an important role in the pathogenesis of diabetes, however the cellular processes involved are poorly defined. Autophagy, ER stress, the UPR and oxidative stress are being studied in insulin resistance but the exact role they play and their interrelationships are yet to be established. Adiponectin is a known insulin sensitizer with anti-diabetic properties but there is limited knowledge of the mechanism by which it exerts its insulin sensitizing effect in skeletal muscle. Through several well-established assays I have demonstrated that impaired autophagy caused ER stress and that UPR activation, specifically peIf2α, activated autophagy. Adiponectin alleviated ER stress by restoring autophagy, and a correlation between autophagy induction and insulin sensitization by adiponectin was observed. Alleviating oxidative stress with NAC improved insulin sensitivity independent of ER stress and autophagy, and there appeared to be a correlation between downregulating the UPR and improved insulin sensitivity.

Acknowledgments

My journey though graduate studies in biological research has been incredibly rewarding and from it I take away important insights and values that will help guide me through both my professional and personal life. This experience would not have been possible without my colleagues and my family, and I will always appreciate their support and friendship. Specifically I would like to thank my supervisor Dr. Gary Sweeney for his continuous support, advice and guidance, I would also like to thank all the members of my examining committee, Dr. John McDermott, Dr. Robert Tsushima, and Dr. Tara Haas, for taking their valuable time to discuss and evaluate my thesis, and further I would like to thank all the past and present members of the Sweeney lab including several talented researchers that has become my personal friends: Sanjana Sen, Dr. Carol Chan, Dr. Keith Dadson, Cindy Sung and Phuong Bui. I would also like to extend a special thanks to the “L6 group”; Dr. Palanivel Rengasamy an experienced researcher with extraordinary talent for assay optimization, Suharto Chakma, the newest addition to our team, whom I have had the privilege to teach and work with for the last few months of my project and last, but not least, my dear Esther Rai whose friendship and inexhaustible encouragement I will always value.

Table of Contents

List of Tables

List of Figures

Chapter 1. Introduction

1.1 Diabetes: a Global Health Epidemic

1.1.1 Diabetes Mellitus

Diabetes Mellitus is a chronic metabolic disorder hallmarked by a dysregulation of whole body glucose homeostasis resulting in glucose intolerance and hyperglycemia, causing serious health complications including kidney failure, heart disease, stroke, nerve damage, and blindness [1]. There are two main types of diabetes, type 1 and type 2. Type 1 diabetes is a chronic autoimmune disease, typically with onset in younger individuals, characterized by an inability to produce insulin due to the destruction of pancreatic beta-cells. Type 1 diabetes accounts for approximately 5-10% of all diabetes cases [1, 2]. Conversely, type 2 diabetes is the result of insulin resistance in peripheral tissues such as muscle, liver and adipose. Diminished response to normal levels of insulin prompts an increase in production of insulin from beta-cells to control blood glucose levels, eventually leading to diminished beta-cell function and exogenous insulin dependency [3]. Type 2 diabetes corresponds to 90-95% of all diabetes cases and is the focus of my research (hereafter simply referred to as diabetes) [2, 4].

1.1.2 Obesity and Diabetes Prevalence

A change over the last few decades to a sedentary life-style coupled with a high calorie diet has led to a staggering increase in obesity prevalence [5]. In 2005, the global obese population was estimated at 396 million, and with the current trend continuing the projected number of obese people in the world is expected to rise to 1.12 billion in 2030. This represents a rise in world-wide obesity prevalence from 9.8% in 2005 to 19.7% in 2030 [6], and as obesity is associated with a large number of medical complications, including cardiovascular disease, cancer and metabolic disorders, it poses a major global health issue [4].

Diabetes is a metabolic disorder that correlates with obesity and it has been found that 80% of diabetes cases are directly related to obesity [7], with obesity being the single most important predictor for developing diabetes [8]. The increase in obesity prevalence has been closely followed by a similarly striking increase in the incidence of diabetes, with more than double the number of people suffering from diabetes now compared to 30 years ago. The continuous increase in diabetes prevalence has so far exceeded most predictions [4, 5, 9], for example in 1995 the prevalence of adults with diabetes was estimated to 135 million and predicated to rise to 300 million in 2025 [10], but with an estimated 285 million adults world-wide with diabetes in 2010 the prediction has now increased to 439 million adults in 2030. This trend indicates that the current pandemic will continue to increase in severity, constituting a growing health concern [4].

1.1.3 Progression from Obesity to Diabetes

The pathogenesis of obesity has been studied over the last few decades to understand the link between obesity and diabetes, and it is now considered that adipokines secreted from adipose tissue hold a key to this link [11]. Accumulation of adipose tissue, especially visceral adipose tissue, is associated with insulin resistance, hyperglycemia, dyslipidemia, hypertension and pro-inflammatory conditions [12]. Systemic tissue inflammation is induced both by the lipotoxicity acting on a variety of tissues causing an intracellular inflammatory response, and also through the altered adipokine profile that results from the accumulation of visceral fat tissue [13].

1.2 Adiponectin

1.2.1 Adipose Tissue: an Endocrine Organ

Historically adipose tissue and adipocytes were considered to be passive energy storage depots, but with the discovery of bioactive adipocyte secreted molecules, termed adipokines, its endocrine function has come under increasing investigation and it is now well accepted that

adipose tissue functions as an active endocrine organ with many metabolic functions [14]. Several adipokines have to date been identified and characterized as playing a role in obesity and diabetes including leptin, adiponectin, chemerin, visfatin, omentin, tumor necrosis factor alpha (TNFα), resistin, retinol-binding protein 4 (RBP4) and interleukin 6 (IL-6) and vaspin [11, 14-17].

1.2.2 Adiponectin Action

One of the adipocytes secreted from adipose tissue, adiponectin, has been the subject of a lot of research over the last two decades and it is now known to act on a number of target tissues including, liver, heart, adipose, muscle, endothelium, and the hypothalamus to exert several beneficial effects. Adiponectin is generally considered to be anti-diabetic, insulin sensitizing, insulin mimetic, cardio-protective, anti-inflammatory and anti-apoptotic [18-20] and the interest in studying adiponectin was amplified by the finding that its plasma levels were inversely correlated with obesity and diabetes; indeed central fat distribution was an independent negative predictor of circulating adiponectin levels suggesting that adiponectin might represent a link between obesity and the development of insulin resistance and diabetes [21-24].

1.2.3 Structure and Oligomeric Forms

Adiponectin was discovered to consist of 247 amino acids; an approximately 30 kDa polypeptide with four domains: an N-terminal signal sequence, a variable domain, a collagen-like domain, and a C-terminal globular domain [25-28]. The gene encoding adiponectin is located on chromosome 3q27 [29], a locus that has been linked with susceptibility to diabetes and cardiovascular disease [30].

Plasma concentrations of adiponectin in healthy subjects range between 1.9-17 μg/ml [22], with 5-10μg/ml being considered normal levels, making adiponectin highly abundant and corresponding to approximately 0.01% of all plasma protein. There are three oligomeric forms of

adiponectin secreted into the blood stream: low molecular weight (LMW; trimer), medium molecular weight (MMW; hexamer), and high molecular weight (HMW; oligomers) [31]. Globular adiponectin is a fourth form of adiponectin with biological activity, present in plasma and produced by proteolytic cleavage to release the 17 kDa globular domain. Globular adiponectin makes up about 1% of total plasma adiponectin [32].

1.2.4 Regulation and Assembly

Assembly and release of adiponectin is regulated by the endoplasmic reticulum (ER). It has been shown that pools of folded adiponectin is retained in adipocytes by being bound to the ER chaperone ER protein 44 (ERp44), while another ER chaperone, ER oxidoreductin 1p (Ero1-Lα), mediates its release from ERp44 and subsequently from the adipocyte [33]. The metabolic state of the cell regulates the levels of these ER chaperones which also play an important role in the assembly of HMW oligomers of adiponectin [33]. A disulfide-bond oxidoreductase-like protein (DsbA-L) has been shown to be a key regulator of adiponectin assembly and multimerization, it is highly expressed in adipose tissue with a negative correlation with obesity in both mice and human. DsbA-L is stimulated by the insulin sensitizer rosiglitazone and inhibited by the inflammatory cytokine TNFα [34].

The availability of adiponectin is regulated also at the gene expression level and is mediated through the transcription factors CCAAT/enhancer binding protein (C/EBP) [35], sterol regulatory element-binding protein 1c (SREBP1c) [36], peroxisome proliferator-activated receptor gamma (PPARY) [37] and sirtuin 1 (SirT1) [38]. After translation the adiponectin peptide goes through post-translational modifications such as hydroxylation of proline and lysine residues and glycosylation of hydroxylysines which produces multiple isoforms that assemble into the LMW, MMW, and HMW adiponectin oligomers secreted into the circulation [39]. Secretion of HMW adiponectin complexes is stimulated by SIRT1 via suppression of PPARγ causing an upregulation of Ero1-Lα [40] and as the biological function of adiponectin might be

dependent on oligomer formation [41], with HMW being the most biologically active form, the level of HMW more so than total adiponectin might be important for its anti-diabetic and anti-inflammatory role [42].

1.2.5 Adiponectin Receptors

The adiponectin receptors AdipoR1 and AdipoR2 identified by Yamaquichi and colleges were found to contain seven-transmembrane domains but to be both structurally and functionally distinct from guanine nucleotide-binding protein (G-protein) coupled receptors in that they do not associate with any G-proteins and have a reverse membrane polarity with a cytoplasmic N-terminus and a short extracellular C-terminus [43, 44]. Their importance in metabolism was established by a double knock-out study producing mice that presented with elevated insulin levels and glucose intolerance. AdipoR1 is mainly expressed in liver, skeletal muscle, macrophages and hypothalamus, while AdipoR2 is highly expressed in liver, white adipose tissue and vasculature [18].

1.2.6 Signaling

The signalling cascade initiated by adiponectin binding to AdipoR1 and AdipoR2 has not been completely elucidated and requires further study, but one immediate downstream mediator of adiponectin signalling, adaptor protein phosphotyrosine interaction PH domain and leucine zipper containing 1 (APPL1), has been identified. Other downstream effects of adiponectin regulate glucose and lipid metabolism via activation of adenosine monophosphate-activated protein kinase (AMPK) and PPARγ, increasing lipid oxidation and mitochondrial biogenesis while decreasing gluconeogenesis. Full adiponectin-mediated AMPK activation is dependent on calcium/calmodulin-dependent protein kinase beta (CaMKKβ) and AMP/liver kinase B1 (LKB1) [18, 45]. Adiponectin binding to AdipoR stimulates APPL1 association with the receptor which leads to an interaction between APPL1 and ras-related protein 5 (Rab5), causing an increased glucose transporter type 4 (GLUT4) membrane translocation and glucose uptake in skeletal

muscle. This crosstalk between adiponectin and insulin signaling pathways makes APPL1 a critical regulator of the insulin mimetic action of adiponectin [46].

1.2.7 Functional Significance

In early loss-of-function studies there was some variability in the report of adiponectin's influence on insulin sensitivity; some studies demonstrated reduced insulin sensitivity [47], some reported improvements only in high-fat diet (HFD) fed mice [48] while some did not show any effect on insulin signaling at all [49]. However delivery of adiponectin in conditions of obesity and diabetes have consistently been shown to stimulate AMPK and PPARγ activity, increasing lipid oxidation, reducing free fatty acid (FFA) levels and improving insulin sensitivity and glucose tolerance [17, 50, 51] making adiponectin action relevant in the study of obesity and diabetes.

The strong inverse correlations between adiponectin and both insulin resistance and inflammatory states has been well established [52, 53]. Interestingly it has been shown (in non-human primates) that adiponectin levels decline before obesity and insulin resistance develops, suggesting that hypoadiponectinemia might be involved and contribute to the pathogenesis of obesity resulting in insulin resistance [54, 55].

1.2.8 Therapeutic Potential

Weight-loss and exercise are the initial recommendations to help control blood glucose levels in diabetic patients, but if this approach is not enough to manage the disease there are several types of medications that can be prescribed to help manage blood glucose levels. These, however, are typically associated with adverse effects including weight-gain, digestive problems, or even liver damage [56]. Hence identification of new therapeutic targets and their specific mechanisms remain relevant research areas.

The decreased circulating levels of adiponectin in obesity and diabetes together with the beneficial effects of adiponectin administration on insulin resistance suggest potential as a

diabetes treatment. Indeed it has been shown that one category of diabetes medications, thiazolidinediones (TZDs), might partially elicit its beneficial effect via an upregulation of HMW adiponectin expression and secretion through PPARγ activation [57-62]. Direct administration of adiponectin as a diabetes treatment, however, is not cost-effective as its production requires mammalian expression systems and is a time-consuming and labour intensive process. Additionally, adiponectin is a protein and would be broken down in the digestive system and therefore needs to be administered intravenously which is not an ideal method of delivery. Currently there is a lot of interest in finding chemical molecules that can bind and activate AdipoR1 and AdipoR2 and mimic adiponectin action in a convenient and cost-effective manner [63], and this field of research is expected to accelerate with the recent publication of AdipoR's crystal structure [64].

1.2.9 Adiponectin and Skeletal Muscle

Skeletal muscle is one of the most important tissues involved in whole body glucose homeostasis, and insulin resistance in skeletal muscle plays a key role in the pathogenesis of diabetes making it an important tissue to study in the context of obesity, insulin resistance and diabetes [65, 66]. It has recently been shown that in addition to being a receptor of endocrine adiponectin action via AdipoR, skeletal muscle express adiponectin, establishing adiponectin as a myokine, and the autocrine action of adiponectin has been shown to, at least in part, mediate its beneficial anti-diabetic metabolic effects as local production leads to increased glucose uptake and improved insulin sensitivity [62, 67].

Although the beneficial metabolic effects by adiponectin on skeletal muscle is well established, the cellular mechanisms involved have not yet been elucidated [68]; our lab have recently published a study that investigated the effect of adiponectin in HFD fed mice on insulin sensitivity, which showed that induction of autophagy via AMPK and a reduction of oxidative stress was involved in the insulin sensitizing effect of adiponectin [69] but further research is still

needed to elucidate the exact mechanism of insulin sensitization by adiponectin in skeletal muscle.

1.3 Skeletal Muscle Insulin Resistance

1.3.1 Insulin Signaling

In healthy subjects, elevated glucose levels cause secretion of insulin from the pancreas acting on peripheral tissues such as liver, adipose and muscle. Insulin binding to the insulin receptor (IR) induces a conformational change resulting in autophosphorylation and activation of its intrinsic tyrosine kinase. Activated IR is bound by insulin receptor substrate (IRS) via phospho-tyrosine binding (PTB) domains and, upon binding, IR phosphorylate tyrosine residues on IRS, allowing it to interact with Scr homology 2 (SH2) domains in the p85 regulatory subunit of phosphotidylinositol-3-kinase (PI3K). Interaction with IRS activates the p110 catalytic subunit of PI3K which mediate the conversion of phosphatidylinositol 4,5-bisphosphate (PIP2) to phosphatidylinositol 3,4,5-triphosphate (PIP3), recruiting and inducing a conformational change in AKT allowing its phosphorylation and activation by phosphoinositide-dependent kinase-1 (PDK-1) on threonine 308 and by mammalian target of rapamycin complex 2 (mTORC2) on serine 473. Activated AKT then induces GLUT4 translocation to the plasma membrane via Rab5, increasing glucose uptake to the cell [70-73]. Additionally IR activates the mitogen-activated protein kinase (MAPK) pathways involved in cell growth and differentiation [72].

1.3.2 Disruption of Insulin Action in Obesity and Diabetes; JNK

The ability of IR to phosphorylate IRS-1 on tyrosine residues, required for IRS activation, is severely impaired in obese and diabetic subjects compared to healthy, lean subjects. MAPK signaling, however, is not affected, suggesting that impairment of insulin signaling occurs at the IRS-1 level [74]. It is believed that increased serine phosphorylation of IRS-1 is the cause for the impaired tyrosine phosphorylation and, indeed, it has been shown that preventing serine

phosphorylation by mutation of serine residues in IRS-1 prevent development of insulin resistance in mice on HFD [75].

The factors responsible for the serine phosphorylation of IRS and the exact mechanism by which this happens has not been fully established, but c-Jun N-terminal kinase 1 (JNK1) has been suggested as one potential negative regulator of insulin signaling [76]. JNK is activated in obesity by inflammatory pathways such as TNFα [76, 77], and knocking out JNK1 has been shown to protect against obesity related insulin resistance, placing JNK1 as a link between inflammation and metabolic pathways [76, 78].

1.3.3 Cellular Events Involved in the Development of Insulin Resistance

In an environment of disrupted cellular homeostasis, such as insulin resistance, a variety of cellular responses and signalling cascades are likely to be involved. ER stress and unfolded protein response (UPR) signalling as well as autophagy, are important for sensing changes in the intracellular milieu, and disruptions in cellular homeostasis can lead to oxidative stress. All of these cellular conditions and processes are therefore relevant to study in the context of developing insulin resistance and have been implicated in the pathogenesis of obesity and diabetes, but their role in skeletal muscle have yet to be fully established [71, 79-84].

Although it was suggested 30 years ago that skeletal muscle insulin resistance is a main contributor to the glucose intolerant state of diabetes, the exact molecular mechanisms that leads to development of insulin resistance are still not fully characterized [66, 71]. To be able to understand how adiponectin elicits beneficial effects in muscle it is important to understand how insulin resistance in muscle develops and which cellular processes are involved. The following sections will therefore examine the suggested role of ER stress, UPR signalling, oxidative stress and autophagy in skeletal muscle insulin resistance; what is known about the integration between these complex cellular events and what is yet to be established.

1.4 ER Stress and UPR Signaling

1.4.1 Endoplasmic Reticulum

The ER is a cellular organelle responsible for processing of newly synthesized secretory, plasma membrane and organelle proteins. It plays an important role in protein synthesis, folding and trafficking, calcium homeostasis and lipid synthesis. The ER is a sensor of changes in the intracellular milieu, it functions as a communicator between the cytosol and nucleus and induces changes in gene expression to maintain cellular homeostasis in response to a variety of stimuli [85-88].

Proteins that require processing in the ER contain a sequence that targets the ribosome to the ER, the poly-peptide sequence is then translocated into the ER lumen during translation where the signal peptide is cleaved off [89, 90]. The unfolded poly-peptide chain is folded into secondary and tertiary structures with the help of a variety of ER chaperones and folding enzymes, and the protein structure is stabilized by disulfide bonds and often assembled into multimeric complexes, processes that are dependent on the oxidizing environment of the ER lumen [85, 90]. Proper folding is sensitive to ER homeostasis which can be disrupted in response to a variety of pathophysiological conditions, for example in obesity and diabetes [79, 91].

1.4.2 ER Stress and UPR Signaling

When protein folding and ER function gets compromised it leads to an accumulation of unfolded proteins, a condition known as ER stress [86, 92]. ER stress activates the UPR, a signaling cascade with downstream targets functioning to alleviate ER stress by increasing the folding capacity of the ER, reducing the protein folding load and activating ER associated degradation (ERAD) [86, 93].

This response is mediated through three ER membrane proteins, protein kinase-like ER kinase (PERK), inositol-requiring enzyme-1 (IRE1) and activating transcription factor 6 (ATF6)

[85-87]. The ER luminal domain of PERK, IRE1 and ATF6 are bound by the ER chaperone glucose-regulated protein 78 (GRP78) keeping them inactive, however with an accumulation of unfolded proteins GRP78 is titrated away binding to the unfolded proteins, causing activation and initiation of PERK, IRE1, ATF6 and their respective downstream signaling cascades. These signaling cascades ultimately regulate ER chaperones, folding enzymes, antioxidants, lipid synthesis, protein degradation and translational attenuation [87, 88, 94, 95].

Dissociation of GRP78 from PERK leads to activation if its serine/threonine kinase activity through dimerization and autophosphorylation, pPERK then phosphorylates eukaryotic translation initiation factor 2 (eIf2α) which prevents general translation to reduce the protein folding load while allowing selective translation of activating transcription factor 4 (ATF4) which activates the expression of UPR target genes including chaperones and folding enzymes [94, 96].

Activation of IRE1 occurs in the same way as PERK, dissociation of GRP78 from the ER luminal domain causing dimerization and autophosphorylation. Phosphorylation of IRE1 activates its RNase activity cleaving X-box binding protein 1 (XBP1) mRNA allowing translation of an active transcription factor that act on a several UPR target genes. Activation of IRE1 also leads to phosphorylation and activation of JNK via TNF receptor-associated protein factor 2 (TRAF2) and apoptosis signal-regulating kinase 1 (ASK1) [94], and additionally pIRE1 degrade mRNA to reduce the protein folding load of the ER [86].

ATF6 is also activated by dissociation of GRP78, however activation of ATF6 is mediated by translocation to Golgi where it is cleaved by site-1 protease (S1P) and site-2 protease (S2P) to form a 50kDa active transcription factor that translocate to the nucleus to active UPR target genes such as chaperones and genes involved in lipid synthesis [86, 97].

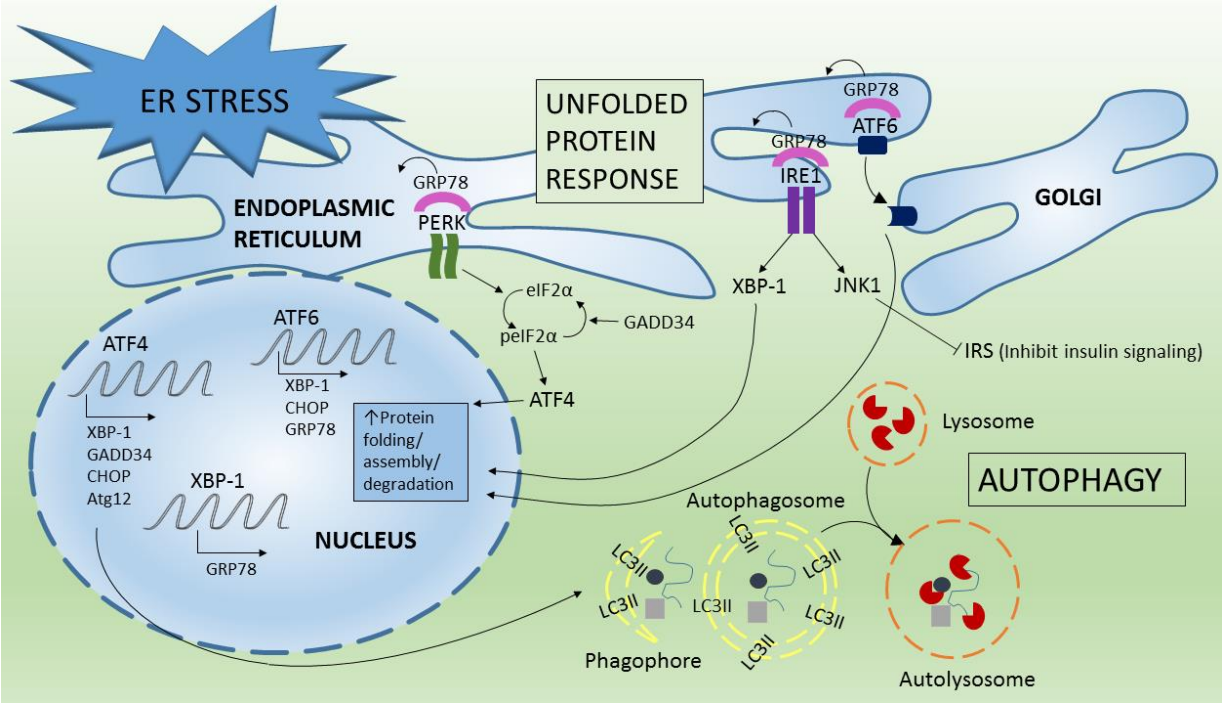

Figure 1.1. ER stress and UPR signaling. Disruption of normal Endoplasmic Reticulum (ER) function leads to an accumulation of unfolded protein, a condition termed ER stress. Increasing ER stress cause an activation of the unfolded protein response (UPR). There are three branches of the UPR controlled by three ER transmembrane proteins: PERK, IRE1, and ATF6. In normal conditions the ER chaperone GRP78 is bound to their ER luminal domain keeping them inactive, however the increased levels of unfolded proteins in ER stress conditions cause GRP78 to dissociate allowing their activation (phosphorylation of PERK and IRE1 and cleavage of ATF6) and initiation of their respective downstream signaling cascades. The function of these signaling cascades is to increase the capacity for protein folding and assembly but also to decrease the protein folding load by increasing ER associated degradation (ERAD) of unfolded proteins [86, 88, 92, 97]. In addition to ERAD it has been suggested that unfolded proteins associated with ER stress are degraded by autophagy with the UPR potentially inducing autophagy via activation eIf2α downstream of PERK, but this mechanism is yet to be fully established [98-100].
Endoplasmic Reticulum (ER); Unfolded Protein Response (UPR); ER associated degradation (ERAD).

1.4.3 ER Stress Induced Protein Degradation; Autophagy

Autophagy has been suggested as one mechanism that alleviates ER stress via degradation of unfolded proteins [98, 101] and autophagy deficient models have been shown to be more susceptible to developing ER stress and insulin resistance [102, 103]. Autophagy is thought be induced in response to ER stress via the UPR and the activation of PERK and eIF2α

[98, 101]. Another mechanism via which autophagy is induced in response to ER stress is via the IRE1-JNK pathway, which has been shown to be required for autophagy activation after ER stress [103]. Additionally XBP1 has been shown to regulate forkhead box protein O1 (FOXO1) which is involved in autophagy regulation [104, 105]. However, the exact role of autophagy in ER stress needs to be further established.

1.4.4 ER and ROS Production

Balance of the sensitive environment in the ER lumen is greatly influenced by redox potential, and a close relationship between ER stress and oxidative stress has been demonstrated [94] although this relationship is not fully understood as the interaction between ER stress, the UPR and oxidative stress is complex. It is known that exposure to oxidative stress causes an activation of the UPR [106], that protein folding and disulfide bond formation is responsible for 25% of reactive oxygen species (ROS) generation in cells [107], and that changes to the redox state of the ER affect its folding capacity leading at an accumulation of unfolded proteins and ER stress [85, 94]. Further, ER stress induces release of calcium from the ER lumen which triggers production of mitochondrial ROS, and energy depletion (caused by energy dependent protein folding) stimulate mitochondrial oxidative phosphorylation to produce more adenosine triphosphate (ATP), a process that produces ROS. Several links between oxidative stress, ER stress and the UPR has thus been found, but the complex interactions between these processes warrant further study, especially in the context of insulin resistance and diabetes.

1.4.5 ER Stress and the UPR in Insulin Resistance and Diabetes

A strong correlation between obesity, insulin resistance and diabetes have been well established, and one key underlying mechanism has been suggested to be ER stress [82, 108, 109]. Indeed it has been demonstrated that relieving ER stress through treatment with chemical

chaperones or upregulation of the ER chaperone GRP78 lead to restoration of insulin sensitivity and glucose tolerance in obese and diabetic mouse models [109-111].

The link between ER stress and insulin resistance has been shown to involve activation of JNK and subsequent phosphorylation of IRS-1 on serine residues, attenuating insulin signaling by preventing activating tyrosine phosphorylation of IRS-1 [109, 112]. However, it has recently been questioned whether UPR induced JNK activation is directly involved in insulin resistance by interfering with insulin signaling, or if these are merely concurrent events [113]. Further, although the role of ER stress in obesity related insulin resistance has been well established in several tissues such as adipose, pancreas and liver, its involvement in skeletal muscle has not yet been established [91] and more research is needed to fully elucidate the role of ER stress and the UPR in insulin resistance, especially in skeletal muscle.

1.5 Oxidative Stress

1.5.1 ROS Production and Oxidative Stress

Reactive oxygen species (ROS) is produced as a natural by-product of oxygen in cellular events such as enzymatic reactions involving oxidases and energy production in the mitochondria [114]. In normal physiological conditions the accumulation of ROS is counteracted by the endogenous antioxidant capacity of a cell which involve defenses such as catalase reductase, superoxide dismutase (SOD), and redox systems including oxidized glutathione/reduced glutathione (GSSG/GSH). In response to cellular stress, however, an increase in ROS production can cause an imbalance between ROS production and the antioxidant defense, leading to an accumulation of ROS, a condition referred to as oxidative stress [94].

1.5.2 Oxidative Stress in Diabetes and Insulin Resistance

Oxidative stress is known to damage cellular constituents such as proteins, lipids and nucleic acids and can therefore disrupt organelles and compromise cell viability [115]. Oxidative stress is currently being investigated in a number of disease states, including obesity, insulin resistance and diabetes [116], and it has been shown that increased levels of ROS together with declining cellular antioxidant capacity can lead to the development of insulin resistance, as established both by experimental and clinical studies [81, 84, 116, 117].

Several experimental studies have shown that antioxidant treatments can ameliorate the diabetic state [94, 117, 118]. However the failure of clinical trials to mimic this beneficial effects [119, 120] points to fact that the role of ROS might be more complex than initially perceived. Studies investigating cellular localisation of ROS production and antioxidant response has indeed established that ROS and redox signalling plays an important role in normal physiological conditions and that production of ROS and oxidative stress are complex and compartmentalised events capable of causing molecular modification to regulate a wide variety of cellular processes. One cellular process that is suggested to be regulated by ROS is autophagy [120, 121].

1.5.3 Redox Signaling and Autophagy

Studies examining the connection between redox signaling and autophagy has so far shown that reactive oxygen species are essential for starvation induced autophagy and that they directly stimulate the formation of autophagosomes via autophagy related gene-protein 4 (ATG4) [122, 123]. Production of ROS activates autophagy and, reciprocally, if the autophagic machinery is not functioning properly it can lead to the accumulation of ROS. As oxidative stress is widely accepted to be involved in insulin resistance and impaired autophagy also has been suggested to play a role in developing insulin resistance, the relationship between oxidative

stress and autophagy is of relevance to study in the context of insulin resistance and diabetes [80, 82, 124].

1.6 Autophagy

1.6.1 Autophagy Regulation and Function

Macroautophagy (hereafter referred to as autophagy) is a cellular bulk degradation process in which a double membrane structure is formed around proteins and organelles destined for degradation, this membrane elongates and closes around cargo to form an autophagosome. The autophagosome then fuses with a lysosome to form an autolysosome, undergoes acidification and the proteins and organelles are broken down by proteases and the remaining components released back into the cytosol [125]. A complete cycle of autophagy resulting in the degradation of cargo is termed autophagic flux [126].

Autophagy is responsible for degradation and turnover of long-lived proteins and organelles allowing major biochemical changes in the cell. Autophagy is upregulated in response to external stressors including metabolic changes and hormonal imbalance, and internal stressors such as accumulation of proteins aggregates (ER stress) and reactive oxygen species (oxidative stress). A constitutive, low level of autophagy is involved in maintenance of cellular homeostasis and too much or too little autophagy has been shown to be detrimental; properly regulated autophagy is thus important for a variety of cellular needs and in keeping cells healthy and viable [127].

The cytoplasmic regulation of autophagy (Fig. 1.2) has been well studied [128-136], however recently it has been suggested that the autophagic response occurs in three phases. The cytoplasmic regulation being the first level response, followed by gene regulation as the second level response and with epigenetic control and chromatin remodelling being the third level response creating an “autophagic memory” having long lasting effects on the process of autophagy [137].

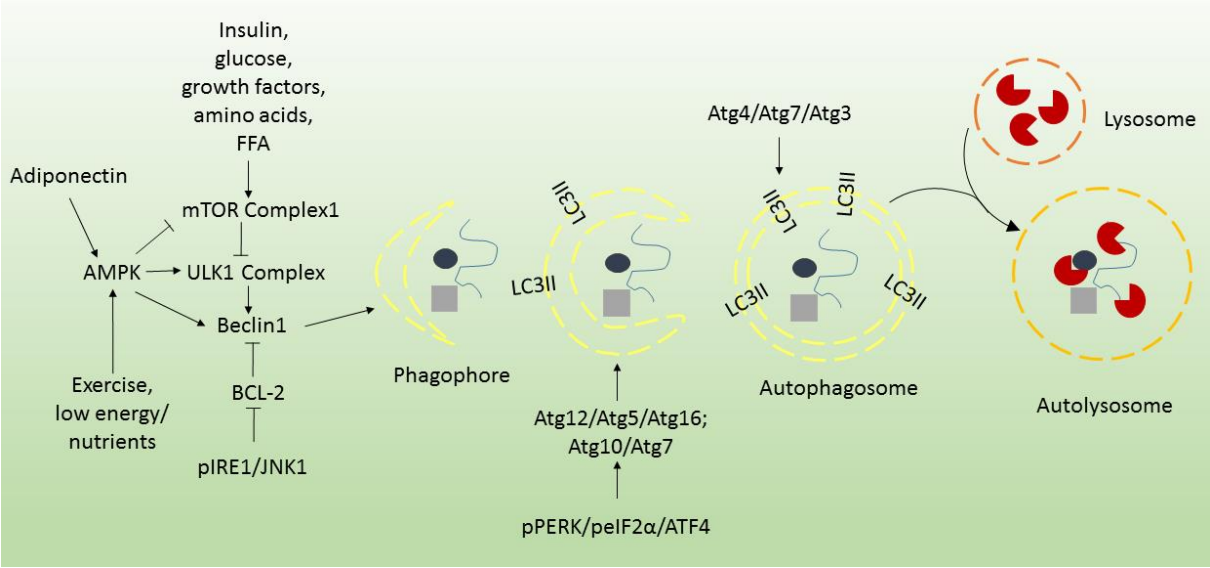

Figure 1.2. Cytoplasmic regulation of autophagy. Autophagy involves the formation of a double-membrane phagophore structure that form around proteins and organelles targeted for degradation. The phagophore membrane elongates and eventually close to form an autophagosome. Exercise and low energy/nutrients, as well as adiponectin, are known to positively regulate autophagy via AMPK. Activation of AMPK inhibit mTOR complex 1 and mediate selective phosphorylation of ULK1 complex on ULK1 S555 which, together with Beclin 1, initiate formation of the phagophore membrane [69, 138-141]. Activation of mTOR, however, negatively regulates autophagy through phosphorylation of ULK1 S757, and known activators of mTOR include insulin, growth factors and high energy/nutrient conditions [128-131, 142-146]. Two conjugation events are subsequently involved in vesicle elongation. The first one include covalent conjugation of ATG12 to ATG5, mediated by ATG7 and ATG10, allowing interaction with ATG16. The ATG5/12/16 complex then promote the second conjugation event in which pro-LC3 is cleaved by ATG4 where after ATG7 and ATG3 mediate conjugation of PE to LC3 forming LC3II [147-149]. LC3II gets incorporated into the phagophore membrane and function in cargo recognition as well as phagophore expansion [150]. The autophagosome then fuses with a lysosome and goes through acidification to form an autolysosome in which the protein and organelle cargo, as well as the inner membrane of the autolysosome, are degraded and components released back into the cytosol [125, 151]. Going through the complete cycle of this process is termed autophagic flux [126]. Autophagy related gene-protein (ATG); unc-51 like autophagy activating kinase 1 (ULK1); mammalian target of rapamycin (mTOR); microtubule-associated protein 1A/1B-light chain 3 (LC3); phosphatidylethanolamine (PE).

1.6.2 The Role of Autophagy in Insulin Resistance and Diabetes

The role of autophagy in sensing the nutritional state of the cell and responding to metabolic stress to maintain cellular homeostasis, together with the observations that autophagy is closely connected to ER and oxidative stress regulation and signaling, both well established

as playing a role in obesity and diabetes, has resulted in autophagy receiving increasing attention in the context of obesity and diabetes, and dysregulation of autophagy have been suggested to play a role in the progression of insulin resistance and diabetes in obesity [82].

It has been shown that in conditions of metabolic stress, beta-cell specific autophagy deficiency leads to development of diabetes [82]. Overexpression of ATG5 enhances autophagy and leads to increased insulin sensitivity and better tolerance to oxidative damage in mice [152], but autophagy knockout in specific insulin target tissues, such as muscle and liver, produced a variety of phenotypes [82]. Some demonstrate that autophagy deficiency is involved in pathogenesis of insulin resistance and diabetes [153], while some show leanness and resistance to diet induced obesity and diabetes [154], highlighting the fact that further studies are necessary to elucidate the role of autophagy in obesity, insulin resistance and diabetes.

1.7 Objectives

1.7.1 Research Questions and Experimental Model

Currently available diabetes medications are associated with a variety of side effects and novel therapeutic targets, aimed at finding better treatment options with fewer and milder side effects, are continually being investigated [56, 155]. Adiponectin has been shown to improve metabolic dysfunctions in obesity and diabetes and is currently under investigation as a potential diabetes treatment [156, 157]. While skeletal muscle has been identified as an important target of adiponectin action [68], the cellular mechanisms involved in the pathogenesis of insulin resistance and diabetes, and how these are regulated by adiponectin are poorly defined.

ER stress, UPR signaling, oxidative stress and autophagy are widely accepted to play a role in insulin resistance and diabetes [94, 117], however few studies have examined their coordinated role in skeletal muscle [91]. As muscle mass makes up 40-50% of the human body, and skeletal muscle plays an essential role in metabolism and whole body glucose

homeostasis, the cellular processes involved in the pathogenesis of insulin resistance in skeletal muscle is of critical relevance to study [158], and further, the interrelationship between these cellular processes need to be investigated, especially in the context of skeletal muscle insulin resistance.

Exposure to high insulin and high glucose media (HIHG) for 24hrs has previously been shown to induce insulin resistance in L6 skeletal muscle, and extensive evaluation of its effect on mediators of insulin signaling and glucose uptake established these conditions as a relevant model to examine cellular changes involved in insulin resistance [159] making this model also a suitable to examine the mechanisms involved in the insulin sensitizing effect of adiponectin in skeletal muscle.

1.7.2 Study Aims and Hypotheses

Using this *in vitro* insulin resistant skeletal muscle model I aim to: Firstly, characterize changes in oxidative stress, ER stress, UPR signaling and autophagy in skeletal muscle insulin resistance; Secondly, establish the effect of adiponectin on oxidative stress, ER stress, the UPR, autophagy and skeletal muscle insulin sensitivity. Thirdly, examine the interrelationship between oxidative stress, ER stress, UPR signaling and autophagy in the context of skeletal muscle insulin resistance.

I hypothesise that 1. insulin resistant skeletal muscle cells will exhibit increased levels of oxidative stress and ER stress, activation of UPR signaling and impaired autophagy, 2. adiponectin will alleviate oxidative stress and ER stress, activate UPR signaling and increase autophagy in insulin resistant skeletal muscle, and 3. improving insulin sensitivity and reducing ER stress by adiponectin is dependent on autophagy.

Chapter 2. Material and Methods

2.1 Cell Culture

2.1.1 Culture Conditions

L6 myoblasts were maintained in alpha-minimum essential medium (AMEM; 5.5mM glucose) supplemented with 10% fetal bovine serum (FBS) in 75 cm2 flasks at 37°C in 5% CO_2. Differentiation from myoblasts (MB) to myotubes (MT) was induced by serum starvation in 2% FBS AMEM for 6 days. Prior to treatments, cells were starved for 3 hours in 0.5% FBS AMEM with relevant chemical inducers/inhibitors added after 2 hours of starvation allowing a 1 hour pre-treatment before inducing insulin resistance. All AMEM contained 5% antibiotic-antimyotic solution, and 10% FBS AMEM used for growing stable cell lines contained puromycin to continuously select for transgene expressing cells. Culture media and solutions were purchased from Wisent Bio Products.

Cells were incubated in High Insulin (HI; 100nM Humulin R, purchased from Eli Lilly and Company) and High Glucose (HG; 25mM D-glucose purchased from Sigma-Aldrich) 0.5% FBS AMEM (HIHG) for 24 hours to induce insulin resistance.

2.1.2 Cell Lines

L6 GLUT4myc cell line. A stable L6 cell line transfected to overexpress GLUT4 with a myc epitope was used to assess insulin stimulated glucose uptake in L6 MB [160].

GRP78mCherry reporter cell line. A stable L6 GRP78mCherry reporter cell line containing a truncated version of the GRP78 promoter controlling the expression of mCherry allowed mCherry fluorescence signal to be used a readout of GRP78 gene expression, generally accepted as a readout of UPR activation due to its central role in the UPR signaling cascade. Inducing ER stress by several well-established pharmacological approaches has been shown to cause a marked increase in mCherry red fluorescence [161], although it should be noted that

using a fluorescent protein as a readout of gene expression have inherent limitation as there are many regulatory steps between gene expression and production of a functional fluorescing proteins that could affect the level of fluorescence independent of gene expression regulation, such as modifications/alterations that affect translation and protein processing [162, 163] .

Tandem-fluorescence LC3 cell line. A stable L6 Tandem Fluorescence LC3 cell line (TFLC3) containing the gene for LC3 fused to the gene for green fluorescence protein (GFP) and red fluorescence protein (RFP) allowed assessment of autophagy in response to selected treatments. In this cell line, GFP and RFP co-localize indicating the presence of LC3 by yellow fluorescence signal; accumulation of LC3 resulting in 'puncta' indicate autophagosomes. As the green fluorescence is quenched in the acidic conditions present inside autolysosomes but not inside autophagosomes, while the red florescence is preserved also in acidic conditions, the red/green fluorescence signal is used as a measurement of autophagic flux indicating completion of full cycles of autophagy.

Atg5K130R mutant cell line. A stable L6 Atg5K130R (Atg5K) dominant negative mutant cell line was used as a molecular model of autophagy inhibition. This point mutation prevents conjugation to ATG12 and blocks LC3II incorporation and elongation of the autophagosome membrane [164-167]. Empty vector (EV) cells were used as control.

The L6 GLUT4-myc cell line was a kind gift from Dr. Amira Klip (The Hospital for Sick Children, Toronto) and GRP78mCherry, TFLC3 and Atg5K130R cells lines were generated by retroviral infection as previously described [69]. In short, viral vectors containing the genes of interest were transfected into EcoPack 2-293 (Clontech Laboratories, Inc.), a human embryonic kidney-derived packaging cell line, and the virus-containing culture media was collected 48 hours post-transfection. After incubation for 24 hours with virus-containing media, L6 cells stably overexpressing the transgenes were selected by puromycin antibiotic resistance and maintained in puromycin containing growth media. No notable differences in morphology or growth was

observed between WT L6 cells and GLUT4-myc, GRP78mCherry, or TFLC3 cell lines. Atg5K cells, however, grew slower in comparison EV and WT L6 cells taking an average of 4-6 days to reach 100% confluence after seeding, compared to an average of 2-3 days for EV and WT cells. Additionally Atg5K MB failed to differentiate into MT and showed no signs of elongation or fusion after 8 days in differentiation media (2%FBS AMEM), while EV and WT cells were observed as elongated multinucleated MT between day 5-7. This atypical growth and differentiation patterns might be attributed to the potential role of autophagy in skeletal muscle differentiation and cell cycle regulation [140, 168, 169].

2.1.3 Reagents

Adiponectin was dissolved in phosphate buffered saline (PBS) to a stock concentration of 0.1µg/µl and 50µl/ml was added for a final concentration of 5µg/ml;

Salubrinal was dissolved in dimethyl sulfoxide (DMSO) to a stock concentration of 3mM and 10µl/ml was added for a final treatment concentration of 30µM;

N-acetyl cysteine (NAC) was diluted in PBS to a stock concentration of 500µM and 2µl/ml was added for a final concentration of 1mM;

Tunicamycin was dissolved in DMSO, to a stock concentration of 5mM, and 1.6 µl/ml was added for a final treatment concentration of 8µg/ml;

Rapamycin was dissolved in PBS, to a stock concentration of 27.4µM, and 36.5µl/ml was added for a final treatment concentration of 1µM;

Bafilomycin A1 (Bafilomycin) was dissolved in DMSO, to a stock concentration of 100µM, and 2µl/ml was added for a final treatment concentration of 200nM.

Adiponectin (mouse, mammalian expression system) was purchased from Antibody Immunoassay Services (Hong Kong) and all other reagents were purchased from Sigma-Aldrich.

2.2 Assays

2.2.1 Western blotting

Upon completion of treatment, L6 cells were lysed in denaturing RIPA lysis buffer (50mM Tris, 150mM NaCl, 0.1% SDS, 1% Triton X, and 0.5% sodium deoxycholate) containing β-mercaptoethanol, protease and phosphatase inhibitors, heated for 10 minutes in 90°C, and centrifuged at 12000 rpm for 3-15 minutes depending on protein of interest. Samples were loaded and ran in 8-15% sodium dodecyl sulfate polyacrylamide gel electrophoresis (SDS-PAGE). Proteins were transferred onto a polyvinylidene fluoride (PVDF) membrane at 110V for 70-85 minutes depending on protein of interest, blocked in 3% bovine serum albumin (BSA) blocking buffer, immunoblotted with primary antibodies (pPERK, peIf2α, LC3, pAKT, pmTOR, pULK1S757, pAMPK, pULK1S555, β-actin and GAPDH purchased from Cell Signaling, pIRE1 purchased from Novus Biologicals and ATF6 purchased from Santa Cruz) and subsequently with secondary horseradish peroxidase (HRP)-conjugated antibody (anti-rabbit, purchased from Cell Signaling). Protein bands were visualized using enhanced chemiluminescence (ECL) reagent and developing of exposed film. Band densitometry was determined using Image J, and corrected for loading control, β-actin or GAPDH.

2.2.2 Glucose Uptake

L6 GLU4myc cells were stimulated with 10 and 100nM insulin for 20 minutes before glucose uptake was assessed as previously described [160]. In short, insulin stimulated cells were incubated with HEPES-buffered saline solution containing 2-deoxy-D-[3H]glucose, washed in saline solution and lysed with NaOH. Cell lysates were put into scintillation vials containing 3ml of scintillation fluid for radioactivity counting.

2.2.3 Thioflavin T – KDEL Immunofluorescence

Thioflavin T (ThT) dye exhibit increased fluorescence when bound by protein aggregates and the levels of fluorescence has been shown to correlate directly with established ER stress inducers [93]. ThT dye was added to live cells for 40 minutes (1µM/ml), media was aspirated and cells were washed before fixing in 4% paraformaldehyde for 20 minutes. Coverslips were mounted on slides in Vectashield mounting media containing DAPI.

When ThT assay was combined with KDEL immunofluorescence, after fixing, the cells were quenched in 0.1% glycine in PBS for 10 minutes, washed with PBS and permeabilized for 3 minutes in 0.1% Triton X 100. The cells were blocked for 30min in 3% BSA, and then incubated overnight at 4°C with 1:500 primary KDEL antibody. After primary incubation the cells were washed and subsequently incubated with 1:1000 secondary antibody Alexa Fluor 594 for 1 hour in the dark at room temperature and washed before coverslips were mounted on slides in DAKO mounting media.

2.2.4 Magic Red

Magic Red is a cell permeable substrate that fluoresces upon cleavage by cathepsin B and increased cathepsin B activity therefore results in more fluorescence signal. Cathepsin B targets a wide range of intracellular proteins in lysosomes and Magic Red fluorescence intensity can be used as a general measurement of lysosomal activity [170]. After fixing with 4% paraformaldehyde for 20 min, the cells were quenched in 0.1% glycine for 10 minutes. Cells were permeabilized in 0.1% Triton X 100 for 3 minutes and blocked for 30 minutes in 3% BSA, and Magic Red reagent added at 1x concentration according to manufacturer's protocol and incubated for 30 minutes. Cells were washed before coverslips were mounted on slides in Vectashield mounting media containing DAPI.

2.2.5 Catalase Activity

Catalase activity was determined using BioVision Catalase Activity Colorimetric Assay Kit (#K773-100) according to manufacturer's instructions. In short, cell lysates were incubated with H_2O_2 (3%, 0.88M) and catalase present in the cell lysates was allowed to convert H_2O_2 to water and oxygen before OxiRed was added. OxiRed reacts with unconverted H_2O_2 to produce as product that can be detected colorimetrically, with catalase activity being reversely proportional to the signal detected.

2.2.6 CellRox Green

CellRox Green reagent is a cell permeable fluorogenic dye that exhibit bright fluorescence when oxidized by reactive oxygen species and was used a measure of oxidative stress. Upon completion of treatments, cells were incubated with CellRox Green according to the manufacturer's instructions (#C10444, Molecular Probes Life Technologies) before coverslips were mounted on slides in Vectashield mounting media containing DAPI.

2.3 Analysis

2.3.1 Fluorescence Confocal Microscopy Imaging

Microscopy slides prepared from GRP78mCherry and TFLC3 cells lines, as wells as slides prepared from ThT-KDEL, MagicRed and CellRox Green assays, were imaged in Zeiss LSM 700 Laser Confocal Microscope using solid state lasers; 405nm (blue channel: 405/435 filter setting), 488nm (green channel: 488/518 filter setting) and 555nm (red channel: 555/585 filter setting). Gain and offset parameters were optimized for each experiment but kept constant between different treatments within an experiment.

2.3.2 Quantification

Stacked images (12 slices) were taken for GRP78mCherry experiment and quantified in Image J software as average fluorescence intensity per cell for 40 cells/treatment/replicate experiment; all other images were taken as single images. TFLC3 experiments were quantified

as total red/green fluorescence intensity per image for 8-10 images using Zen 2012 Blue Edition. ThT–KDEL, CellRox Green and Magic Red were quantified as total green or red fluorescence intensity per image divided by the number of cells in the view for 5-10 images using Zen 2012 Blue Edition.

2.3.3 Statistical Analysis

Comparison between two groups were done using unpaired one-tailed t-test and comparisons between multiple groups were done by one-way ANOVA. Significant ANOVAs were followed by Tukey's HSD post hoc test when differences between all groups were of interest and Dunnett's post hoc test when all groups were compared to control. $P<0.05$ was accepted as significant.

Chapter 3. Results

3.1 Characterization of Autophagy, ER stress, the UPR and Oxidative Stress in Skeletal Muscle Insulin Resistance

3.1.1 HIHG Treatment Impaired Insulin Signaling and Insulin Stimulated Glucose Uptake in L6 Skeletal Muscle Cells

To validate my insulin resistant model I treated L6 myotubes with HIHG for 24 hours and measured the level of AKT phosphorylation in response to 100nM of insulin at 0, 1, 3, 6, 8 and 10 minutes. In control conditions there was a marked increase in AKT phosphorylation in response to insulin stimulation, peaking around 3-6 minutes, while HIHG treated cells showed no increase in AKT phosphorylation in response to insulin stimulation (Fig. 3.1A). In line with this, 5 minutes of 100nM insulin stimulation resulted in increased glucose uptake for control, but not HIHG treated cells (Fig. 3.1B), however 5 minutes of 10nM insulin stimulation did not cause an increase in glucose uptake in control or HIHG condition (Fig. 3.1B). The level of AKT phosphorylation in response to 5 minutes of 100nM insulin stimulation gradually decreased in response to HIHG treatment, measured at 2, 6 and 24 hours, with significantly lower AKT phosphorylation for HIHG compared to control condition at each time point (Fig. 3.1C and D). These data together demonstrate that HIHG treatment induced insulin resistance in skeletal muscle cells.

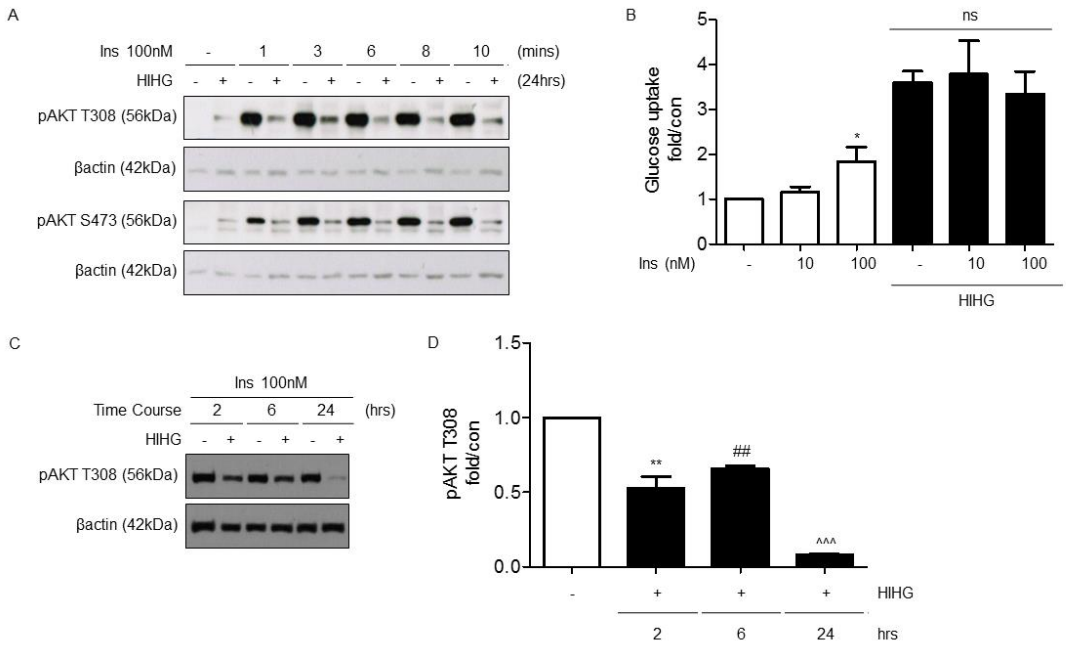

Figure 3.1. Skeletal muscle insulin resistance was induced by exposing L6 cells to HIHG condition.

(A, C and D) L6 WT MB were differentiated into MT in 6-well cell culture plates in 2% FBS AMEM, starved in 0.5% FBS AMEM for three hours and treated with high insulin and high glucose media (HIHG; 0.5% FBS AMEM with 100nM insulin and 25mM glucose) for 2, 6 or 24 hrs. Upon completion of treatments cells were stimulated with 100nM insulin for 0-10 minutes (A) and for 5 minutes (C and D), cell lysates were prepared and protein content analyzed by western blotting. Representative blots are shown (A and C; n=3) and quantification of band densitometry is represented as fold over control (D; n=3) with standard error of mean displayed as error bars.

(B) L6 GLUT4myc MB were grown to 100% confluency in 24-well cell culture plates in 10% FBS AMEM, starved in 0.5% FBS AMEM for three hours and treated with HIHG for 24 hours. After 5 minutes of 0, 10 or 100nM insulin stimulation (^{3}H)2-deoxy-d-glucose uptake assay was performed and represented as fold over control (B; n=3) with standard error of mean displayed as error bars.

AKT phosphorylation in response to 100nM insulin at 0, 1, 3, 6, 8, and 10 minutes in cells treated with 24 hrs of HIHG showed more basal phosphorylation of AKT than control conditions, but no insulin stimulated increase in pAKT. Although there was some fluctuation in AKT phosphorylation over the insulin time course in controls cells, there was a clear increase compared to HIHG conditions at each time point (A; n=3). Comparing insulin stimulated AKT phosphorylation for 2, 6 and 24 hours of HIHG treatment showed a gradual reduction in HIHG treated compared to control cells (C and D; p<0.0001). Glucose uptake was not stimulated by 10nM of insulin in control or HIHG condition while a significant increase in glucose uptake was seen with 100nM insulin stimulation in control but not HIHG condition (B; n=3).

*(B) *Significantly different compared to no-insulin control (P=0.05)*

*(D) **/##Significantly different compared to control and 24 hours HIHG treatment. ^^^Significantly different compared to control, 2 and 6 hours HIHG treatment. (p<0.0001). *P < 0.05; **P < 0.01; ***P < 0.001.*

3.1.2 HIHG Treatment Impaired Autophagosome Formation and Decreased Autophagic Flux

Next I examined different stages of autophagy using a variety of well-established assays. I observed a decrease in the autophagosome marker protein LC3II, concurrent with an increase in LC3I, in response to 24 hours of HIHG treatment (Fig. 3.2E and F). TFLC3 microscopy data further supported a decrease in autophagosome formation as demonstrated by the decrease in TFLC3 puncta signifying autophagosomes (Fig. 3.2A). Calculating the red/green fluorescence ratio from TFLC3 images confirmed a decrease in autophagic flux in response to HIHG treatment (Fig. 3.2A and D) but, contrary to expectation, the decrease in autophagic flux in HIHG treated cells was associated with an increase, not decrease, in lysosomal activity as determined by MagicRed assay measuring Cathepsin B activity (Fig. 3.2B and C).

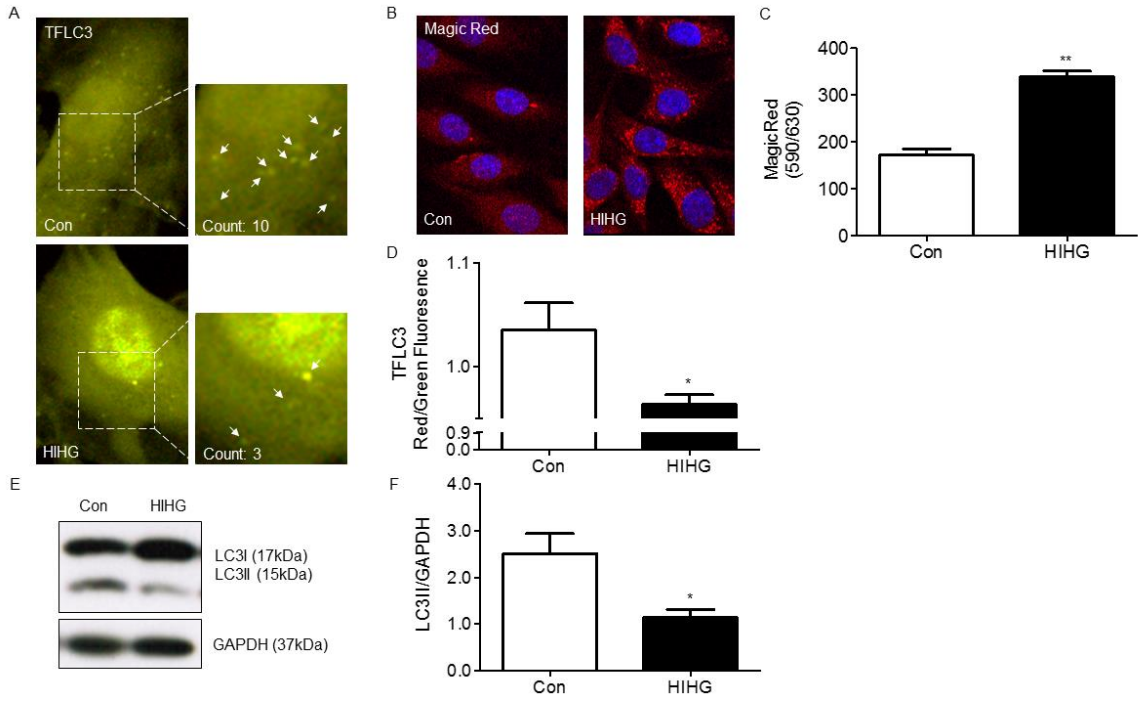

Figure 3.2. Autophagy was impaired in insulin resistant skeletal muscle cells.
(A-B and D-E) TFLC3 and WT L6 MB were grown on coverslips to 70% confluency in 12-well cell culture plates in 10% FBS AMEM, starved in 0.5% FBS AMEM for three hours before 24 hours HIHG treatment. TFLC3 L6 MB were fixed upon completion of treatment and MagicRed assay was performed on WT L6 MB; 7-9 images per condition were taken by fluorescence confocal microscopy. Representative images are shown (A and B; n=6-10); quantification of TFLC3 total red/green (D; n=4) and quantification of total MagicRed fluorescence/cell (C; n=3) is represented as mean values with standard error of mean displayed as error bars.
(C and F) L6 WT MB were differentiated into MT in 6-well cell culture plates in 2% FBS AMEM, starved in 0.5% FBS AMEM for three hours before the 24 hour HIHG. Upon completion of treatments cell lysates were prepared and protein content analyzed by western blotting. Representative blots are shown (E; n=7) and quantification of band densitometry is represented as fold over control (F; n=7) with standard error of mean displayed as error bars. HIHG treatment decreased TFLC3 puncta (A), red/green fluorescence (D; p=0.0133) and LC3II (E and F; p=0.0496) compared to control, while lysosomal activity, assessed by Magic Red assay, was increased in HIHG condition (B and c; p<0.0001)
/ Significant difference compared to control. *P < 0.05; **P < 0.01.*

Looking closer at the temporal induction of impaired autophagy in response to HIHG treatment I found that the decrease in autophagy occurred gradually, measured at 2, 6 and 24 hours, with a significant decrease in LC3II at 2 and 24 hours but interestingly not at 6 hours, while LC3I was unchanged at 2 hours but significantly increased at 6 and 24 hours (Fig. 3.3E, H and I). Similarly as for LC3II, there was a gradual decrease in TFLC3 red/green fluorescence ratio and therefore autophagic flux, measured at 2, 6 and 24 hours, however autophagic flux was significantly different at each time point, both compared to control and compared to the other time points (Fig. 3.3A and B). Although there was a marginal increase in LC3II at 6 hours compared to 2 hours of HIHG treatment, together these results demonstrated a gradual impairment of autophagy in response to HIHG treatment, and I hypothesized that the decrease in autophagy was caused by changes in early regulatory events, downregulating autophagosome formation, resulting in decreased autophagy.

Examining early autophagy regulators by western blotting I showed that the autophagy inhibitor pmTOR, together with its downstream autophagy specific target, pULK1S757, were downregulated compared to control at 2 hours of HIHG treatment but increased at 6 and 24 hours (Fig. 3.3C-E). pAMPK is known to stimulate autophagy via pULK1S555 but, although there was a decrease in both pAMPK and pULK1S555 at 2 hours of HIHG treatment, they followed a similar pattern as pmTOR and pULK1S757 with an increase at 6 hours. At 24 hours, however, pULK1555 was again downregulated while pmTOR and pULK1S757 were upregulated (Fig. 3.3E-G). This regulatory pattern is consistent with the biphasic decrease in LC3II, potentially indicating an attempted recovery following the initial impairment in autophagy, and these data demonstrate decreased initiation of autophagosome formation in response to HIHG treatment at 24 hours.

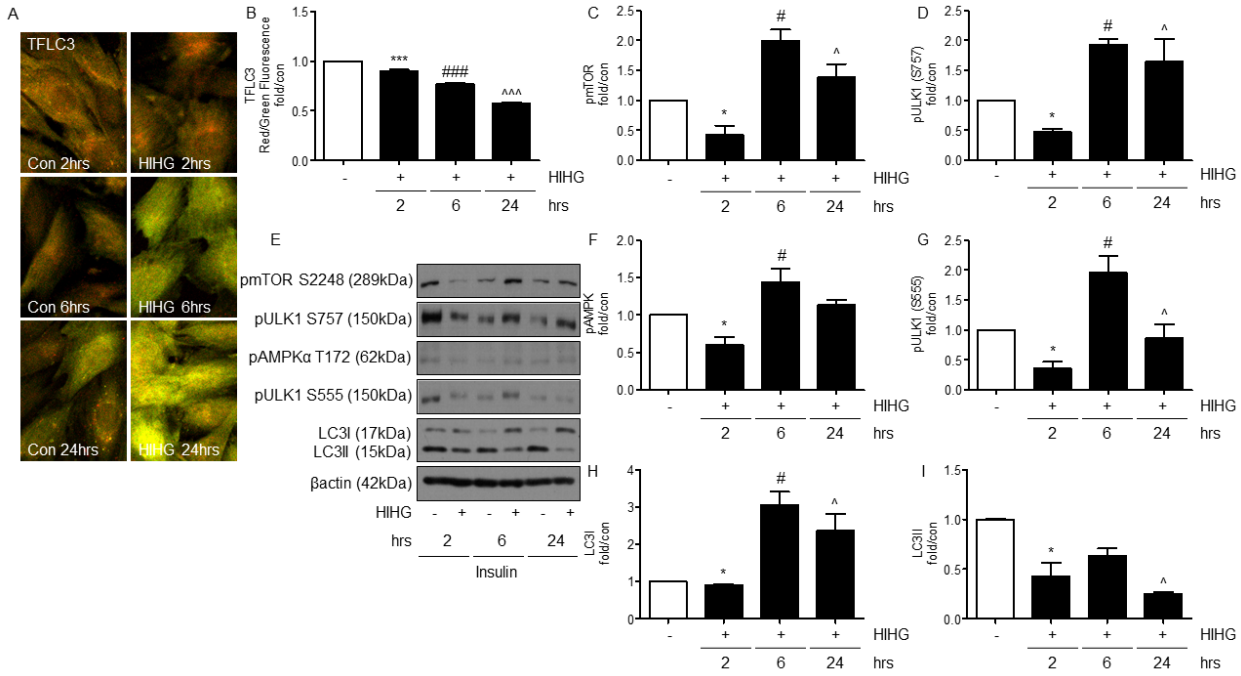

Figure 3.3. Autophagy gradually decreased in response to HIHG treatment.
(A and B) TFLC3 L6 MB were grown on coverslips to 70% confluency in 12-well cell culture plates in 10% FBS AMEM, starved in 0.5% FBS AMEM for three hours before 2, 6, or 24 hours of HIHG treatment. TFLC3 L6 MB were fixed and mounted upon completion of treatment and 5-9 images per condition was taken by fluorescence confocal microscopy. Representative images are shown (A; n=3) and quantification of TFLC3 total red/green fluorescence is represented as fold over control (B; n=3) with standard error of mean displayed as error bars.
(C-G and H-I) L6 WT MB were differentiated into MT in 6-well cell culture plates in 2% FBS AMEM, starved in 0.5% FBS AMEM for three hours before 2, 6, or 24 hour HIHG treatment. Upon completion of treatments cells were stimulated with 100nM of insulin for 5 minutes, cell lysates were subsequently prepared and protein content analyzed by western blotting. Representative blots are shown (E) and quantification of band densitometry is represented as fold over control (C-D and F-I; n=3) with standard error of mean displayed as error bars. pmTOR and pULK1 S757 were decreased at 2 hours but increased at 6 and 24 hours (E, C; p=0.0090 and D; p=0.0258). pAMPK and pULKS555 were similarly decreased at 2 hours but increased at 6 hours, however at 24 hours there was no difference compared to control in pAMPK, while pULK1 S555 was decreased (E and F; p=0.0278, G; p=0.0181). LC3II showed a gradual decrease at 2, 6 and 24 hours compared to control with significant difference at 2 and 24 hours (E and I; p=0.0114), and a corresponding increase in LC3I for HIHG compared to control at 6 and 24 hours (E and H; p=0.0004). There was a gradual decrease in TFLC3 red/green fluorescence in response to HIHG treatment with significant differences at 2, 6 and 24 hours (A and B; p<0.0001).
*(B) ***/###/^^^ Significant difference between all conditions. p<0.0001*
*(C) *Significant difference compared to 6 and 24 hrs. #Significant difference compared to control and 2 hrs. ^Significant difference compared to 2 hrs. p=0.0100*
*(D) *Significant difference compared to 6 and 24 hrs. #Significant difference compared to 2 hrs. ^Significant difference compared to 2 hrs. p=0.0206*
*(F) *Significant difference compared to 2hrs. #Significant difference compared to 6 hrs. p=0.0278*

*(G) *Significant difference compared to 6 hrs. #Significant difference compared to 2 hrs. ^Significant difference compared to 6 hrs. p=0.0181*
*(H) *Significant difference compared to 6 hrs. #Significant difference compared to control and 2 hrs. p=0.0148*
*(I) *Significant difference compared to control. ^^Significant difference compared to control. p=0.0097*
**P < 0.05; **P < 0.01; ***P < 0.001.*

3.1.3 HIHG Treatment Increased ER Stress and UPR Activation

To examine whether the impairment in autophagy, caused by HIHG treatment, was associated with an increase in ER stress, I performed ThT assay directly assessing the level of unfolded proteins, the hallmark of ER stress, which showed an increase of unfolded proteins compared to control after 24 hours of HIHG treatment (Fig. 3.4A and B). The increase in ER stress was, as expected, accompanied by an increase in UPR activation, determined by a GRP78mCherry reporter assay in which mCherry red fluorescence was used a general readout of UPR activation (Fig. 3.4C and D). Looking in detail at the UPR response, examining activation of the individual branches involved, namely IRE1, PERK and ATF6, I showed that their activation was increased in response to 24 hours of HIHG treatment (Fig. 3.5A-D), while the downstream target of pPERK, peIf2α, was downregulated (Fig. 3.5A and E).

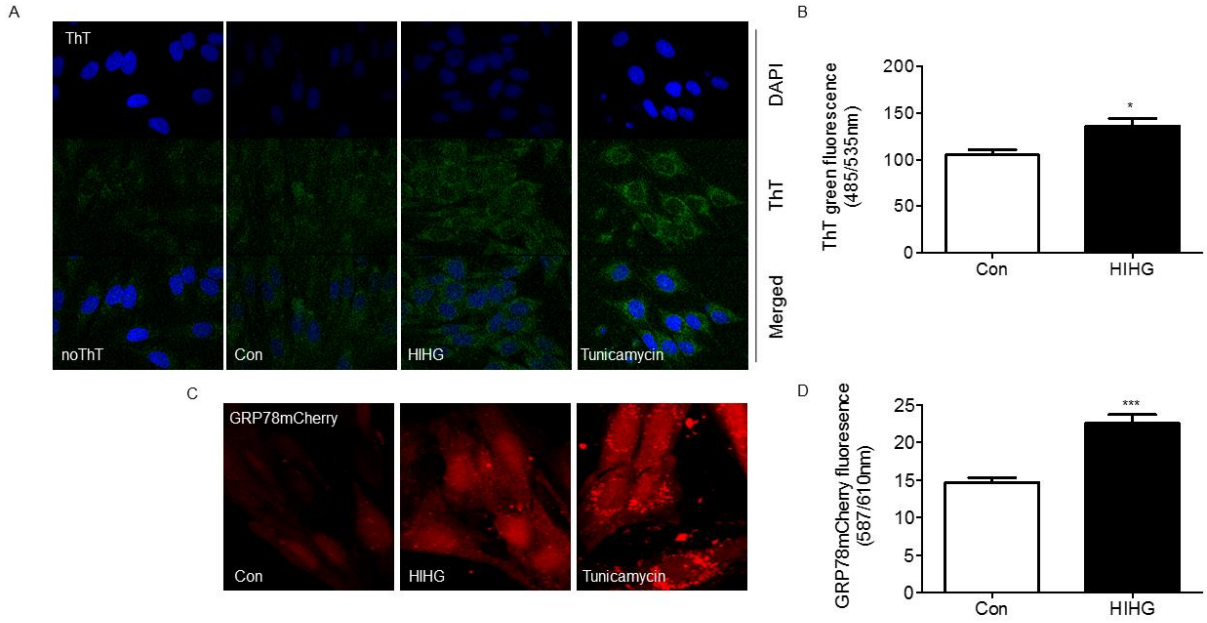

Figure 3.4. ER stress and UPR activation was increased in insulin resistance skeletal muscle cells.
(A-D) GRP78mCherry and WT L6 MB were grown on coverslips to 70% confluency in 6-well cell culture plates in 10% FBS AMEM, starved in 0.5% FBS AMEM for three hours before 24 hours HIHG treatment. GRP78mCherry L6 MB were fixed and mounted upon completion of treatment and ThT assay was performed on WT L6 MB, then fixed and mounted in DAPI; 9-12 images per condition was taken by fluorescence confocal microscopy and representative images are shown (A and C; n=3-7). Quantification of total ThT green fluorescence/cell and mean mCherry fluorescence/cell are represented as mean values (B and D; n=3-7) with standard error of mean displayed as error bars.
HIHG increased ThT fluorescence, and thus the level of unfolded proteins, compared to control (A and B; p=0.0178) correlating with increased UPR activation as measured by red fluorescence using GRP78mCherry reporter cells (C and D; p=0.0007). Tunicamycin is a known ER stress inducer used as a positive control also showing increased ThT and GRP78mCherry induction (A and C).
/* Significantly different compared to control.*
**P < 0.05; **P < 0.01; ***P < 0.001.*

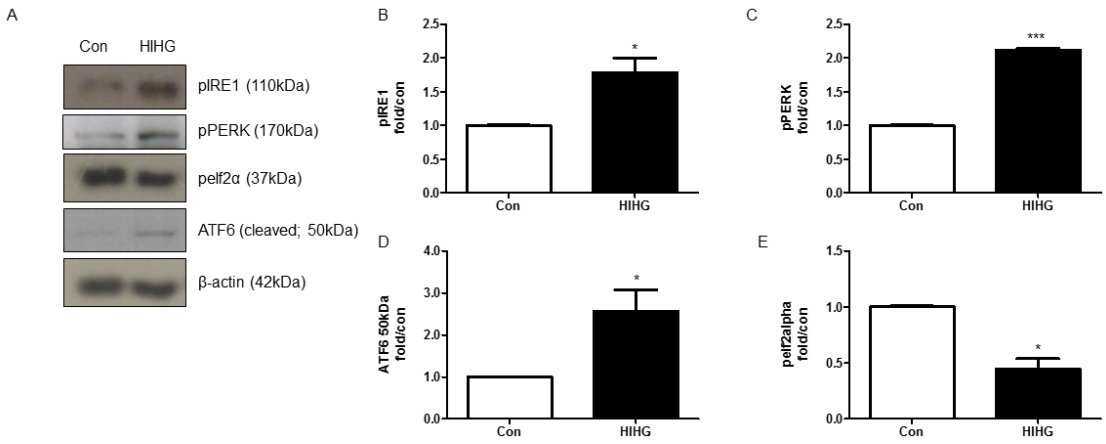

Figure 3.5. All three branches of the UPR were activated in insulin resistant skeletal muscle cells.
L6 WT MB were differentiated into MT in 6-well cell culture plates in 2% FBS AMEM, starved in 0.5% FBS AMEM for three hours before 24 hours HIHG treatment. Upon completion of treatments cell lysates were prepared and protein content analyzed by western blotting. Representative blots are shown (A; n=4-7) and quantification of band densitometry is represented as fold over control (B-E; n=4-7) with standard error of mean displayed as error bars.
All there mediators of the UPR response were upregulated in response to HIHG treatment (A, B; p=0.013, C; p<0.0001, D; p=0.0454), pelf2α however was decreased despite being directly downstream of pPERK (E; p=0.0134).
*/***Significantly different compared to control. *P < 0.05; **P < 0.01; ***P < 0.001.*

To confirm that the unfolded proteins detected using ThT assay were indeed localized to the ER, I performed a co-localization assay with ThT and KDEL immunofluorescence (Fig. 3.6). KDEL is an ER retention sequence present in most ER chaperones and foldases, a well-established marker of the ER, and merged imaged of ThT and KDEL fluorescence demonstrated that increased ThT green fluorescence correlated with increased yellow fluorescence caused by co-localization with KDEL red fluorescence (Fig. 3.6A and D). Using Manders co-localization coefficient (M1) I confirmed that the observed ThT green fluorescence signal almost exclusively localized to areas with red fluorescence (Fig. 3.6E; M1=0.99) demonstrating that the increase in unfolded proteins was ER specific, and indeed signified ER stress. Further supporting an increase in UPR activation there was also an increase in KDEL after 24 hours of HIHG treatment but examining ER stress and UPR activation at 4 hours showed no increase in KDEL or ER stress (Fig. 3.6A, C and D), demonstrating that ER stress and UPR activation in response to HIHG treatment increased later, between 4 and 24 hours. Examining the individual branches of the UPR confirmed that also ATF6 and pPERK activation in response to HIHG was apparent only at 24 hours (Fig. 3.6B) however, interestingly, pIRE1 activation was increased in response to HIHG treatment at 2, 6 and 24 hours (Fig. 3.6B), and peIf2α showed an initial increase after 2 hours, no difference compared to control after 6 hours and a decrease after 24 hours of HIHG treatment (Fig. 3.6B).

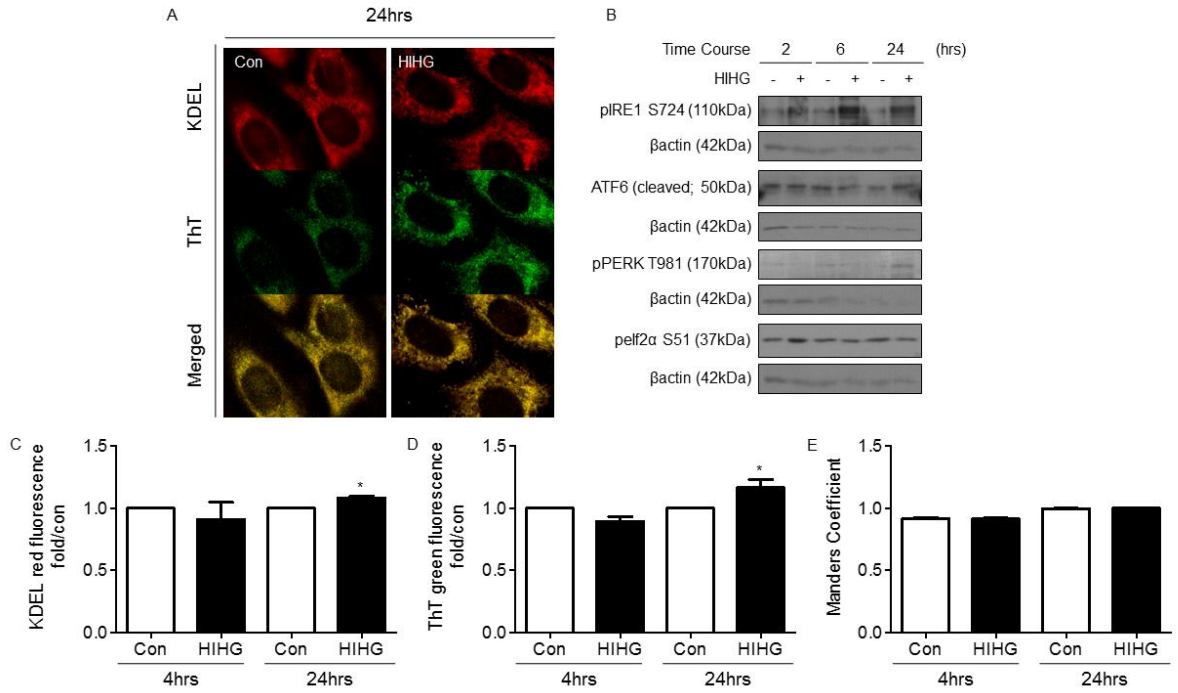

Figure 3.6. ER stress is increased in response to 24 but not 4 hours of HIHG treatment.
(A and C-E) L6 MB were grown on coverslips to 70% confluency in 12-well cell culture plates in 10% FBS AMEM, starved in 0.5% FBS AMEM for three hours before the 4 or 24 hours HIHG treatment. ThT-KDEL co-immunofluorescence assay was performed and 5-9 images per condition was taken by fluorescence confocal microscopy. Representative images of 24 hours HIHG treatment are shown (A) and quantification of total fluorescence/cells is represented as fold over control (C and D; n=4) with standard error of mean displayed as error bars.
(B) L6 WT MB were differentiated into MT in 6-well cell culture plates in 2% FBS AMEM, starved in 0.5% FBS AMEM for three hours before 2, 6 and 24 hours HIHG treatment. Upon completion of treatments cell lysates were prepared and protein content analyzed by western blotting. Representative blots are shown (B; n=3).
ThT assay showed increased levels of unfolded proteins at 24 but not 4 hours of HIHG treatment (A, D; p=0.0024) and KDEL was similarly increased at 24 but not 4 hours in response to HIHG treatment (C; p=0.002). Manders Coefficient analysis of co-localization of ThT to KDEL fluorescence (M1) showed that the increase in unfolded proteins was ER specific (E; M1=0.99 for 24 hours and 0.92 for 4 hours). Assessment of UPR signaling proteins in response to 2, 6 and 24 hours of HIHG treatment showed that pIRE1 is gradually increased at 2, 6 and 24 hours while ATF6 and pPERK were increased only at 24 hours (B). pelf2α increased at 2 hours, showed no difference at 6 hours, and decreased at 24 hours in HIHG compared to control condition (B).
**P < 0.05.*

3.1.4 HIHG Increased Oxidative Stress

I investigated whether oxidative stress was induced in response to HIHG treatment, and using CellRox Green for detection of intracellular ROS, I showed that there was an increase in ROS accumulation in response to 24 hours of HIHG treatment (Fig. 3.7A and B). Interestingly, catalase activity was also increased (Fig. 3.7C), however the inability of the increased antioxidant response to mitigate ROS production, leading to ROS accumulation, support that HIHG treatment increased oxidative stress.

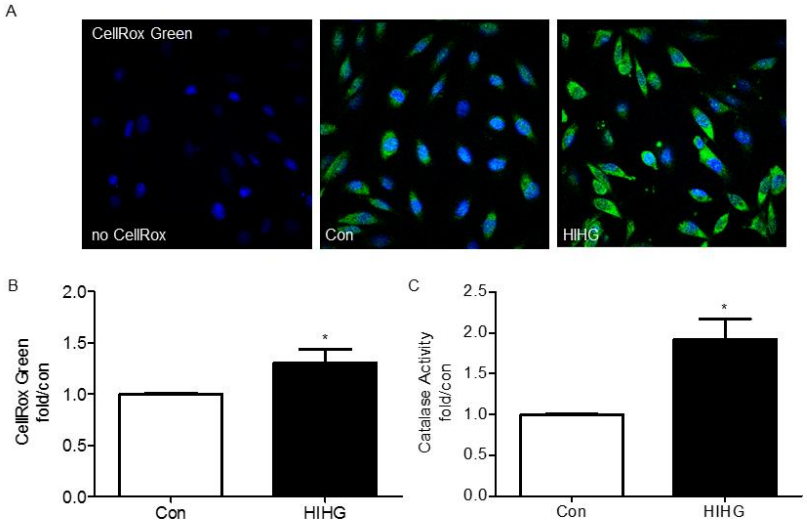

Figure 3.7. Oxidative stress was increased in insulin resistant skeletal muscle cells.
(A-B) WT L6 MB were grown on coverslips to 70% confluency in 6-well cell culture plates in 10% FBS AMEM, starved in 0.5% FBS AMEM for three hours before the 24 hours HIHG treatment. Upon completion of treatment CellRox Green assay was performed and 9-12 images per condition was taken by fluorescence confocal microscopy. Representative images are shown (A; n=3) and quantification of total green fluorescence/cell is represented as mean fold over control (B; n=3) with standard error of mean displayed as error bars.
(C) L6 WT MB were grown in in 96-well cell culture plates in 10% FBS AMEM, starved in 0.5% FBS AMEM for three hours before the 24 hours HIHG treatment. Upon completion of treatment catalase activity was determined and represented as mean fold over control (C; n=3) with standard error of mean displayed as error bars.
HIHG increased ROS (A and B; p=0.0464) and catalase activity (C; p=0.0106) compared to control.
**Significantly different compared to control. *P<0.05.*

3.2 Investigating the Insulin Sensitizing Action of Adiponectin in Skeletal Muscle Insulin Resistance

To examine the effect of adiponectin in skeletal muscle insulin resistance I treated L6 cells with adiponectin in control and HIHG condition and assessed changes in insulin signaling, autophagy, ER stress and the UPR response.

3.2.1 Adiponectin Restored Autophagy and Improved Insulin Sensitivity in HIHG Treated Cells

I first confirmed the insulin sensitizing effect of adiponectin by looking at AKT phosphorylation in HIHG condition with or without adiponectin treatment, demonstrating an increase in insulin stimulated AKT phosphorylation with adiponectin compared to HIHG treatment alone (Fig. 3.8F and E). I further showed that adiponectin directly restored the impaired autophagy seen in response to HIHG treatment, supported by increased LC3II protein, TFLC3 puncta and red/green fluorescence with adiponectin treatment in HIHG condition (Fig. 3.8A, B, C and D).

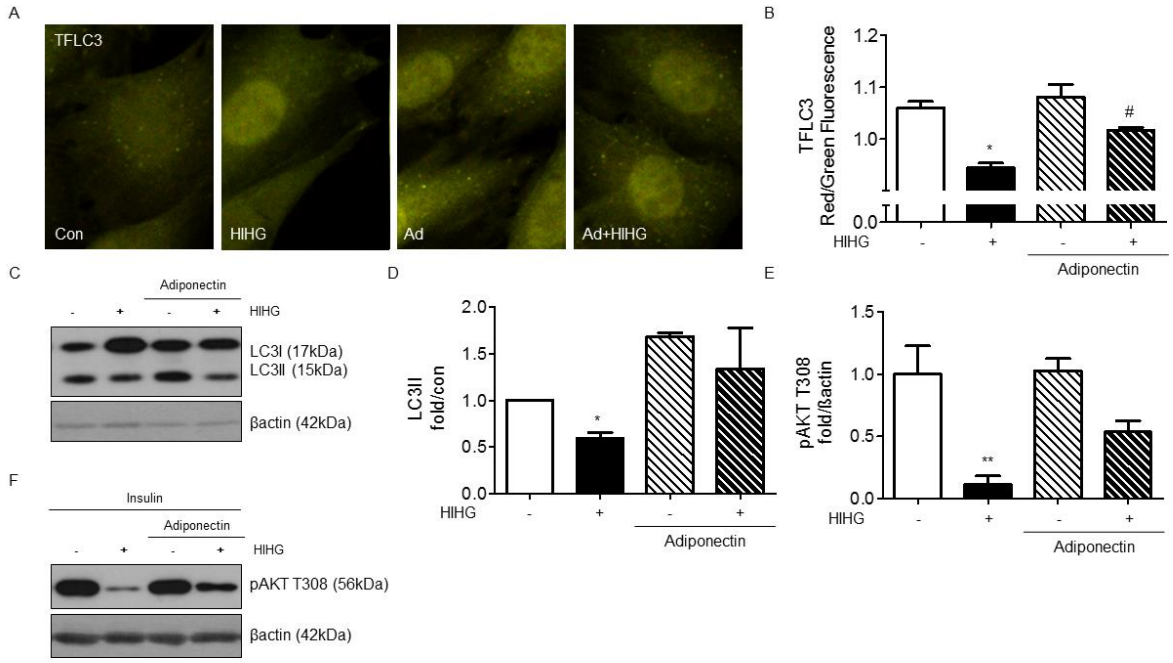

Figure 3.8. Adiponectin increased AKT phosphorylation and autophagy in insulin resistant skeletal muscle cells.
(A-B) TFLC3 L6 MB were grown on coverslips to 70% confluency in 12-well cell culture plates in 10% FBS AMEM, starved in 0.5% FBS AMEM for three hours before 24 hours HIHG treatment ± one hour adiponectin pre-treatment. TFLC3 L6 MB were fixed upon completion of treatment and 5-9 images per condition were taken by fluorescence confocal microscopy. Representative images are shown (A; n=4) and quantification of TFLC3 total red/green fluorescence is represented as mean values (C; n=4) with standard error of mean displayed as error bars.
(C-F) L6 WT MB were differentiated into MT in 6-well cell culture plates in 2% FBS AMEM, starved in 0.5% FBS AMEM for three hours before 24 hours HIHG treatment ± one hour adiponectin pre-treatment. Upon completion of treatments, cells were stimulated with 100nM of insulin for 5 minutes to examine pAKT, cell lysates were subsequently prepared and protein content analyzed by western blotting. Representative blots are shown (C and F) and quantification of band densitometry is represented as fold over control (D and E; n=3-4) with standard error of mean displayed as error bars.
Adiponectin treatment increased TFLC3 puncta (A), red/green fluorescence (B; p=0.0001) and LC3II (C and D; p=0.0172) in HIHG condition. Further, adiponectin also increased insulin stimulated AKT phosphorylation (E; p=0.0043 and F) in HIHG condition.

3.2.2 Adiponectin did not Increase Autophagy or Improve Insulin Sensitivity in HIHG Treated EV or Atg5K Cells

To examine if restoring autophagy was imperative for improving insulin sensitivity I compared insulin stimulated AKT phosphorylation in autophagy deficient Atg5K cells to empty vector control (EV) cells in HIHG condition with or without adiponectin treatment. There was a decrease in pAKT in Atg5K compared to EV in control condition, with a further decrease caused by HIHG treatment in both EV and Atg5K cells, but no significant increase in response to adiponectin treatment in EV or Atg5K cells (Fig. 3.9A and D). Interestingly, however, HIHG treatment of EV cells increased LC3II, in direct contrast with the response observed in wild type (WT) cells, and adiponectin was unable to significantly increase LC3II further in HIHG conditions in EV cells (Fig. 3.9C and F). There was however an increasing trend for both LC3II and pAKT in response to adiponectin in HIHG condition in EV cells. HIHG treatment in Atg5K cells increased pmTOR which was reduced to control levels by adiponectin treatment (Fig. 3.9B and E), and as expected, LC3II was decreased in Atg5K compared to EV cells in both control and HIHG conditions (Fig. 3.9C and F).

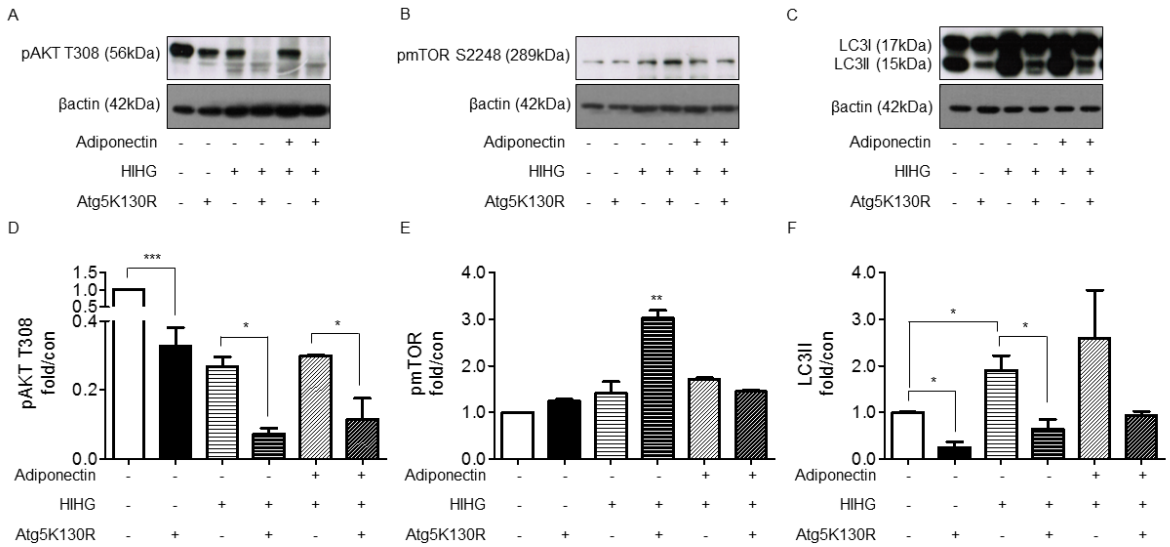

Figure 3.9 Analysis of autophagy and insulin signaling in EV and Atg5K cells and regulation by adiponectin.
L6 EV and Atg5K MB were grown to 100% confluence in 6-well cell culture plates in 10% FBS AMEM, starved in 0.5% FBS AMEM for three hours before 24 hours HIHG treatment ± one hour adiponectin pre-treatment. Upon completion of treatments, cell lysates were prepared and protein content analyzed by western blotting. Representative blots are shown (A-C) and quantification of band densitometry is represented as fold over control (D-F; n=2) with standard error of mean displayed as error bars.
There was a decrease in pAKT in Atg5K compared to EV cells, HIHG treatment reduced pAKT in both EV and Atg5K cells and no increase was seen with adiponectin treatment in either cell type (A and D; $p<0.0001$). HIHG treatment in Atg5K cells increased pmTOR, which was decreased by adiponectin treatment (B and E; $p=0.0020$). LC3II levels were decreased in Atg5K compared to EV cells both in control and HIHG conditions, and HIHG increased LC3II in EV but not Atg5K cells (C and F; $p=0.033$).

3.2.3 Adiponectin Alleviated ER Stress in WT and EV but not Atg5K Cells

Next I examined the effect of adiponectin on ER stress and demonstrated that adiponectin decreased ER stress in HIHG condition as measured by ThT green fluorescence (Fig. 3.10A and C) and increased UPR activation in both control and HIHG condition, as measured by GRP78mCherry red fluorescence (Fig. 3.10B). Activation of pIRE1 and pPERK was unchanged in both control and HIHG conditions (Fig. 3.10F, D and H), while ATF6 was decreased in HIHG conditions in response to adiponectin treatment (Fig. 10F and G). Further, adiponectin treatment resulted in a decreased trend in control conditions and an increased trend in HIHG conditions of peIf2α levels (Fig. 10F and E).

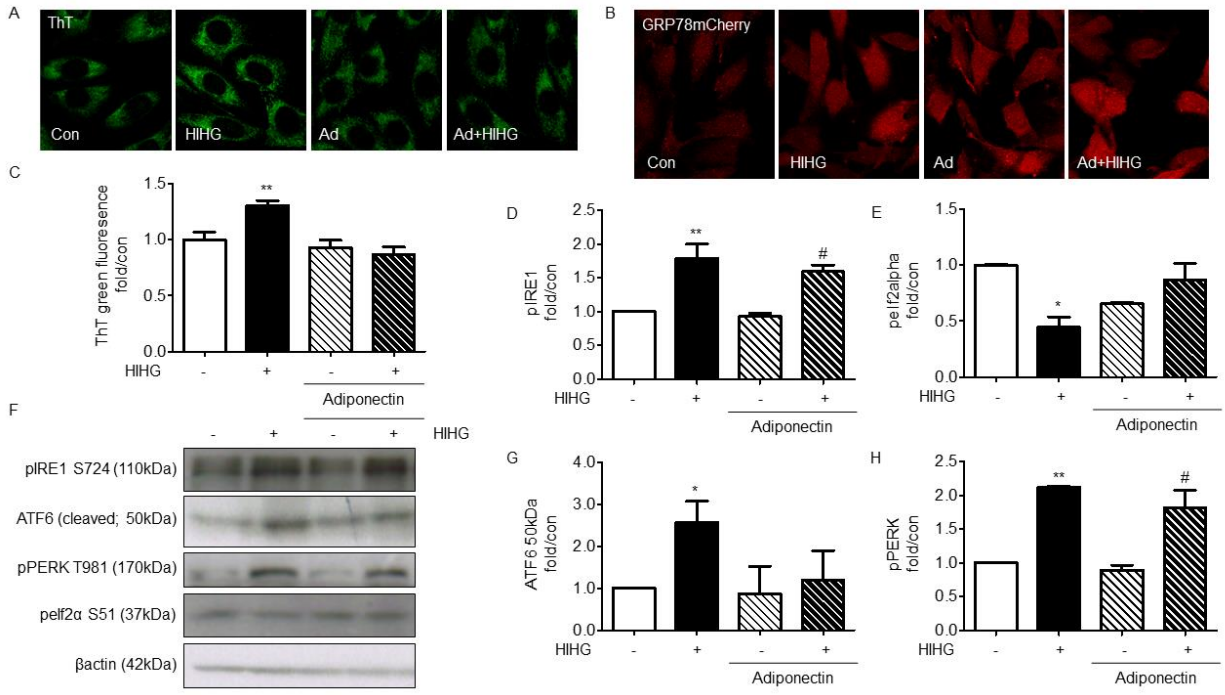

Figure 3.10. Adiponectin stimulated UPR activation and alleviated ER stress in insulin resistant skeletal muscle cells.
(A-C) GRP78mCherry and WT L6 MB were grown on coverslips to 70% confluency in 12-well cell culture plates in 10% FBS AMEM, starved in 0.5% FBS AMEM for three hours before the 24 hours HIHG treatment ± one hour adiponectin pre-treatment. GRP78mCherry L6 MB were fixed upon completion of treatment and ThT assay was performed on WT L6 MB; 5-9 images per condition was taken by fluorescence confocal microscopy. Representative images are shown (A and B; n=3) and quantification of ThT green fluorescence/cell is represented as mean values (C; n=3) with standard error of mean displayed as error bars.
(D-H) L6 WT MB were differentiated into MT in 6-well cell culture plates in 2% FBS AMEM, starved in 0.5% FBS AMEM for three hours before the 24 hours HIHG treatment ± one hour adiponectin pre-treatment. Upon completion of treatments, cell lysates were prepared and protein content analyzed by western blotting. Representative blots are shown (F) and quantification of band densitometry is represented as fold over control (D, E, G and H; n=4-5) with standard error of mean displayed as error bars.
*Adiponectin decreased ThT green fluorescence in HIHG condition (A and C; p=0.0001) and increased GRP78mCherry red fluorescence in both control and HIHG condition (B). Adiponectin pre-treatment did not change pIRE1 (F and D; p=0.0021) or pPERK (F and H; p=0.0005, but reduced ATF6 (F and G; p=0.0454H) and increased pelf2α in HIHG condition (F and E; p=0.0397). *P < 0.05; **P < 0.01.*
*(C) **Significant difference compared to Con, Ad and Ad+HIHG. (p=0.0001)*
*(D) **/#Significant difference compared to Con and Ad+HIHG treatment. (p=0.0021)*
*(E) *Significant difference compared to Con, Ad and Ad+HIHG. (p=0.0397)*
*(G) *Significant difference compared to Con. (p=0.0454)*
*(H) **/#Significant difference compared to Con and Ad. (p=0.0325)*

To test if the increase in autophagy, stimulated by adiponectin in HIHG condition, mediated the adiponectin mediated reduction in ER stress I assessed the ability of adiponectin to alleviate ER stress in Atg5K cells compared to EV cells (Fig. 3.11). Adiponectin reduced ER stress in both control and HIHG conditions in EV cells, but not in Atg5K cells (Fig. 3.11A, B, D and E), however there was a decreased trend in ER stress in response to adiponectin treatment in both control and HIHG condition also in Atg5K cells ($p=0.1044$).

Further I examined the regulation of UPR signaling proteins in EV and Atg5K cells; in EV cells HIHG treatment caused an increase in ATF6, demonstrating similar levels of ATF6 as was seen for Atg5K cells in control conditions but there was no further increase in ATF6 in Atg5K cells with HIHG treatment (Fig. 3.11C and F). Although there was no significant change in pPERK in Atg5K or EV cells with HIHG or adiponectin treatment (Fig. 3.11C and G), peIf2α was increased in Atg5K cells compared to EV cells and by HIHG treatment in both EV and Atg5K cells but there was no change with adiponectin treatment (Fig. 3.11C and H).

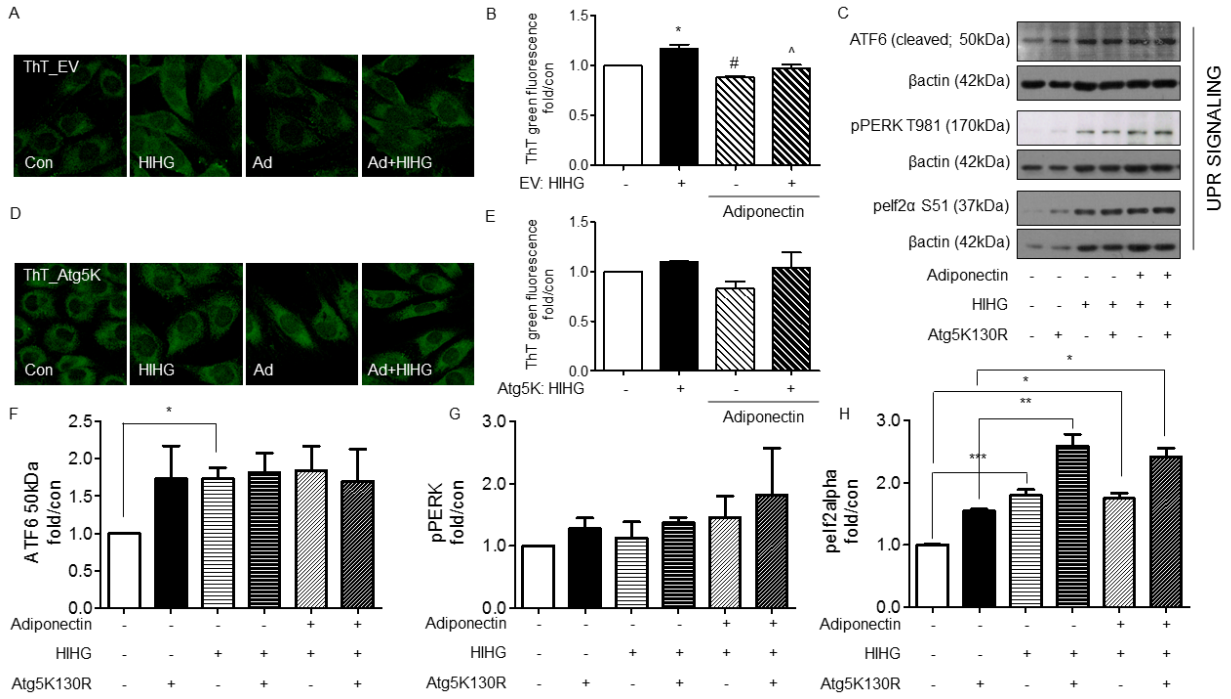

Figure 3.11. ER stress is alleviated by adiponectin in EV but not Atg5K cells.
(A-B and D-E) L6 EV and Atg5K MB were grown on coverslips to 70% confluency in 12-well cell culture plates in 10% FBS AMEM, starved in 0.5% FBS AMEM for three hours before the 24 hours HIHG treatment ± one hour adiponectin pre-treatment. ThT assay was performed and 5-9 images per condition was taken by fluorescence confocal microscopy. Representative images are shown (A) and quantification of total fluorescence/cells is represented as fold over control (B and C; n=3) with standard error of mean displayed as error bars.
(C, F-H) L6 EV and Atg5K MB were grown to 100% confluence in 6-well cell culture plates in 10% FBS AMEM, starved in 0.5% FBS AMEM for three hours before the 24 hours HIHG treatment ± one hour adiponectin pre-treatment. Upon completion of treatments, cell lysates were prepared and protein content analyzed by western blotting. Representative blots are shown (C) and quantification of band densitometry is represented as fold over control (F-H; n=2) with standard error of mean displayed as error bars.
*Adiponectin decreased ER stress in EV (A and B; p=0.0011) but not in Atg5K cells (D and E; p=0.1044). There is no difference in ATF6 and pPERK for any treatments in EV or Atg5K cells (C, F; p=0.4686 and G; p=0.7023), but pairwise comparison indicate that HIHG increased ATF6 in EV cells (C and F; p=0.0192). HIHG increased pelf2α in both EV and Atg5K cells, but there was no change with adiponectin treatment (C and H; p=0.0005). *P < 0.05; **P < 0.01.*

3.3 Examining the Relationship between Autophagy, ER Stress, UPR Signaling, Oxidative Stress and Skeletal Muscle Insulin Resistance

3.3.1 Blocking Autophagy with Bafilomycin Caused ER Stress and Insulin Resistance

To further examine the influence of autophagy on cellular processes implicated in insulin resistance I treated L6 cells with bafilomycin, a known autophagy inhibitor. I first confirmed that bafilomycin treatment inhibited autophagy, and although there was an increase in LC3II in response to bafilomycin (Fig. 3.12D and E), this increase corresponded to an accumulation of autophagosomes (Fig. 3.12A), and assessing TFLC3 red/green fluorescence demonstrated that autophagic flux was decreased in response to bafilomycin treatment (Fig. 3.12A and C). Further, decreased autophagic flux was accompanied with increased lysosomal activity (Fig. 3.12B).

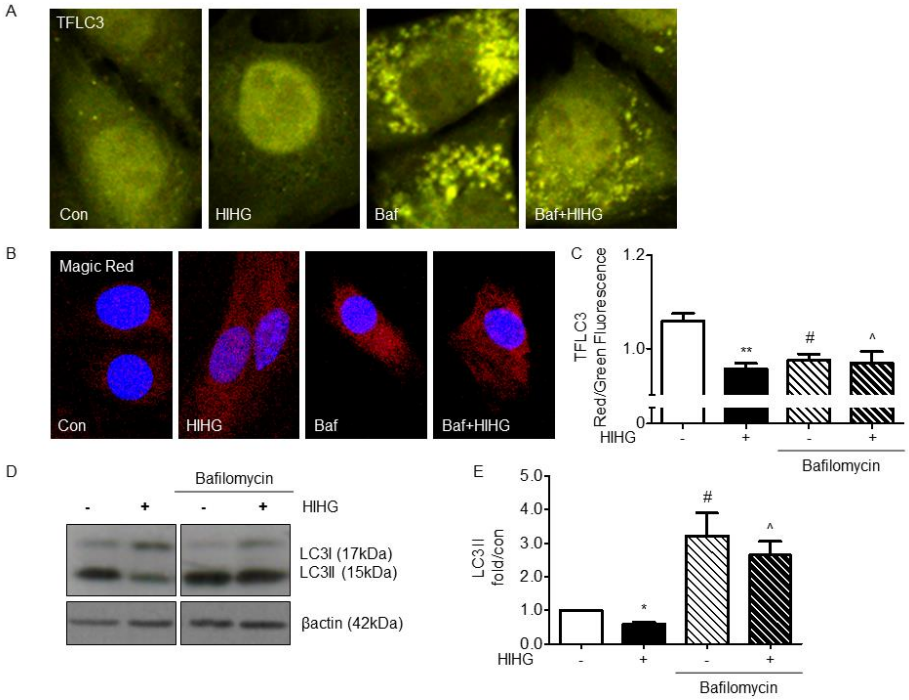

Figure 3.12. Bafilomycin treatment decreased autophagy.
(A-C) TFLC3 and WT L6 MB were grown on coverslips to 70% confluency in 12-well cell culture plates in 10% FBS AMEM, starved in 0.5% FBS AMEM for three hours before 24 hours HIHG treatment ± one hour bafilomycin pre-treatment. TFLC3 L6 MB were fixed upon completion of treatment and MagicRed assay was performed on WT L6 MB; 5-9 images per condition was taken by fluorescence confocal microscopy. Representative images are shown (A and B; n=3-4) and quantification of TFLC3 total red/green fluorescence is represented as mean values (C; n=4) with standard error of mean displayed as error bars.
(D and E) L6 WT MB were differentiated into MT in 6-well cell culture plates in 2% FBS AMEM, starved in 0.5% FBS AMEM for three hours before the 24 hours HIHG treatment ± one hour bafilomycin pre-treatment. Upon completion of treatments, cell lysates were prepared and protein content analyzed by western blotting. Representative blots are shown (D) and quantification of band densitometry is represented as fold over control (E; n=4) with standard error of mean displayed as error bars.
Bafilomycin treatment decreased TFLC3 red/green fluorescence in both control and HIHG conditions (A and C, p=0.0043) but increased TFLC3 puncta accumulation (A) and LC3II (D and E, p=0.0125). Lysosomal activity increased in response to bafilomycin treatment (B).
*(C) **/#/^ Significant difference compared to control.*
*(E) * Significant difference compared to control, Baf and Baf+HIHG treatment. #/^ Significant difference compared to control and HIHG. *P < 0.05; **P < 0.01.*
For uncut blots see Appendix A, Supplementary Figure 1.

I then looked at the functional significance of impaired autophagy in the context of insulin resistance and its regulation of cellular processes involved. I demonstrated that bafilomycin treatment was associated with increased ER stress (Fig. 3.13A and C), and further that bafilomycin caused a decrease in insulin stimulated AKT phosphorylation (Fig. 3.13B and E).

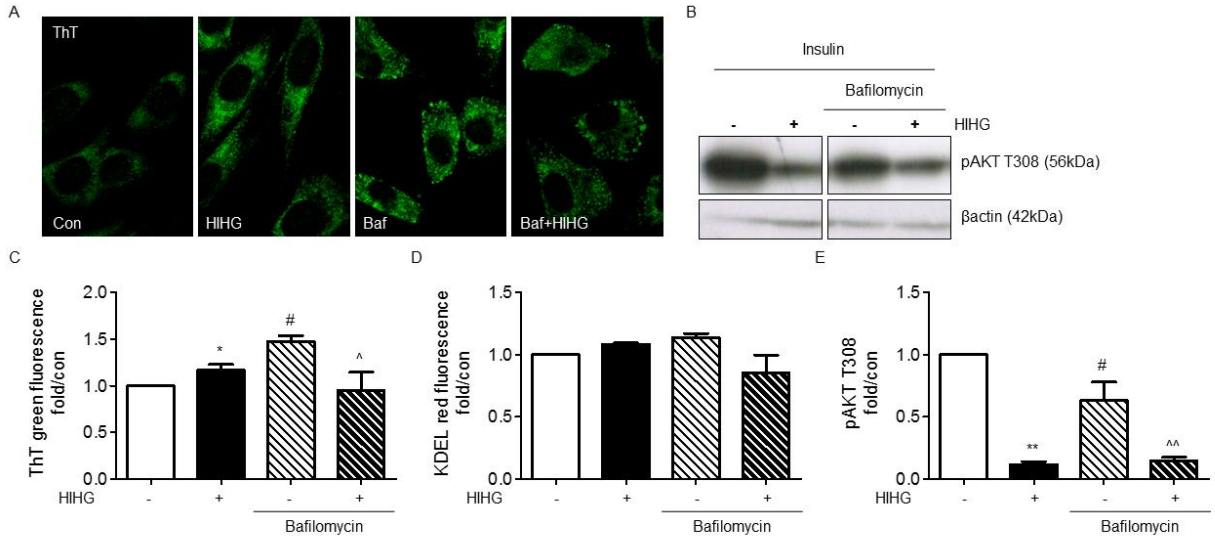

Figure 3.13. Inhibiting autophagy with bafilomycin treatment increased ER stress and decreased AKT phosphorylation.
(A, C and D) L6 MB were grown on coverslips to 70% confluency in 12-well cell culture plates in 10% FBS AMEM, starved in 0.5% FBS AMEM for three hours before 24 hours HIHG treatment ± one hour bafilomycin pre-treatment. ThT-KDEL co-immunofluorescence assay was performed and 5-9 images per condition was taken by fluorescence confocal microscopy. Representative images of ThT are shown (A) and quantification of total fluorescence/cells is represented as fold over control (C and D; n=4) with standard error of mean displayed as error bars.
(B and E) L6 WT MB were differentiated into MT in 6-well cell culture plates in 2% FBS AMEM, starved in 0.5% FBS AMEM for three hours before the 24 hours HIHG treatment ± one hour bafilomycin pre-treatment. Upon completion of treatments cells were stimulated with 100nM of insulin for 5 minutes, cell lysates were subsequently prepared and protein content analyzed by western blotting. Representative blots are shown (B) and quantification of band densitometry is represented as fold over control (E; n=4) with standard error of mean displayed as error bars.
Bafilomycin treatment increased ER stress (A and C; p=0.0208). KDEL immunofluorescence however did not show any difference with bafilomycin treatment (D; p=0.1391). Bafilomycin decreased AKT phosphorylation in both control and HIHG conditions (B and E; p<0.0001).
*(C) *Significant difference compared to control. #Significant difference compared to control and HIHG treatment.*

*(E) *Significant difference compared to control. #Significant difference compared to control, HIHG and Baf+HIHG treatment. ^Significant difference compared to control and Baf treatment. *P < 0.05; **P < 0.01.*
For uncut blots see Appendix A, Supplementary Figure 1.

3.3.2 Rapamycin Treatment Reduced ER Stress in EV but not in Atg5K Cells

After establishing that bafilomycin caused ER stress and insulin resistance, I wanted to determine whether inducing autophagy by rapamycin, a known pmTOR inhibitor and autophagy stimulator, could alleviate ER stress and insulin resistance induced by HIHG treatment. I first confirmed that rapamycin treatment induced autophagy, demonstrated by the increased TFLC3 red/green fluorescence ratio in response to rapamycin in control condition and further that rapamycin treatment restored autophagy in HIHG treated cells (Fig. 3.14A and B). Rapamycin also alleviated ER stress in EV cells treated with HIHG (Fig. 3.14C and E), however in Atg5K cells there was no significant reduction in ER stress in HIHG condition by rapamycin treatment (Fig. 3.14D and F).

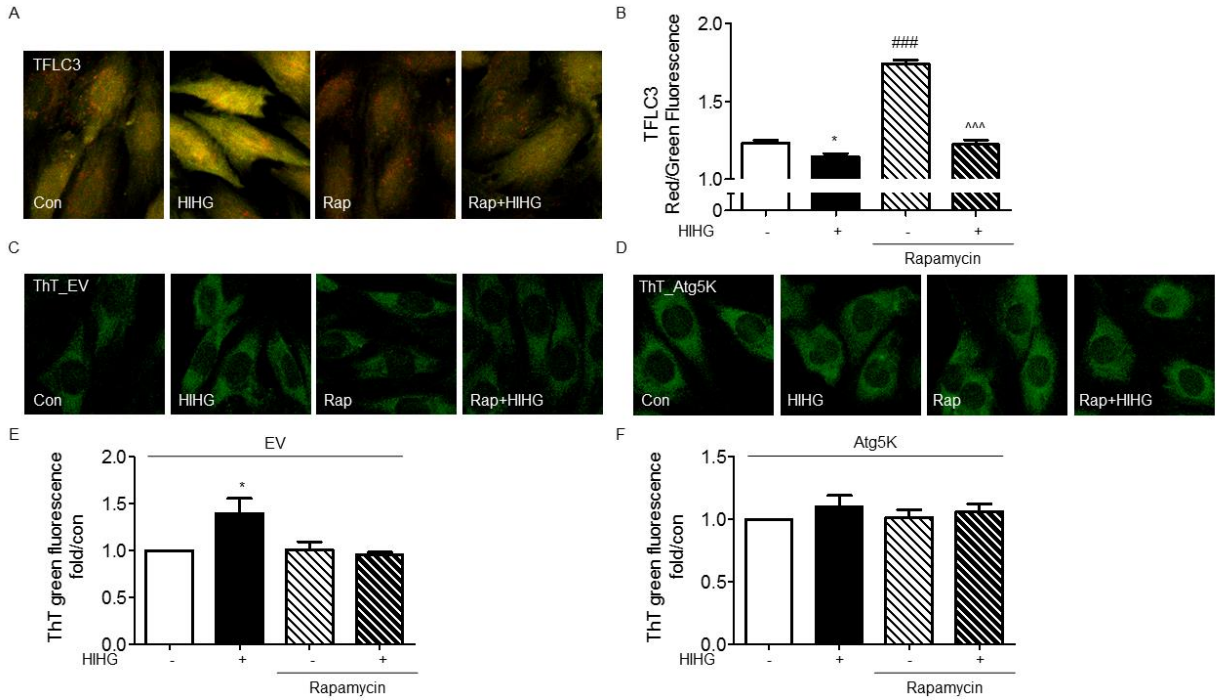

Figure 3.14. Rapamycin treatment increased autophagic flux and decreased HIHG induced ER stress in EV but not Atg5K cells.
TFLC3, EV and Atg5K L6 MB were grown on coverslips to 70% confluency in 12-well cell culture plates in 10% FBS AMEM, starved in 0.5% FBS AMEM for three hours before 24 hours HIHG treatment ± one hour rapamycin pre-treatment. TFLC3 L6 MB were fixed upon completion of treatment and ThT assay was performed on EV and Atg5K L6 MB; 5-9 images per condition was taken by fluorescence confocal microscopy. Representative images are shown (A, C and D) and quantification of total fluorescence/cells is represented as fold over control (B, E and F; n=4) with standard error of mean displayed as error bars.
Rapamycin stimulated autophagic flux in both control and HIHG conditions (A and B; $p<0.0001$). ER stress was reduced by rapamycin in HIHG condition in EV cells (C and E; $p=0.0177$) but not in Atg5K cells (D and F; $p=0.6669$).
*(B) *Significant difference compared to control and Rap treatments. ###Significant difference compared to control, HIHG, Rap+HIHG. ^^^Significant difference compared to control and Rap treatments.*
*(E) *Significant difference compared to control, Rap and Rap+HIHG. *$P < 0.05$; **$P < 0.0$; ***$P < 0.001$.*

To examine the effect of rapamycin treatment on proteins involved in autophagy, insulin signaling and the UPR response in HIHG condition, and to confirm that responses were caused by the autophagy stimulating effect of rapamycin, I examined protein expression in HIHG condition in EV and Atg5k cells, with or without rapamycin treatment. These results surprisingly showed that rapamycin reduced pmTOR phosphorylation in Atg5K but not EV cells (Fig. 3.15A and B) and similarly that rapamycin increased AKT phosphorylation in Atg5K but not in EV cells (Fig. 3.15A and D). Although there was an increased trend in LC3II in EV cells with rapamycin treatment, this increase was not significant (Fig. 3.15A and C). I also examined pPERK and peIf2α which were decreased by rapamycin treatment in Atg5K cells (Fig. 3.15A, F and G), there was also a decreased trend in ATG6, although this reduction was not significant (Fig. 3.15A and E). These proteins were not altered in EV cells by rapamycin treatment in HIHG condition (Fig. 3.15A, E, F and G).

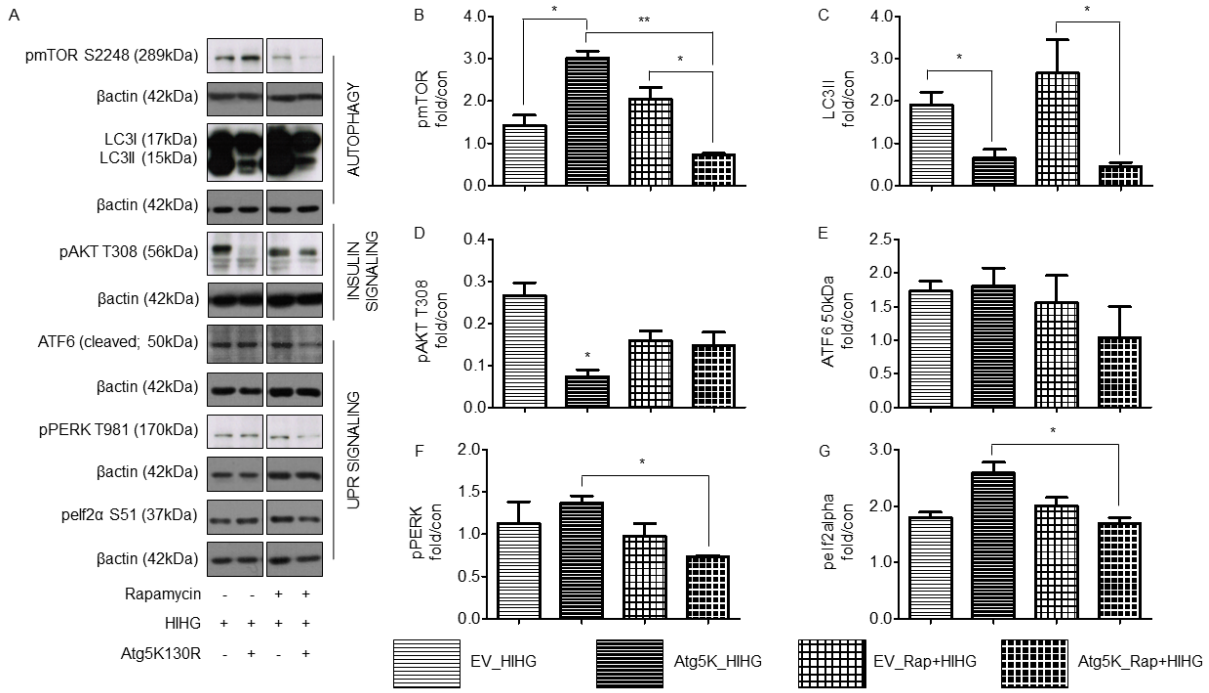

Figure 3.15. Regulation of proteins involved in the UPR response, insulin signaling and autophagy by rapamycin in EV and Atg5K cells.
L6 EV and Atg5K MB were grown to 100% confluence in 6-well cell culture plates in 10% FBS AMEM, starved in 0.5% FBS AMEM for three hours before 24 hours HIHG treatment ± one hour rapamycin pre-treatment. Upon completion of treatments, cell lysates were prepared and protein content analyzed by western blotting. Representative blots are shown (A) and quantification of band densitometry is represented as fold over control (B-G; n=2) with standard error of mean displayed as error bars.
*Rapamycin reduced pmTOR in Atg5K but not EV cells (B; p=0.0057) however no significant increase in LC3II was seen in response to rapamycin treatment in either EV or Atg5K cells, although LC3II showed an increased trend in EV cells (C; p=0.0616). In Atg5K cells there is less pAKT than in EV cells in HIHG conditions, and in EV cells rapamycin treatment lowered pAKT but increased it in Atg5K cells (D; p=0.0288). Rapamycin did not change the levels of ATF6 (E; p=0.4710) or pPERK (F; p=0.1580), although individual analysis of each cell type suggest that rapamycin decreased pPERK in Atg5K cells (F; p=0.0082) and similarly rapamycin decreased pelf2α in Atg5K cells (G; p=0.0339). *P < 0.05; **P < 0.01.*
For uncut blots see Appendix A, Supplementary Figure 2.

3.3.3 Salubrinal Treatment Reduced ER Stress and Increased Autophagy

Salubrinal is a known inhibitor of ER stress and specifically inhibits dephosphorylation of peIf2α leading to increased levels of peIf2α keeping the UPR response active. As expected, peIf2α was increased in response to salubrinal treatment in HIHG condition, however there was no significant increase in control (Fig. 3.16A and E). I confirmed that salubrinal reduced ER stress, both in control and HIHG condition (Fig. 3.16F and G), and demonstrated that ATF6, pPERK, and pIRE1 was not changed in control, but decreased in HIHG conditions (Fig. 3.16A, B, C and D).

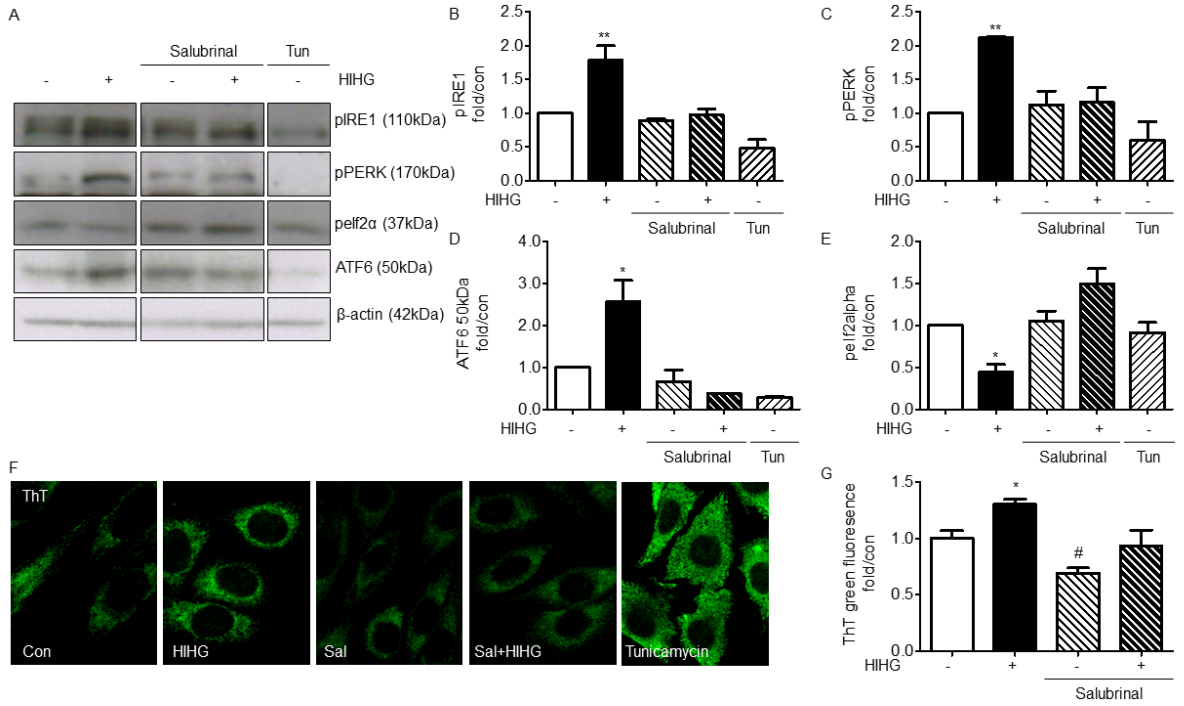

Figure 3.16. Salubrinal decreased ER stress and UPR activation in insulin resistant skeletal muscle cells.

(A-E) L6 WT MB were differentiated into MT in 6-well cell culture plates in 2% FBS AMEM, starved in 0.5% FBS AMEM for three hours before the 24 hours HIHG treatment ± one hour salubrinal, or tunicamycin pre-treatment. Upon completion of treatments, cell lysates were prepared and protein content analyzed by western blotting. Representative blots are shown (A) and quantification of band densitometry is represented as fold over control (B-E; n=3-4) with standard error of mean displayed as error bars.

(F and G) L6 MB were grown on coverslips to 70% confluency in 12-well cell culture plates in 10% FBS AMEM, starved in 0.5% FBS AMEM for three hours before the 24 hours HIHG treatment ± one hour salubrinal pre-treatment. ThT assay was performed and 5-9 images per condition was taken by fluorescence confocal microscopy. Representative images are shown (F) and quantification of total fluorescence/cells is represented as fold over control (G; n=4) with standard error of mean displayed as error bars.

Salubrinal treatment decreased ER stress in both control and HIHG conditions while tunicamycin increased ER stress (F and G; P<0.001). pelf2α was increased by salubrinal (A and E; p=0.0140). pIRE1, ATF6 and pPERK were increased by HIHG treatment and reduced by salubrinal treatment (A, B; p=0.0002, C; p=0.0021, D; p=0.0074).

*(B,C) **Significant difference compared to control, Sal, Sal+HIHG and Tun. (p=0.0002, p=0.0021)*

*(D) *Significant difference compared to control, Sal, Sal+HIHG and Tun. (p=0.0074)*

*(E) *Significant difference compared to control and Sal+HIHG. (p=0.0140)*

(G) Significant difference compared to control, Sal and Sal+HIHG. # Significant difference compared to control and HIHG treatment. (p<0.0001)*

**P < 0.05; **P < 0.01.*

For uncut blots see Appendix A, Supplementary Figure 1.

Investigating the effect of salubrinal treatment on autophagy I showed increased TFLC3 red/green fluorescence in both control and HIHG conditions (Fig. 3.17A and B), and increased autophagosome formation, based on increased TFLC3 puncta (Fig. 3.17A) and LC3II (Fig. 3.17C and D). Salubrinal also decreased lysosomal activity in both control and HIHG conditions (Fig. 3.17E).

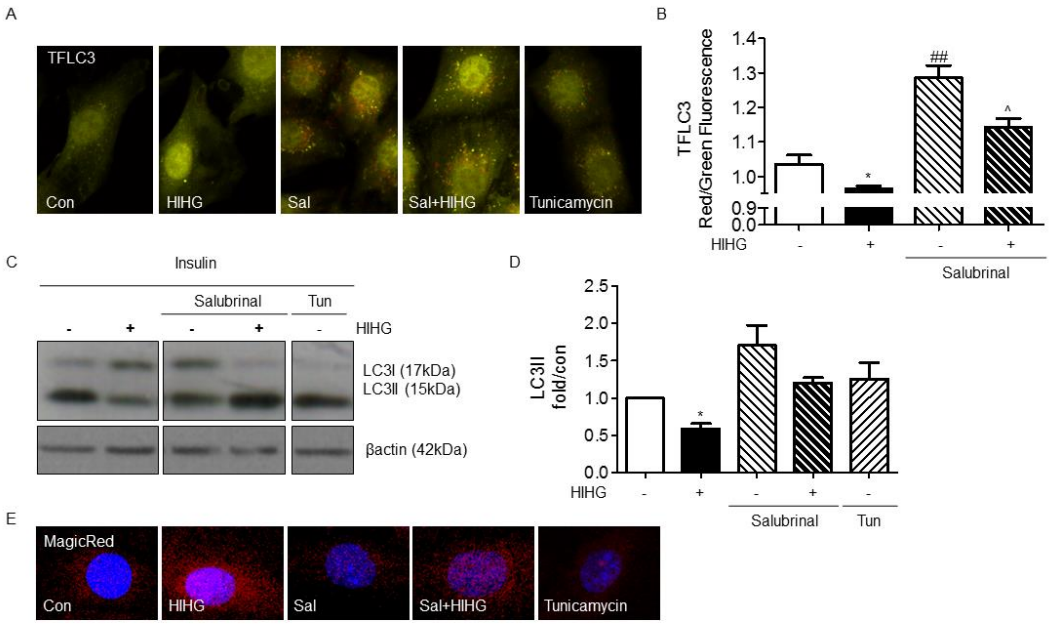

Figure 3.17. Salubrinal increased autophagy.
(A, B and E) TFLC3 and WT L6 MB were grown on coverslips to 70% confluency in 12-well cell culture plates in 10% FBS AMEM, starved in 0.5% FBS AMEM for three hours before the 24 hours HIHG treatment ± one hour salubrinal pre-treatment. TFLC3 L6 MB were fixed upon completion of treatment and MagicRed assay was performed on WT L6 MB; 5-9 images per condition was taken by fluorescence confocal microscopy. Representative images are shown (A and E; n=3-4) and quantification of TFLC3 total red/green fluorescence is represented as mean values (B; n=3) with standard error of mean displayed as error bars.
(C and D) L6 WT MB were differentiated into MT in 6-well cell culture plates in 2% FBS AMEM, starved in 0.5% FBS AMEM for three hours before the 24 hours HIHG treatment ± one hour salubrinal pre-treatment. Upon completion of treatments, cell lysates were prepared and protein content analyzed by western blotting. Representative blots are shown (D) and quantification of band densitometry is represented as fold over control (E; n=3-4) with standard error of mean displayed as error bars.
Salubrinal increased TFLC3 puncta (A), red/green fluorescence (B; p<0.0001) and LC3II levels (C and D; p=0.0243) in both control and HIHG condition and reduced lysosomal activity as measured by Cathepsin B and MagicRed assay (E). Tunicamycin also induced autophagy and reduced lysosomal activity.

*(B) *Significant difference compared to control, Sal and Sal+HIHG. ##Significant difference compared to control, HIHG and Sal+HIHG treatment. ^Significant difference compared to control, HIHG and Sal treatment.*
*(D) *Significant difference compared to control and Sal.*
**P < 0.05; **P < 0.01.*
For uncut blots see Appendix A, Supplementary Figure 1.

Inducing ER stress with tunicamycin reduced insulin stimulated AKT phosphorylation, however alleviating ER stress with salubrinal treatment did not alter AKT phosphorylation in control or HIHG conditions (Fig. 3.18A and B).

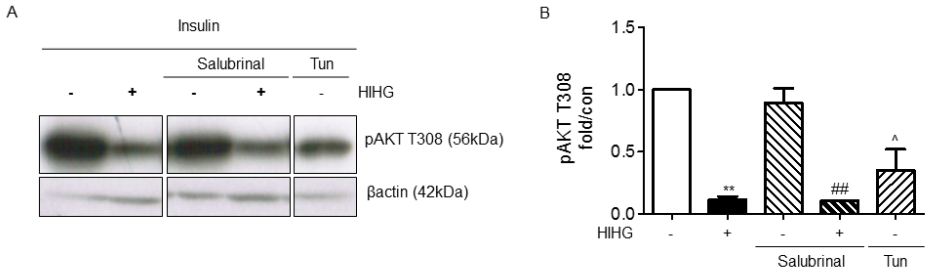

Figure 3.18. Salubrinal treatment did not alter insulin stimulated AKT phosphorylation. L6 WT MB were differentiated into MT in 6-well cell culture plates in 2% FBS AMEM, starved in 0.5% FBS AMEM for three hours before 24 hours HIHG treatment ± one hour salubrinal pre-treatment. Upon completion of treatments cells were stimulated with 100nM of insulin for 5 minutes, cell lysates were subsequently prepared and protein content analyzed by western blotting. Representative blots are shown (A) and quantification of band densitometry is represented as fold over control (B; n=3) with standard error of mean displayed as error bars. Salubrinal did not influence AKT phosphorylation in HIHG or control condition however tunicamycin decreased pAKT (A and B; p<0.0001, ANOVA, TPH).
*(B) **Significant difference compared to control and Sal treatment. ##Significant difference compared to control and Sal treatment. ^Significant difference compared to control and Sal treatment. *P < 0.05; **P.*
For uncut blots see Appendix A, Supplementary Figure 1.

3.3.4 ER Stress was Alleviated by Salubrinal in EV but not Atg5K Cells

After I showed that salubrinal decreased ER stress (Fig. 3.16) and concurrently increased autophagy (Fig. 3.17), I wanted to investigate if the reduction in ER stress was dependent on autophagy stimulation. To examine this I compared the ability of salubrinal to reduce ER stress in EV compared to Atg5K cells in HIHG condition, demonstrating that that the reduction in ER stress observed for EV cells (Fig. 3.19A and C) was not observed for Atg5K cells (Fig. 3.19B and D).

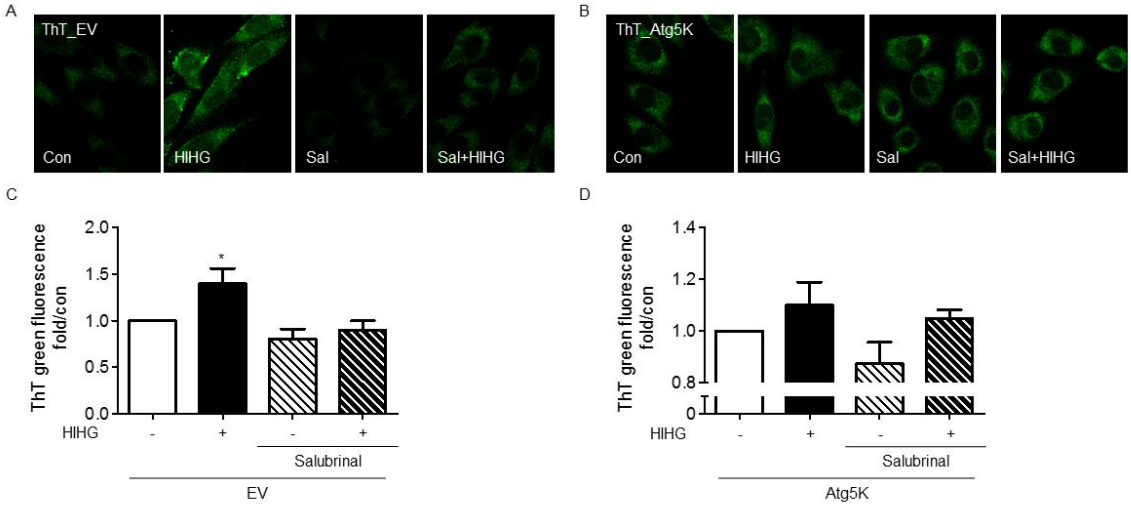

Figure 3.19. Salubrinal reduced ER stress in EV but not Atg5K cells.
L6 EV and Atg5K MB were grown on coverslips to 70% confluency in 12-well cell culture plates in 10% FBS AMEM, starved in 0.5% FBS AMEM for three hours before the 24 hours HIHG treatment ± one hour salubrinal pre-treatment. ThT assay was performed and 5-9 images per condition was taken by fluorescence confocal microscopy. Representative images are shown (A) and quantification of total fluorescence/cells is represented as fold over control (B and C; n=4) with standard error of mean displayed as error bars.
Salubrinal treatment decreased ER stress in HIHG treated EV (A and C; p=0.0147) but not ATG5K cells (B and D; p=0.1015).
*(C) *Significant difference compared to control, Sal and Sal+HIHG. *P < 0.05.*

I further went on to look at proteins involved in autophagy, insulin and UPR signaling and how they were regulated by salubrinal in HIHG condition in EV and Atg5K cells. pmTOR was unchanged in EV but decreased in Atg5K cells (Fig. 3.20A and B), LC3II was reduced in Atg5K compared to EV cells and this was not altered by salubrinal treatment (Fig. 3.20A and C). There was no change in pAKT or ATF6 in response to salubrinal treatment in EV or Atg5K cells (Fig. 3.20A, C and D). pPERK was unchanged in EV cells but showed a decreased trend ($p=0.0557$) in Atg5K cells in response to salubrinal treatment (Fig. 3.20A and F), peIf2α was decreased in Atg5K cells but unchanged in EV cells (Fig. 3.20A and G).

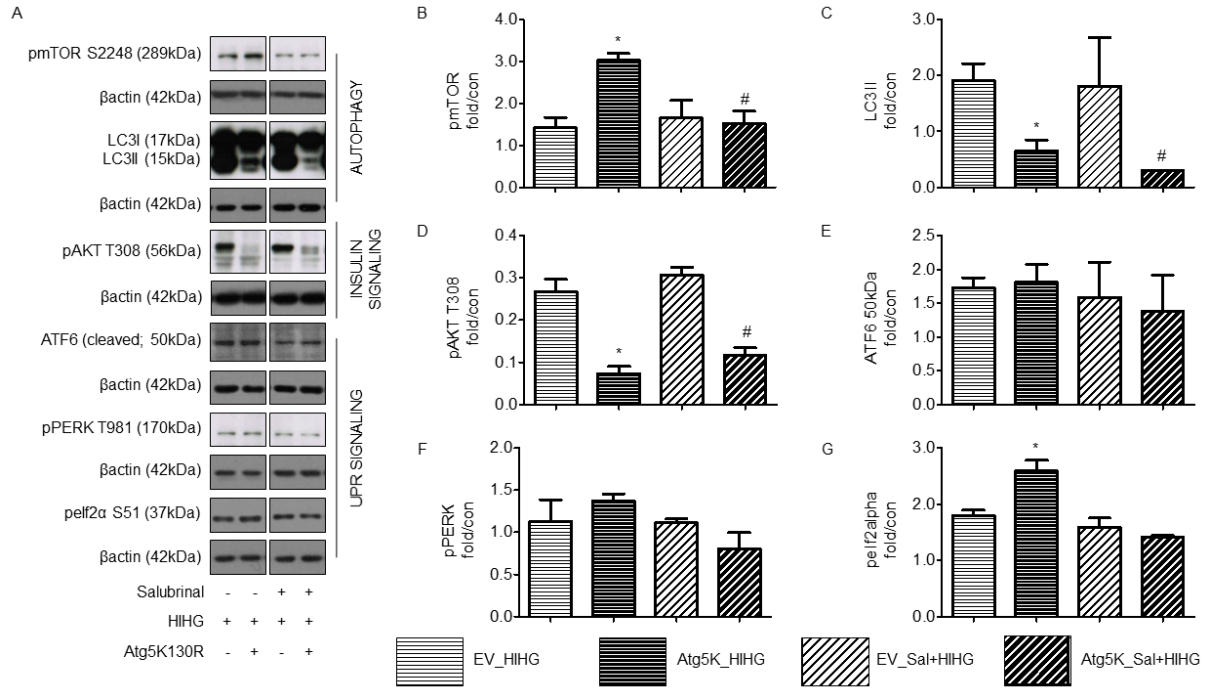

Figure 3.20. Regulation of the UPR, insulin signaling and autophagy proteins by salubrinal in EV and Atg5K cells.
L6 EV and Atg5K MB were grown to 100% confluence in 6-well cell culture plates in 10% FBS AMEM, starved in 0.5% FBS AMEM for three hours before the 24 hours HIHG treatment ± one hour salubrinal pre-treatment. Upon completion of treatments, cell lysates were prepared and protein content analyzed by western blotting. Representative blots are shown (A) and quantification of band densitometry is represented as fold over control (B-G; n=2) with standard error of mean displayed as error bars.
*Salubrinal decreased pmTOR in Atg5K but not in EV cells (B; p=0.05) however there were no increase in LC3II (C; p=0.1613) or pAKT (D; p=0.0039) in response to salubrinal treatment in either EV or Atg5K cells. Similarly salubrinal did not change ATF6 (E; p=0.8772) or pPERK (F; p=0.2648) in either EV or Atg5K cells. However peIf2α was significantly lowered with salubrinal treatment in Atg5K cells (G; p=0.0118). *P < 0.05; **P < 0.01.*
For uncut blots see Appendix A, Supplementary Figure 2.

3.3.5 Alleviating Oxidative Stress by NAC Treatment Improved Insulin Sensitivity and Restored Autophagy

To examine regulation by oxidative stress of cellular processes involved in insulin resistance I used NAC treatment, a well-established insulin sensitizer known to alleviate oxidative stress, and I confirmed that NAC had an insulin sensitizing effect as measured by its ability to improve insulin stimulated AKT phosphorylation in HIHG condition (Fig. 3.21A and B).

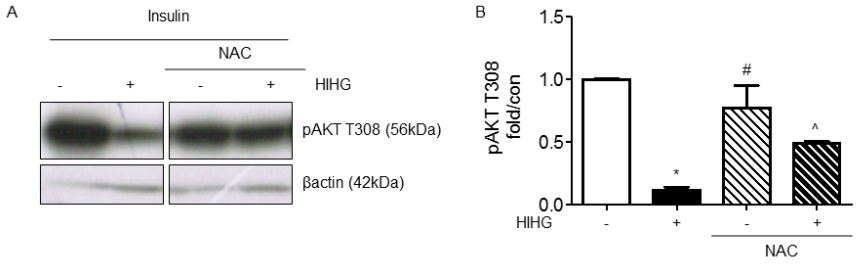

Figure 3.21. NAC increased insulin stimulated AKT phosphorylation in insulin resistant skeletal muscle cells. L6 WT MB were differentiated into MT in 6-well cell culture plates in 2% FBS AMEM, starved in 0.5% FBS AMEM for three hours before the 24 hours HIHG treatment ± one hour NAC pre-treatment. Upon completion of treatments cells were stimulated with 100nM of insulin for 5 minutes, cell lysates were subsequently prepared and protein content analyzed by western blotting. Representative blots are shown (A) and quantification of band densitometry is represented as fold over control (B; n=3) with standard error of mean displayed as error bars.
NAC increased pAKT in HIHG but not in control condition (A and B; p=0.0006).
*(B) *Significant difference compared to control and NAC treatment. #Significant difference compared to HIHG and NAC+HIHG. ^Significant difference compared to control. (p=0.0006)*
**P < 0.05.*
For uncut blots see Appendix A, Supplementary Figure 1.

Then I investigated the effect of NAC on autophagy and I observed increased TFLC3 puncta (Fig. 3.22A), increased red/green fluorescence (Fig. 3.22C), but decreased LC3II (Fig. 3.22D and E), and the increased autophagic flux in response to NAC treatment was associated with decreased lysosomal activity (Fig. 3.22B).

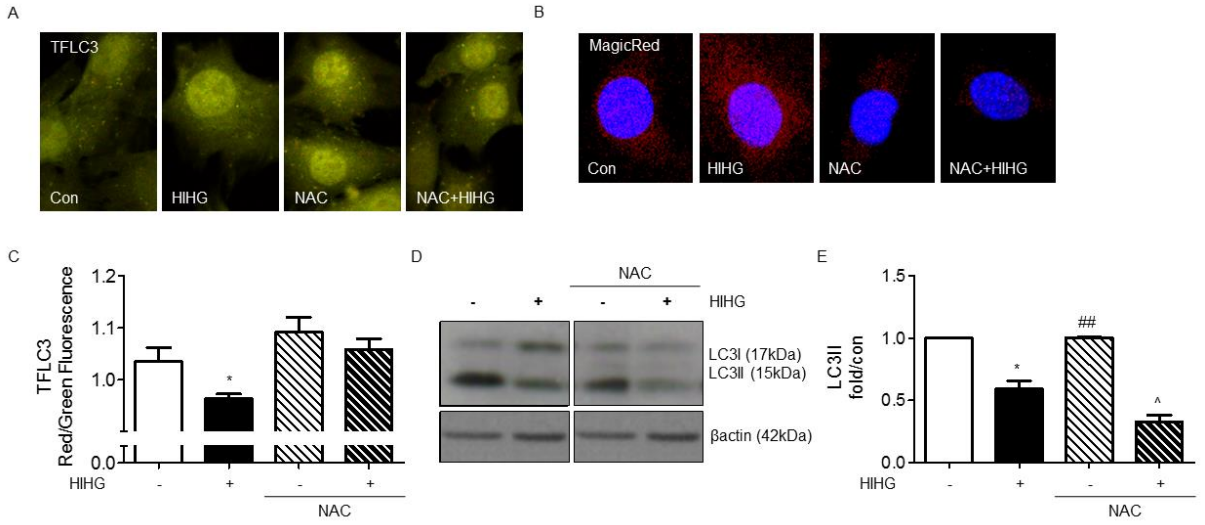

Figure 3.22. NAC increased autophagy in insulin resistant skeletal muscle cells.
(A-C) TFLC3 and WT L6 MB were grown on coverslips to 70% confluency in 12-well cell culture plates in 10% FBS AMEM, starved in 0.5% FBS AMEM for three hours before 24 hours HIHG treatment ± one hour NAC pre-treatment. TFLC3 L6 MB were fixed upon completion of treatment and MagicRed assay was performed on WT L6 MB; 5-9 images per condition was taken by fluorescence confocal microscopy. Representative images are shown (A and B; n=3) and quantification of TFLC3 total red/green fluorescence is represented as mean values (C; n=3) with standard error of mean displayed as error bars.
(D-E) L6 WT MB were differentiated into MT in 6-well cell culture plates in 2% FBS AMEM, starved in 0.5% FBS AMEM for three hours before the 24 hours HIHG treatment ± one hour NAC pre-treatment. Upon completion of treatments, cell lysates were prepared and protein content analyzed by western blotting. Representative blots are shown (D) and quantification of band densitometry is represented as fold over control (E; n=4-7) with standard error of mean displayed as error bars.
NAC treatment increased TFLC3 puncta (A) and red/green fluorescence (C; p=0.0040), but decreased LC3II in HIHG but not control condition (D and E; p<0.0001). NAC treatment increased and lysosomal activity as measured by MagicRed assay (B).
*(C) *Significant difference compared to control, NAC and NAC+HIHG. (p=0.0040)*
*(E) *Significant difference compared to control, NAC and NAC+HIHG. #Significant difference compared to HIHG and NAC treatment. ^Significant difference compared to control, HIHG and NAC. (p=0.0001)*
**P < 0.05; **P < 0.01.*
For uncut blots see Appendix A, Supplementary Figure 1.

3.3.6 NAC Downregulated the UPR and Increased ER Stress

Interestingly, alleviation of oxidative stress and induction of autophagy was not associated with a reduction in ER stress, contrarily NAC treatment increased ER stress (Fig. 3.23A and B). However KDEL fluorescence was decreased with NAC treatment in HIHG condition (Fig. 3.23C), and further, I showed that all three branches of UPR: pIRE1, ATF6 and pPERK, and also peIf2α, were decreased in response to NAC treatment in HIHG condition (Fig. 3.24A-E).

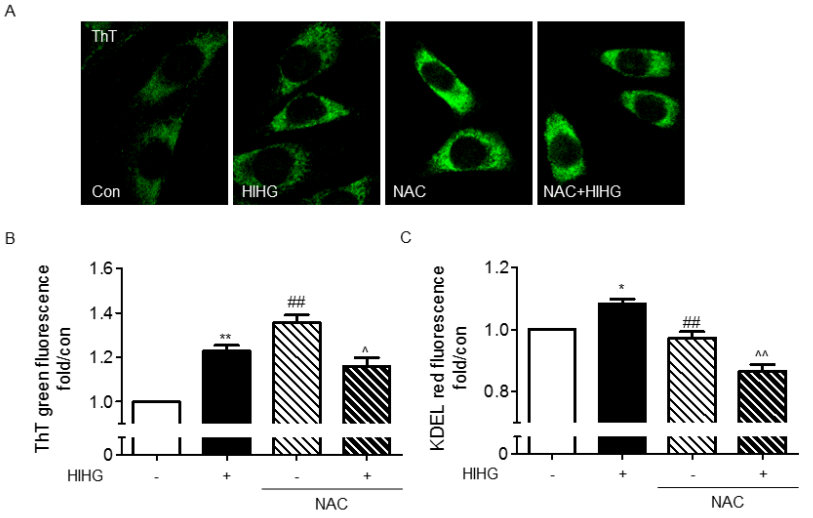

Figure 3.23. NAC treatment increased ER stress.
L6 MB were grown on coverslips to 70% confluency in 12-well cell culture plates in 10% FBS AMEM, starved in 0.5% FBS AMEM for three hours before the 24 hours HIHG treatment ± one hour NAC pre-treatment. ThT-KDEL co-immunofluorescence assay was performed and 5-9 images per condition was taken by fluorescence confocal microscopy. Representative images are shown (A) and quantification of total fluorescence/cells is represented as fold over control (B and C; n=3) with standard error of mean displayed as error bars.
NAC treatment increased ER stress in control but not HIHG condition (A and B; p=0.0002) and decreased KDEL immunofluorescence in HIHG but not control condition (C; p=0.0001).
*(B) **Significant difference compared to Con, NAC and NAC+HIHG. ##Significant difference compared to Con and NAC+HIHG. ^Significant difference compared to Con and NAC. (p=0.0002)*
*(C) *Significant difference compared to Con, NAC and NAC+HIHG. ##Significant difference compared to HIHG and NAC+HIHG. ^^Significant difference compared to Con, HIHG and NAC. (p=0.0001)*
**P < 0.05; **P < 0.01.*

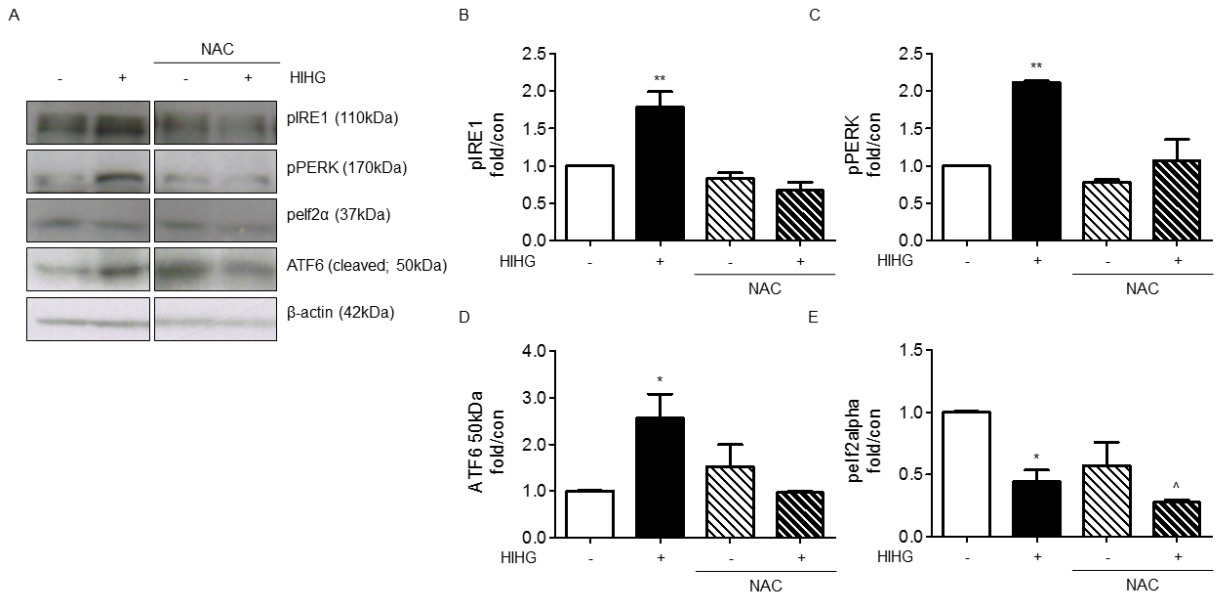

Figure 3.24. NAC downregulated UPR signaling in insulin resistant skeletal muscle cells. L6 WT MB were differentiated into MT in 6-well cell culture plates in 2% FBS AMEM, starved in 0.5% FBS AMEM for three hours before 24 hours HIHG treatment ± one hour NAC pre-treatment. Upon completion of treatments, cell lysates were prepared and protein content analyzed by western blotting. Representative blots are shown (A) and quantification of band densitometry is represented as fold over control (B-G; n=3-4) with standard error of mean displayed as error bars.
NAC decreased pIRE1, pPERK and ATF6 in HIHG condition but induced no change in control condition (A, B, C) while pelf2α was not changed in HIHG or control condition (E).
*(B) **Significant difference compared to Con, NAC and NAC+HIHG (p=0.0010)*
*(C) **Significant difference compared to Con, NAC and NAC+HIHG (p=0.0007)*
*(D) *Significant difference compared to Con and NAC+HIHG (p=0.0454)*
*(E) *Significant difference compared to Con (p=0.0325)*
**P < 0.05; **P < 0.01.*
For uncut blots see Appendix A, Supplementary Figure 1.

3.3.7 NAC Treatment Improved Insulin Sensitivity in both EV and Atg5K Cells

Next I evaluated the importance of autophagy in mediating the insulin sensitizing effect of NAC. I compared changes in proteins involved in autophagy, the UPR and insulin signaling in EV and Atg5K cells by NAC treatment in HIHG condition. I observed that HIHG treatment in Atg5K cells increased pmTOR which was decreased to control levels by NAC treatment (Fig. 3.25A and B), however NAC also decreased LC3II and increased pAKT in both EV and Atg5K cells (Fig. 3.25A, C and D). There was a decreased trend in ATF6 in EV cells ($p=0.0860$) and in pPERK in Atg5K cells ($p=0.0566$; Fig. 3.25A, E and F), and peIf2α was significantly decreased in both EV and Atg5K cells with NAC treatment in HIHG condition (Fig. 3.25A and G).

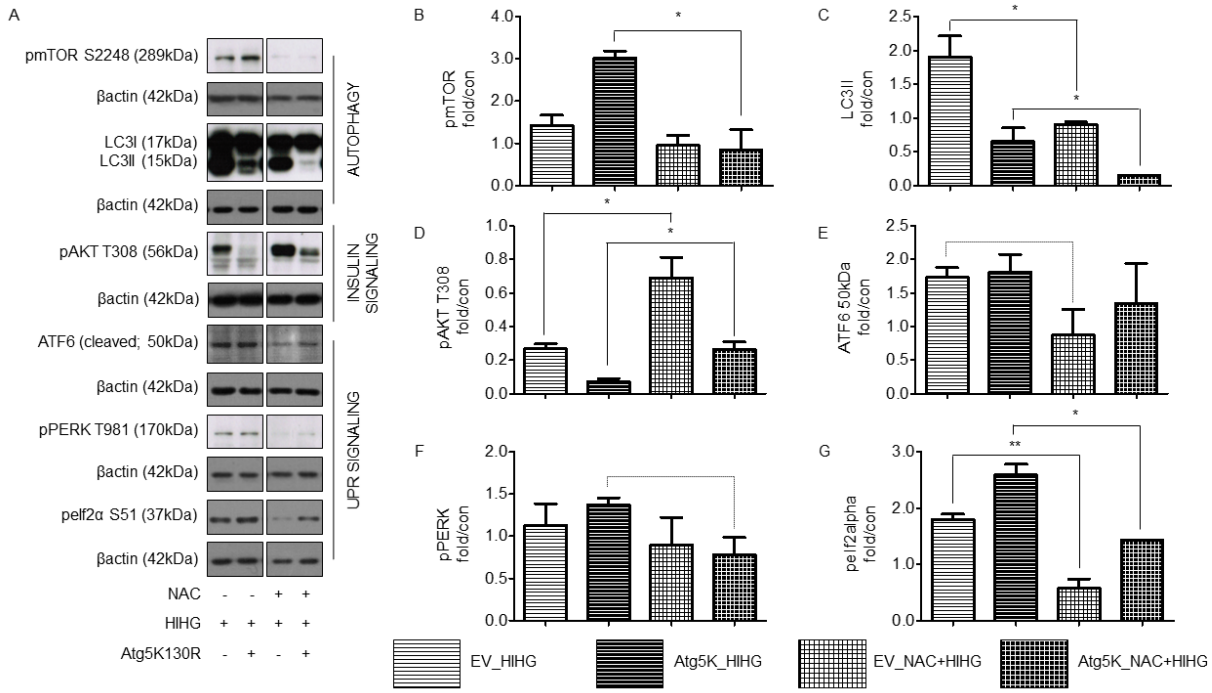

Figure 3.25. Regulation of proteins involved in the UPR, insulin signaling and autophagy in HIHG condition by NAC in EV and Atg5K cells.
L6 EV and Atg5K MB were grown to 100% confluency in 6-well cell culture plates in 10% FBS AMEM, starved in 0.5% FBS AMEM for three hours before 24 hours HIHG treatment ± one hour NAC pre-treatment. Upon completion of treatments, cell lysates were prepared and protein content analyzed by western blotting. Representative blots are shown (A) and quantification of band densitometry is represented as fold over control (B-G; n=2) with standard error of mean displayed as error bars.
NAC reduced pmTOR in Atg5K but not EV cells (B: p=0.0222) however LC3II was decreased in response to NAC treatment in both EV and Atg5K cells (C: p=0.0106). NAC increased pAKT in both EV and Atg5K cells (D: p=0.0390), and ATF6 showed a decreased trend in EV cells (E: 0.0860) and pPERK showed a decreased trend in Atg5K cells (F: p=0.0566). pelf2α was decreased in both EV and Atg5K cells in response to NAC treatment in HIHG condition (G: p=0.0122).
**P < 0.05; **P < 0.01.*
For uncut blots see Appendix A, Supplementary Figure 2.

Chapter 4. Discussion

The staggering increase in obesity prevalence over the last few decades has been closely followed by a similar increase in diabetes prevalence, and it is now known that obesity is the single most important predictor of developing diabetes with 80% of cases being directly related to obesity [7, 8]. Diabetes is a known risk factor for a number of medical conditions and thus poses a major and growing health concern [4, 5], and accordingly a lot of research have been aimed towards understanding the progression of obesity to diabetes [11, 12]. The hallmark of diabetes is insulin resistance and glucose intolerance [1] and, as skeletal muscle is an important target for insulin action and a major regulator of whole-body glucose homeostasis, the relevance of studying skeletal muscle in the context of insulin resistance is significant [65, 66]; firstly, to better understand the complex cellular events involved in the disturbed metabolic condition of insulin resistance and diabetes, and secondly, to identify pathways that can be potential therapeutic targets. Although skeletal muscle insulin resistance is a well-accepted contributor to the pathogenesis of diabetes, the exact molecular mechanisms involved in developing insulin resistance in skeletal muscle is not fully known [71] and therefore the first objective of my study was to characterize changes in cellular processes and signalling responses that exhibited an altered profile in insulin resistant skeletal muscle.

I started by validating an already established *in vitro* model of skeletal muscle insulin resistance in which L6 skeletal muscle cells were treated with HIHG for 24 hours, resulting in impaired insulin signaling and an attenuation of insulin stimulated glucose uptake due to a reduction in GLUT4 translocation to the plasma membrane [159]. I confirmed that HIHG treatment impaired insulin signaling, and that the impaired insulin signaling resulted in a lack of insulin stimulated glucose uptake (Fig. 3.1), and then showed that HIHG treatment impaired autophagy (Fig. 3.2), increased ER stress and UPR activation (Fig. 3.4), and caused oxidative stress (Fig. 3.7).

The adipokine adiponectin have been extensively studied in the context of obesity and diabetes but, although adiponectin is well known to have an insulin sensitizing effect in the disturbed metabolic profile of those conditions, its cellular mechanism of action remains largely unknown, especially in skeletal muscle, [21, 68]. Our lab has recently published that adiponectin stimulate autophagy via AMPK and further that adiponectin stimulate expression of genes involved in the antioxidant response in skeletal muscle of HFD fed mice [69], however a causative relationship between autophagy induction or alleviation of oxidative stress in mediating the insulin sensitizing effects of adiponectin still needs to be demonstrated and its effect on ER stress and the UPR in skeletal muscle remains to be established. The second objective of my study was therefore to further our understanding of the insulin sensitizing mechanism of adiponectin in skeletal muscle, examining autophagy, ER stress, the UPR and oxidative stress.

I confirmed that adiponectin treatment improved insulin sensitivity, restored autophagy and alleviated ER stress in HIHG treated cells (Fig. 3.8A-F and Fig. 3.10A,C), and I demonstrated that the ability of adiponectin to alleviate ER stress in HIHG condition was dependent on autophagy using an autophagy deficient cell line, Atg5K (Fig. 3.11A,B,D,E). To determine if the insulin sensitizing effect of adiponectin was autophagy dependent I again used Atg5K cells, but surprisingly adiponectin was not able to improve insulin sensitivity in either Atg5K or EV control cells (Fig. 3.9A,D). However adiponectin treatment did similarly not increase autophagy in Atg5K or EV cells (Fig. 3.9C,F), and although HIHG treatment caused insulin resistance in Atg5K and EV cells, it increased autophagy in both Atg5K and EV cells, contrary to the findings in WT cells (Fig. 3.2A-F and Fig. 3.9A,D,C,F). It is therefore conceivable that adiponectin was unable to stimulate autophagy further beyond the increase caused by HIHG treatment. No definitive conclusion regarding the necessity of autophagy stimulation in the insulin sensitizing effect of adiponectin can be drawn based on the obtained data but the

correlation between the ability of adiponectin to induce autophagy and adiponectin's ability to improve insulin sensitivity highlight that this warrants further study.

Oxidative stress and ER stress have been extensively studied in the context of insulin resistance and diabetes, especially in beta-cells, and alleviating ER stress in metabolically challenged mouse models has been shown to improve insulin sensitivity and glucose tolerance [109-111], and oxidative stress has similarly been shown to be involved in developing insulin resistance [171-173] and alleviating oxidative stress has been shown to improve insulin sensitivity [174, 175]. Recently there has also been a growing interest in studying the process of autophagy in a variety of conditions and disease states including diabetes [176]; it has been suggested that dysregulation of autophagy might play an essential role in the progression from obesity to diabetes and an increasing body of research is establishing the central role of autophagy in regulating whole body metabolism [82]. The relevance of autophagy, ER stress, the UPR and oxidative stress in insulin resistance and the close relationship between ER stress, the UPR and oxidative stress, that has been suggested to also involve autophagy, makes the interrelationship between the processes, especially in the context of insulin resistance, of critical importance and examining the relationship between autophagy, ER stress, the UPR and oxidative stress in the context of insulin resistance was therefore the third objective of my study.

Temporal analysis of induction of ER stress, UPR activation and autophagy impairment in HIHG induced insulin resistance demonstrated that both insulin signaling and autophagy gradually decreased starting somewhere between 0-2 hours, being decreased also at 6 hours and further decreased at 24 hours (Fig. 3.1C-D and Fig. 3.3A-B, H-I), while ER stress was induced later somewhere between 4-24 hours (Fig. 3.6A, D). Interestingly there was a differential activation of the UPR with all three signaling branches of the UPR being activated at 24 hours (Fig. 3.5A-E and Fig. 3.6B), but with pIRE1 demonstrating a gradual increase at 2, 6 and 24 hours while pPERK and ATF6 only were increased at 24 hours (Fig. 3.6B).

Table 4.1 Summary of time course analysis.

pAKT	↓		↓	↓	Insulin Sensitivity
Red/Green	↓		↓	↓	Autophagy
LC3II	↓		↓	↓	
ThT green		=		↑	ER Stress
pIRE1	↑		↑	↑	UPR
pPERK	=		=	↑	
ATF6	=		=	↑	
peIf2α	↑		=	↓	
HIHG	2	4	6	24	(hours)

↑	increased compared to control
↓	decreased compared to control
=	no difference compared to control
Red/Green	TFLC3 red/green fluorescence

Taken together these data suggests that impaired autophagy or activation of pIRE1 might be involved in developing insulin resistance while the ER stress observed at 24 hours of HIHG treatment is likely to be a concurrent event to the observed insulin resistance, as supposed to playing a causative role in its development. Further, since autophagy has been demonstrated to alleviate ER stress [99, 100], the impairment in autophagy might directly cause the observed increase in ER stress.

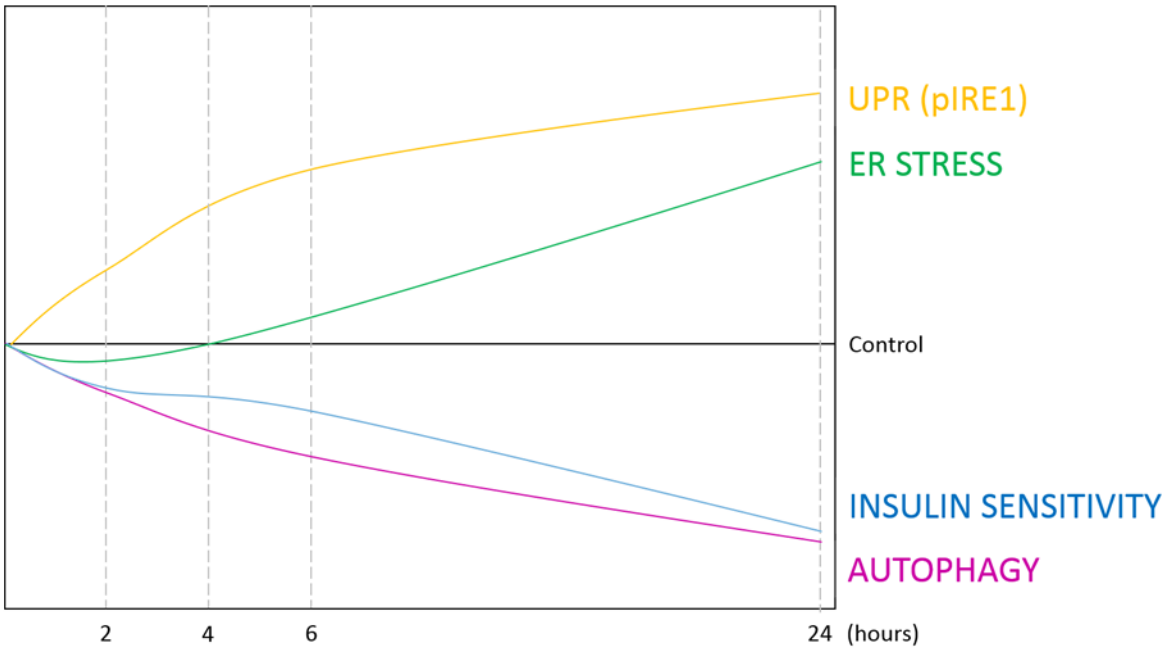

Figure 4.1.Graphical representation of time course analysis.

Indeed recently published data from our lab demonstrated that insulin resistance was induced both by chemical and molecular impairment of autophagy [69], and to further evaluate the role of autophagy in developing insulin resistance and to determine if impaired autophagy caused ER stress I directly assessed these processes both in response to chemical inhibition of autophagy, by bafilomycin treatment, and in a molecular model of impaired autophagy, Atg5K cells. I confirmed previous findings that inhibiting autophagy caused insulin resistance (Fig. 3.9A,D and Fig. 3.13B,E) and additionally showed that ER stress was increased by both chemical and molecular inhibition of autophagy (Fig. 3.13A,C and Fig. 3.14C-F). To further investigate if impaired autophagy directly caused ER stress, I inhibited mTOR with rapamycin treatment which induced autophagy and also alleviated the ER stress observed in skeletal muscle insulin resistance, and the ER stress lowering effects of rapamycin was shown to be autophagy dependent (Fig. 3.14A-F). This demonstrated that the impaired autophagy in HIHG induced insulin resistance indeed caused ER stress.

Looking in detail at proteins that are part of the UPR signaling cascades I observed that although all three branches of the UPR, namely pIRE1, pPERK and ATF6, were upregulated in response to HIHG treatment, the UPR effector protein immediately downstream of pPERK, peIf2α, was decreased. In addition to being an important mediator of the UPR, peIf2α is also thought to be a link between UPR activation and autophagy induction making the decrease in peIf2α, especially in the context of impaired autophagy, an interesting observation. Temporal analysis of peIf2α in progressing insulin resistance revealed that peIf2α showed an early increase, at 2 hours, and then gradually decreased, at 6 hours demonstrating similar a level as control and at 24 hours being significantly lowered compared to control (Fig. 3.6B and Fig. 3.5A,E). This pattern in peIf2α can be explained by a self-regulatory mechanism which functions to prevent over-activation of peIf2α induced pathways; specifically, activation of peIf2α is known to stimulate the expression of GADD34 which dephosphorylates peIf2α to downregulate its activity [177]. I observed several instances of a correlation between increased autophagy and increased peIf2α, for example in WT cells there was an increase in autophagy in response to adiponectin treatment and also an increase in peIf2α (Fig. 3.10E,F) and in both EV and Atg5K cells, HIHG treatment increased autophagy and also increased peIf2α (Fig. 3.9C,F and Fig. 3.11C,H). I thus wanted to examine if, in the context of insulin resistance, directly preventing peIf2α dephosphorylation would prevent autophagy impairment and alleviate ER stress, and to investigate whether this would improve insulin sensitivity.

Salubrinal is a well-established pharmacological inhibitor of peIf2α dephosphorylation [178], and salubrinal treatment not only restored, but significantly increased autophagy, which resulted in a reduction of ER stress (Fig. 3.17A-E and Fig. 3.16F-G). Using Atg5K cells I demonstrated that the ER stress lowering effect of salubrinal was dependent on its ability to induce autophagy (Fig. 3.19A-D), but despite increasing autophagy and alleviating ER stress there was no increase in insulin sensitivity in response to salubrinal treatment (Fig. 3.18A-B). These results support that alleviating ER stress is insufficient to improve insulin sensitivity and I

speculate that the inability of salubrinal to improve insulin sensitivity, despite also increasing autophagy, might be caused by the induction of autophagy surpassing normal levels as both too much and too little autophagy is known to be detrimental [127] highlighting the importance of properly regulated autophagy in maintaining cellular homeostasis or, alternatively, that increased peIf2α in addition to stimulating autophagy also causes cells cycle arrest and increases ER stress induced apoptotic signaling [179] potentially perpetrating cellular dysregulation and an insulin resistant state. Interestingly, although alleviating ER stress does not improve insulin sensitivity in skeletal muscle insulin resistance, increasing ER stress by tunicamycin treatment (Fig. 3.16F) did cause insulin resistance (Fig. 3.18A,B), but also increased autophagy (Fig. 3.17A,C-E).

To determine which of the aforementioned processes are required for insulin sensitization I wanted to examine them in response to NAC, an antioxidant that has been demonstrated to improve insulin sensitivity [118]. While I confirmed the insulin sensitizing effect of NAC in skeletal muscle (Fig. 3.21A,B), I also demonstrated a clear increase in ER stress in response to NAC treatment (Fig. 3.23A,B). This further evidences that alleviating ER stress is insufficient to improve insulin sensitivity and does not appear to even be required to combat insulin resistance, and that insulin resistance observed in response to tunicamycin treatment is likely caused by a secondary event to ER stress and not the ER stress itself. I also showed that NAC treatment increased autophagy in skeletal muscle insulin resistance (Fig. 3.22A-E) however examining the effect of NAC in Atg5K cells I demonstrated that this increase in autophagy was not required for the insulin sensitizing effect of NAC (Fig. 3.25A,D).

Examining the regulation of the UPR in response to NAC treatment I observed a clear decrease in activation of all three UPR signaling proteins, and also peIf2α, in WT cells (Fig. 3.24A-E) with similar trends observed also in EV and Atg5K cells (Fig. 3.24A, E-G). As activation of the UPR, specifically pIRE1, has been linked to phosphorylation of JNK and impaired insulin signaling [112, 180] this is an interesting observation.

Looking at the regulation of UPR signaling proteins in response to other treatments we can see that there appears to be a trend correlation between reducing UPR signaling and improving insulin sensitivity. For example in response to adiponectin treatment there was a decreased trend, significant for ATF6, in the UPR signaling proteins (except peIf2α; Fig. 3.10C-H), and in Atg5K and EV cells adiponectin did not alter ATF6 or pPERK or peIf2α, consistent with its inability to improve insulin sensitivity (Fig. 3.11C,F-H). Rapamycin increased insulin sensitivity in Atg5K but not EV cells, again correlating with a decreased trend in UPR signaling in Atg5K but not EV cells (Fig. 3.15A,D-G) although the regulation of pIRE1 still needs to be examined. Interestingly in response to salubrinal treatment there was a small increased trend in insulin sensitivity in Atg5K cells which correlated with a decreased trend in UPR signaling, a significant decrease in peIf2α and a decrease in autophagy (Fig. 3.20A,D-G).

These results point to a very complex network being involved in improving insulin sensitivity and highlight the importance of a balanced regulation. It is conceivable that all of these processes are involved in different pathways resulting in increased insulin sensitivity, although a close relationship appears to exist between autophagy, oxidative stress and the UPR, and cumulatively these results point to a reduction in UPR activation being the common denominator between the ability of adiponectin, NAC and rapamycin to have an insulin sensitizing effect.

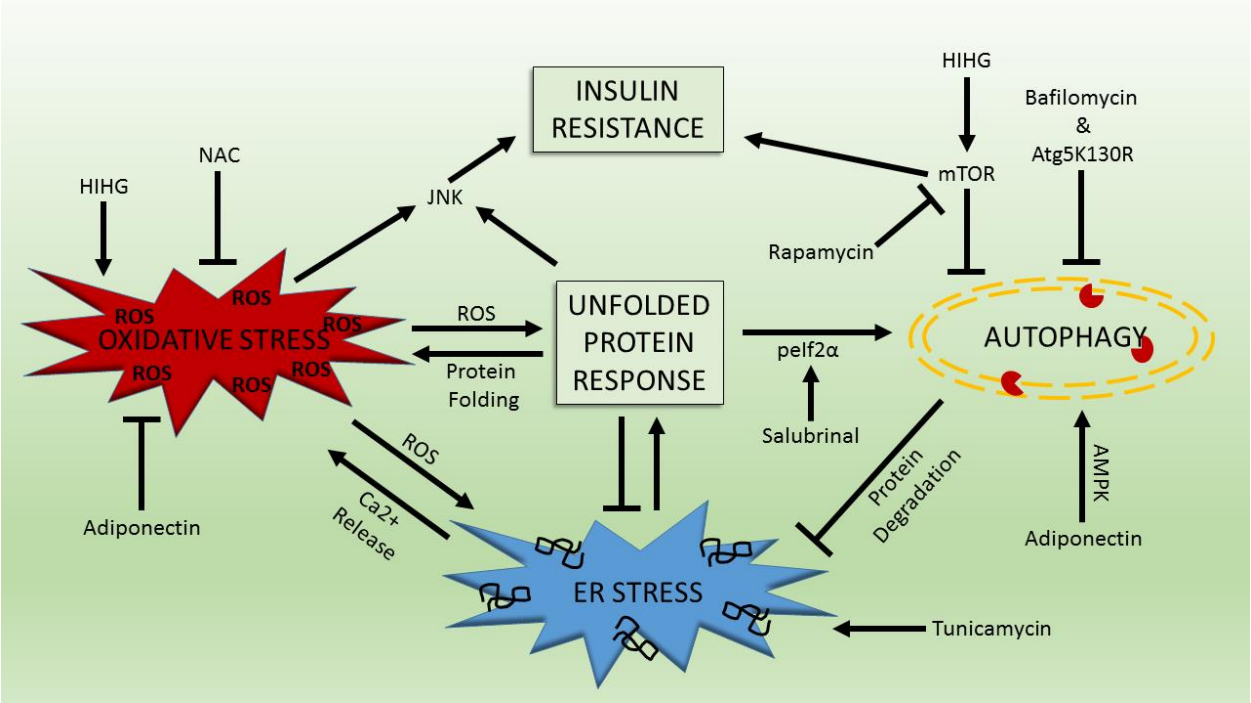

Figure 4.2. Summary of the interrelationship between autophagy, ER stress, the UPR and oxidative stress in skeletal muscle insulin resistance and regulation by adiponectin. HIHG treatment increased pmTOR and impaired autophagy leading ER stress, UPR activation and insulin resistance; HIHG treatment also caused oxidative stress which further exacerbate dysregulation of cellular homeostasis leading to ER stress, UPR activation and insulin resistance. Chemical or molecular impairment of autophagy and induction of ER stress was associated with insulin resistance but alleviating ER stress or inducing autophagy was not necessary to improve insulin sensitivity by NAC treatment, although adiponectin's insulin sensitizing ability appeared to correlate with its ability to induce autophagy. Correlations between improved insulin sensitivity and downregulated UPR signalling suggests its importance in regulation of insulin resistance, potentially via JNK.

In summary, skeletal muscle insulin resistance is associated with impaired autophagy, ER stress, increased UPR activation and oxidative stress. Chemical and molecular inhibition of autophagy leads to insulin resistance and chemical inhibition of protein folding to increase ER stress also caused insulin resistance, however temporal analysis revealed that impaired autophagy is an early event while ER stress happened later, and I have demonstrated that the ER stress in insulin resistance was directly caused by the impairment of autophagy.

Although impairment in autophagy followed a similar pattern as developing insulin resistance and demonstrated a correlation with the ability of adiponectin to improve insulin sensitivity it was not required for the antioxidant NAC to improve insulin sensitivity, and correlations between improved insulin sensitivity and downregulation of the UPR point to this potentially being the converging point between several cellular processes and regulation of insulin sensitivity.

Future studies should examine oxidative stress in the context of skeletal muscle insulin resistance, both by temporal analysis and in response to adiponectin and chemical and molecular regulators of autophagy and ER stress, to help clearly place it in relationship to these processes in the context of skeletal muscle insulin resistance. Future studies should also aim to determine if autophagy is required for the insulin sensitizing properties of adiponectin, if there is a significant correlation between a reduction in UPR and improved insulin sensitivity in response to adiponectin and rapamycin treatment, particularly in pIRE1, and examine whether activation of JNK correlates with these changes thus clearly linking the regulation of UPR activation by autophagy and oxidative stress with insulin resistance.

References

1. van Belle, T.L., K.T. Coppieters, and M.G. von Herrath, *Type 1 diabetes: etiology, immunology, and therapeutic strategies.* Physiol Rev, 2011. **91**(1): p. 79-118.
2. Daneman, D., *Type 1 diabetes.* Lancet, 2006. **367**(9513): p. 847-58.
3. Scheen, A.J., *Pathophysiology of type 2 diabetes.* Acta Clin Belg, 2003. **58**(6): p. 335-41.
4. Shaw, J.E., R.A. Sicree, and P.Z. Zimmet, *Global estimates of the prevalence of diabetes for 2010 and 2030.* Diabetes Res Clin Pract, 2010. **87**(1): p. 4-14.
5. Zimmet, P., K.G. Alberti, and J. Shaw, *Global and societal implications of the diabetes epidemic.* Nature, 2001. **414**(6865): p. 782-7.
6. Kelly, T., et al., *Global burden of obesity in 2005 and projections to 2030.* Int J Obes (Lond), 2008. **32**(9): p. 1431-7.
7. Matthaei, S., et al., *Pathophysiology and pharmacological treatment of insulin resistance.* Endocr Rev, 2000. **21**(6): p. 585-618.
8. Hu, F.B., et al., *Diet, lifestyle, and the risk of type 2 diabetes mellitus in women.* N Engl J Med, 2001. **345**(11): p. 790-7.
9. Chen, L., D.J. Magliano, and P.Z. Zimmet, *The worldwide epidemiology of type 2 diabetes mellitus--present and future perspectives.* Nat Rev Endocrinol, 2012. **8**(4): p. 228-36.
10. King, H., R.E. Aubert, and W.H. Herman, *Global burden of diabetes, 1995-2025: prevalence, numerical estimates, and projections.* Diabetes Care, 1998. **21**(9): p. 1414-31.
11. Rabe, K., et al., *Adipokines and insulin resistance.* Mol Med, 2008. **14**(11-12): p. 741-51.
12. Grundy, S.M., et al., *Definition of metabolic syndrome: report of the National Heart, Lung, and Blood Institute/American Heart Association conference on scientific issues related to definition.* Arterioscler Thromb Vasc Biol, 2004. **24**(2): p. e13-8.
13. Whitehead, J.P., et al., *Adiponectin--a key adipokine in the metabolic syndrome.* Diabetes Obes Metab, 2006. **8**(3): p. 264-80.
14. Kershaw, E.E. and J.S. Flier, *Adipose tissue as an endocrine organ.* J Clin Endocrinol Metab, 2004. **89**(6): p. 2548-56.
15. Fruhbeck, G., et al., *The adipocyte: a model for integration of endocrine and metabolic signaling in energy metabolism regulation.* Am J Physiol Endocrinol Metab, 2001. **280**(6): p. E827-47.
16. Tilg, H. and A.R. Moschen, *Adipocytokines: mediators linking adipose tissue, inflammation and immunity.* Nat Rev Immunol, 2006. **6**(10): p. 772-83.
17. Rosen, E.D. and B.M. Spiegelman, *Adipocytes as regulators of energy balance and glucose homeostasis.* Nature, 2006. **444**(7121): p. 847-53.
18. Yamauchi, T. and T. Kadowaki, *Adiponectin receptor as a key player in healthy longevity and obesity-related diseases.* Cell Metab, 2013. **17**(2): p. 185-96.
19. Ye, R. and P.E. Scherer, *Adiponectin, driver or passenger on the road to insulin sensitivity?* Mol Metab, 2013. **2**(3): p. 133-41.
20. Guillod-Maximin, E., et al., *Adiponectin receptors are expressed in hypothalamus and colocalized with proopiomelanocortin and neuropeptide Y in rodent arcuate neurons.* J Endocrinol, 2009. **200**(1): p. 93-105.
21. Gavrila, A., et al., *Serum adiponectin levels are inversely associated with overall and central fat distribution but are not directly regulated by acute fasting or leptin administration in humans: cross-sectional and interventional studies.* J Clin Endocrinol Metab, 2003. **88**(10): p. 4823-31.
22. Arita, Y., et al., *Paradoxical decrease of an adipose-specific protein, adiponectin, in obesity.* Biochem Biophys Res Commun, 1999. **257**(1): p. 79-83.

23. Lihn, A.S., S.B. Pedersen, and B. Richelsen, *Adiponectin: action, regulation and association to insulin sensitivity.* Obes Rev, 2005. **6**(1): p. 13-21.
24. Hotta, K., et al., *Plasma concentrations of a novel, adipose-specific protein, adiponectin, in type 2 diabetic patients.* Arterioscler Thromb Vasc Biol, 2000. **20**(6): p. 1595-9.
25. Maeda, K., et al., *cDNA cloning and expression of a novel adipose specific collagen-like factor, apM1 (AdiPose Most abundant Gene transcript 1).* Biochem Biophys Res Commun, 1996. **221**(2): p. 286-9.
26. Scherer, P.E., et al., *A novel serum protein similar to C1q, produced exclusively in adipocytes.* J Biol Chem, 1995. **270**(45): p. 26746-9.
27. Nakano, Y., et al., *Isolation and characterization of GBP28, a novel gelatin-binding protein purified from human plasma.* J Biochem, 1996. **120**(4): p. 803-12.
28. Hu, E., P. Liang, and B.M. Spiegelman, *AdipoQ is a novel adipose-specific gene dysregulated in obesity.* J Biol Chem, 1996. **271**(18): p. 10697-703.
29. Saito, K., et al., *Organization of the gene for gelatin-binding protein (GBP28).* Gene, 1999. **229**(1-2): p. 67-73.
30. Stumvoll, M., et al., *Association of the T-G polymorphism in adiponectin (exon 2) with obesity and insulin sensitivity: interaction with family history of type 2 diabetes.* Diabetes, 2002. **51**(1): p. 37-41.
31. Tsao, T.S., et al., *Role of disulfide bonds in Acrp30/adiponectin structure and signaling specificity. Different oligomers activate different signal transduction pathways.* J Biol Chem, 2003. **278**(50): p. 50810-7.
32. Waki, H., et al., *Generation of globular fragment of adiponectin by leukocyte elastase secreted by monocytic cell line THP-1.* Endocrinology, 2005. **146**(2): p. 790-6.
33. Wang, Z.V., et al., *Secretion of the adipocyte-specific secretory protein adiponectin critically depends on thiol-mediated protein retention.* Mol Cell Biol, 2007. **27**(10): p. 3716-31.
34. Liu, M., et al., *A disulfide-bond A oxidoreductase-like protein (DsbA-L) regulates adiponectin multimerization.* Proc Natl Acad Sci U S A, 2008. **105**(47): p. 18302-7.
35. Koshiishi, C., et al., *Regulation of expression of the mouse adiponectin gene by the C/EBP family via a novel enhancer region.* Gene, 2008. **424**(1-2): p. 141-6.
36. Rahmouni, K. and C.D. Sigmund, *Id3, E47, and SREBP-1c: fat factors controlling adiponectin expression.* Circ Res, 2008. **103**(6): p. 565-7.
37. Gustafson, B., et al., *Adiponectin gene activation by thiazolidinediones requires PPAR gamma 2, but not C/EBP alpha-evidence for differential regulation of the aP2 and adiponectin genes.* Biochem Biophys Res Commun, 2003. **308**(4): p. 933-9.
38. Qiao, L. and J. Shao, *SIRT1 regulates adiponectin gene expression through Foxo1-C/enhancer-binding protein alpha transcriptional complex.* J Biol Chem, 2006. **281**(52): p. 39915-24.
39. Richards, A.A., et al., *Adiponectin multimerization is dependent on conserved lysines in the collagenous domain: evidence for regulation of multimerization by alterations in posttranslational modifications.* Mol Endocrinol, 2006. **20**(7): p. 1673-87.
40. Qiang, L., H. Wang, and S.R. Farmer, *Adiponectin secretion is regulated by SIRT1 and the endoplasmic reticulum oxidoreductase Ero1-L alpha.* Mol Cell Biol, 2007. **27**(13): p. 4698-707.
41. Pajvani, U.B., et al., *Structure-function studies of the adipocyte-secreted hormone Acrp30/adiponectin. Implications fpr metabolic regulation and bioactivity.* J Biol Chem, 2003. **278**(11): p. 9073-85.
42. Aso, Y., et al., *Comparison of serum high-molecular weight (HMW) adiponectin with total adiponectin concentrations in type 2 diabetic patients with coronary artery disease using a novel enzyme-linked immunosorbent assay to detect HMW adiponectin.* Diabetes, 2006. **55**(7): p. 1954-60.

43. Yamauchi, T., et al., *Cloning of adiponectin receptors that mediate antidiabetic metabolic effects.* Nature, 2003. **423**(6941): p. 762-9.
44. Cheng, K.K., et al., *Signaling mechanisms underlying the insulin-sensitizing effects of adiponectin.* Best Pract Res Clin Endocrinol Metab, 2014. **28**(1): p. 3-13.
45. Yamauchi, T., et al., *Adiponectin stimulates glucose utilization and fatty-acid oxidation by activating AMP-activated protein kinase.* Nat Med, 2002. **8**(11): p. 1288-95.
46. Mao, X., et al., *APPL1 binds to adiponectin receptors and mediates adiponectin signalling and function.* Nat Cell Biol, 2006. **8**(5): p. 516-23.
47. Kubota, N., et al., *Disruption of adiponectin causes insulin resistance and neointimal formation.* J Biol Chem, 2002. **277**(29): p. 25863-6.
48. Maeda, N., et al., *Diet-induced insulin resistance in mice lacking adiponectin/ACRP30.* Nat Med, 2002. **8**(7): p. 731-7.
49. Ma, K., et al., *Increased beta -oxidation but no insulin resistance or glucose intolerance in mice lacking adiponectin.* J Biol Chem, 2002. **277**(38): p. 34658-61.
50. Yamauchi, T., et al., *Dual roles of adiponectin/Acrp30 in vivo as an anti-diabetic and anti-atherogenic adipokine.* Curr Drug Targets Immune Endocr Metabol Disord, 2003. **3**(4): p. 243-54.
51. Combs, T.P., et al., *A transgenic mouse with a deletion in the collagenous domain of adiponectin displays elevated circulating adiponectin and improved insulin sensitivity.* Endocrinology, 2004. **145**(1): p. 367-83.
52. Chandran, M., et al., *Adiponectin: more than just another fat cell hormone?* Diabetes Care, 2003. **26**(8): p. 2442-50.
53. Diez, J.J. and P. Iglesias, *The role of the novel adipocyte-derived hormone adiponectin in human disease.* Eur J Endocrinol, 2003. **148**(3): p. 293-300.
54. Hotta, K., et al., *Circulating concentrations of the adipocyte protein adiponectin are decreased in parallel with reduced insulin sensitivity during the progression to type 2 diabetes in rhesus monkeys.* Diabetes, 2001. **50**(5): p. 1126-33.
55. Mullen, K.L., et al., *Adiponectin resistance precedes the accumulation of skeletal muscle lipids and insulin resistance in high-fat-fed rats.* Am J Physiol Regul Integr Comp Physiol, 2009. **296**(2): p. R243-51.
56. Mazzola, N., *Review of current and emerging therapies in type 2 diabetes mellitus.* Am J Manag Care, 2012. **18**(1 Suppl): p. S17-26.
57. Pajvani, U.B., et al., *Complex distribution, not absolute amount of adiponectin, correlates with thiazolidinedione-mediated improvement in insulin sensitivity.* J Biol Chem, 2004. **279**(13): p. 12152-62.
58. Tonelli, J., et al., *Mechanisms of early insulin-sensitizing effects of thiazolidinediones in type 2 diabetes.* Diabetes, 2004. **53**(6): p. 1621-9.
59. Maeda, N., et al., *PPARgamma ligands increase expression and plasma concentrations of adiponectin, an adipose-derived protein.* Diabetes, 2001. **50**(9): p. 2094-9.
60. Kubota, N., et al., *Pioglitazone ameliorates insulin resistance and diabetes by both adiponectin-dependent and -independent pathways.* J Biol Chem, 2006. **281**(13): p. 8748-55.
61. Nawrocki, A.R., et al., *Mice lacking adiponectin show decreased hepatic insulin sensitivity and reduced responsiveness to peroxisome proliferator-activated receptor gamma agonists.* J Biol Chem, 2006. **281**(5): p. 2654-60.
62. Liu, Y., et al., *Functional significance of skeletal muscle adiponectin production, changes in animal models of obesity and diabetes, and regulation by rosiglitazone treatment.* Am J Physiol Endocrinol Metab, 2009. **297**(3): p. E657-64.
63. Okada-Iwabu, M., et al., *A small-molecule AdipoR agonist for type 2 diabetes and short life in obesity.* Nature, 2013. **503**(7477): p. 493-9.

64. Tanabe, H., et al., *Crystal structures of the human adiponectin receptors.* Nature, 2015. **520**(7547): p. 312-6.
65. Karlsson, H.K. and J.R. Zierath, *Insulin signaling and glucose transport in insulin resistant human skeletal muscle.* Cell Biochem Biophys, 2007. **48**(2-3): p. 103-13.
66. DeFronzo, R.A., et al., *Effects of insulin on peripheral and splanchnic glucose metabolism in noninsulin-dependent (type II) diabetes mellitus.* J Clin Invest, 1985. **76**(1): p. 149-55.
67. Krause, M.P., et al., *Adiponectin is expressed by skeletal muscle fibers and influences muscle phenotype and function.* Am J Physiol Cell Physiol, 2008. **295**(1): p. C203-12.
68. Liu, Y. and G. Sweeney, *Adiponectin action in skeletal muscle.* Best Pract Res Clin Endocrinol Metab, 2014. **28**(1): p. 33-41.
69. Liu, Y., et al., *Adiponectin stimulates autophagy and reduces oxidative stress to enhance insulin sensitivity during high fat diet feeding in mice.* Diabetes, 2014.
70. O'Neill, H.M., *AMPK and Exercise: Glucose Uptake and Insulin Sensitivity.* Diabetes Metab J, 2013. **37**(1): p. 1-21.
71. Abdul-Ghani, M.A. and R.A. DeFronzo, *Pathogenesis of insulin resistance in skeletal muscle.* J Biomed Biotechnol, 2010. **2010**: p. 476279.
72. Rask-Madsen, C. and C.R. Kahn, *Tissue-specific insulin signaling, metabolic syndrome, and cardiovascular disease.* Arterioscler Thromb Vasc Biol, 2012. **32**(9): p. 2052-9.
73. Vinciguerra, M. and M. Foti, *PTEN and SHIP2 phosphoinositide phosphatases as negative regulators of insulin signalling.* Arch Physiol Biochem, 2006. **112**(2): p. 89-104.
74. Cusi, K., et al., *Insulin resistance differentially affects the PI 3-kinase- and MAP kinase-mediated signaling in human muscle.* J Clin Invest, 2000. **105**(3): p. 311-20.
75. Morino, K., et al., *Muscle-specific IRS-1 Ser->Ala transgenic mice are protected from fat-induced insulin resistance in skeletal muscle.* Diabetes, 2008. **57**(10): p. 2644-51.
76. Hotamisligil, G.S., et al., *IRS-1-mediated inhibition of insulin receptor tyrosine kinase activity in TNF-alpha- and obesity-induced insulin resistance.* Science, 1996. **271**(5249): p. 665-8.
77. Sell, H., J. Eckel, and D. Dietze-Schroeder, *Pathways leading to muscle insulin resistance--the muscle--fat connection.* Arch Physiol Biochem, 2006. **112**(2): p. 105-13.
78. Liu, G. and C.M. Rondinone, *JNK: bridging the insulin signaling and inflammatory pathway.* Curr Opin Investig Drugs, 2005. **6**(10): p. 979-87.
79. Panzhinskiy, E., et al., *Endoplasmic reticulum stress upregulates protein tyrosine phosphatase 1B and impairs glucose uptake in cultured myotubes.* Diabetologia, 2013. **56**(3): p. 598-607.
80. Gonzalez, C.D., et al., *The emerging role of autophagy in the pathophysiology of diabetes mellitus.* Autophagy, 2014. **7**(1): p. 2-11.
81. Giacco, F. and M. Brownlee, *Oxidative stress and diabetic complications.* Circ Res, 2010. **107**(9): p. 1058-70.
82. Quan, W. and M.S. Lee, *Role of autophagy in the control of body metabolism.* Endocrinol Metab (Seoul), 2013. **28**(1): p. 6-11.
83. Flamment, M., et al., *New insights into ER stress-induced insulin resistance.* Trends Endocrinol Metab, 2012. **23**(8): p. 381-90.
84. Houstis, N., E.D. Rosen, and E.S. Lander, *Reactive oxygen species have a causal role in multiple forms of insulin resistance.* Nature, 2006. **440**(7086): p. 944-8.
85. Higa, A. and E. Chevet, *Redox signaling loops in the unfolded protein response.* Cell Signal, 2012. **24**(8): p. 1548-55.
86. Wu, J. and R.J. Kaufman, *From acute ER stress to physiological roles of the Unfolded Protein Response.* Cell Death Differ, 2006. **13**(3): p. 374-84.

87. Engin, F. and G.S. Hotamisligil, *Restoring endoplasmic reticulum function by chemical chaperones: an emerging therapeutic approach for metabolic diseases.* Diabetes Obes Metab, 2010. **12 Suppl 2**: p. 108-15.
88. Ron, D. and P. Walter, *Signal integration in the endoplasmic reticulum unfolded protein response.* Nat Rev Mol Cell Biol, 2007. **8**(7): p. 519-29.
89. Ng, D.T., J.D. Brown, and P. Walter, *Signal sequences specify the targeting route to the endoplasmic reticulum membrane.* J Cell Biol, 1996. **134**(2): p. 269-78.
90. Ma, Y. and L.M. Hendershot, *ER chaperone functions during normal and stress conditions.* J Chem Neuroanat, 2004. **28**(1-2): p. 51-65.
91. Panzhinskiy, E., J. Ren, and S. Nair, *Protein tyrosine phosphatase 1B and insulin resistance: role of endoplasmic reticulum stress/reactive oxygen species/nuclear factor kappa B axis.* PLoS One, 2013. **8**(10): p. e77228.
92. Schroder, M. and R.J. Kaufman, *ER stress and the unfolded protein response.* Mutat Res, 2005. **569**(1-2): p. 29-63.
93. Beriault, D.R. and G.H. Werstuck, *Detection and quantification of endoplasmic reticulum stress in living cells using the fluorescent compound, Thioflavin T.* Biochim Biophys Acta, 2013. **1833**(10): p. 2293-301.
94. Malhotra, J.D. and R.J. Kaufman, *Endoplasmic reticulum stress and oxidative stress: a vicious cycle or a double-edged sword?* Antioxid Redox Signal, 2007. **9**(12): p. 2277-93.
95. Wek, R.C. and T.G. Anthony, *Obesity: stressing about unfolded proteins.* Nat Med, 2010. **16**(4): p. 374-6.
96. Wek, R.C., H.Y. Jiang, and T.G. Anthony, *Coping with stress: eIF2 kinases and translational control.* Biochem Soc Trans, 2006. **34**(Pt 1): p. 7-11.
97. Samali, A., et al., *Methods for monitoring endoplasmic reticulum stress and the unfolded protein response.* Int J Cell Biol, 2010. **2010**: p. 830307.
98. Kouroku, Y., et al., *ER stress (PERK/eIF2alpha phosphorylation) mediates the polyglutamine-induced LC3 conversion, an essential step for autophagy formation.* Cell Death Differ, 2007. **14**(2): p. 230-9.
99. Bartolome, A., C. Guillen, and M. Benito, *Autophagy plays a protective role in endoplasmic reticulum stress-mediated pancreatic beta cell death.* Autophagy, 2012. **8**(12): p. 1757-68.
100. Bachar-Wikstrom, E., et al., *Stimulation of autophagy improves endoplasmic reticulum stress-induced diabetes.* Diabetes, 2013. **62**(4): p. 1227-37.
101. Talloczy, Z., et al., *Regulation of starvation- and virus-induced autophagy by the eIF2alpha kinase signaling pathway.* Proc Natl Acad Sci U S A, 2002. **99**(1): p. 190-5.
102. Quan, W., et al., *Autophagy deficiency in beta cells leads to compromised unfolded protein response and progression from obesity to diabetes in mice.* Diabetologia, 2012. **55**(2): p. 392-403.
103. Ogata, M., et al., *Autophagy is activated for cell survival after endoplasmic reticulum stress.* Mol Cell Biol, 2006. **26**(24): p. 9220-31.
104. Vidal, R.L. and C. Hetz, *Unspliced XBP1 controls autophagy through FoxO1.* Cell Res, 2013. **23**(4): p. 463-4.
105. Zhao, Y., et al., *XBP-1u suppresses autophagy by promoting the degradation of FoxO1 in cancer cells.* Cell Res, 2013. **23**(4): p. 491-507.
106. Xue, X., et al., *Tumor necrosis factor alpha (TNFalpha) induces the unfolded protein response (UPR) in a reactive oxygen species (ROS)-dependent fashion, and the UPR counteracts ROS accumulation by TNFalpha.* J Biol Chem, 2005. **280**(40): p. 33917-25.
107. Tu, B.P. and J.S. Weissman, *Oxidative protein folding in eukaryotes: mechanisms and consequences.* J Cell Biol, 2004. **164**(3): p. 341-6.

108. Hotamisligil, G.S., *Role of endoplasmic reticulum stress and c-Jun NH2-terminal kinase pathways in inflammation and origin of obesity and diabetes.* Diabetes, 2005. **54 Suppl 2**: p. S73-8.
109. Ozcan, U., et al., *Endoplasmic reticulum stress links obesity, insulin action, and type 2 diabetes.* Science, 2004. **306**(5695): p. 457-61.
110. Ozcan, U., et al., *Chemical chaperones reduce ER stress and restore glucose homeostasis in a mouse model of type 2 diabetes.* Science, 2006. **313**(5790): p. 1137-40.
111. Teodoro-Morrison, T., et al., *GRP78 overproduction in pancreatic beta cells protects against high-fat-diet-induced diabetes in mice.* Diabetologia, 2013. **56**(5): p. 1057-67.
112. Aguirre, V., et al., *The c-Jun NH(2)-terminal kinase promotes insulin resistance during association with insulin receptor substrate-1 and phosphorylation of Ser(307).* J Biol Chem, 2000. **275**(12): p. 9047-54.
113. Samuel, V.T. and G.I. Shulman, *Mechanisms for insulin resistance: common threads and missing links.* Cell, 2012. **148**(5): p. 852-71.
114. Finkel, T., *Signal transduction by reactive oxygen species.* J Cell Biol, 2011. **194**(1): p. 7-15.
115. Cabiscol, E., et al., *Oxidative stress promotes specific protein damage in Saccharomyces cerevisiae.* J Biol Chem, 2000. **275**(35): p. 27393-8.
116. Maritim, A.C., R.A. Sanders, and J.B. Watkins, 3rd, *Diabetes, oxidative stress, and antioxidants: a review.* J Biochem Mol Toxicol, 2003. **17**(1): p. 24-38.
117. Kaneto, H., et al., *Oxidative stress, ER stress, and the JNK pathway in type 2 diabetes.* J Mol Med (Berl), 2005. **83**(6): p. 429-39.
118. Haber, C.A., et al., *N-acetylcysteine and taurine prevent hyperglycemia-induced insulin resistance in vivo: possible role of oxidative stress.* Am J Physiol Endocrinol Metab, 2003. **285**(4): p. E744-53.
119. Steinhubl, S.R., *Why have antioxidants failed in clinical trials?* Am J Cardiol, 2008. **101**(10A): p. 14D-19D.
120. Brown, D.I. and K.K. Griendling, *Regulation of signal transduction by reactive oxygen species in the cardiovascular system.* Circ Res, 2015. **116**(3): p. 531-49.
121. Jones, D.P. and Y.M. Go, *Redox compartmentalization and cellular stress.* Diabetes Obes Metab, 2010. **12 Suppl 2**: p. 116-25.
122. Scherz-Shouval, R., et al., *Reactive oxygen species are essential for autophagy and specifically regulate the activity of Atg4.* EMBO J, 2007. **26**(7): p. 1749-60.
123. Scherz-Shouval, R., E. Shvets, and Z. Elazar, *Oxidation as a post-translational modification that regulates autophagy.* Autophagy, 2007. **3**(4): p. 371-3.
124. Tal, M.C., et al., *Absence of autophagy results in reactive oxygen species-dependent amplification of RLR signaling.* Proc Natl Acad Sci U S A, 2009. **106**(8): p. 2770-5.
125. Glick, D., S. Barth, and K.F. Macleod, *Autophagy: cellular and molecular mechanisms.* J Pathol, 2010. **221**(1): p. 3-12.
126. Zhou, C., et al., *Monitoring autophagic flux by an improved tandem fluorescent-tagged LC3 (mTagRFP-mWasabi-LC3) reveals that high-dose rapamycin impairs autophagic flux in cancer cells.* Autophagy, 2012. **8**(8): p. 1215-26.
127. Martinet, W., et al., *Autophagy in disease: a double-edged sword with therapeutic potential.* Clin Sci (Lond), 2009. **116**(9): p. 697-712.
128. Kim, J., et al., *AMPK and mTOR regulate autophagy through direct phosphorylation of Ulk1.* Nat Cell Biol, 2011. **13**(2): p. 132-41.
129. Bach, M., et al., *The serine/threonine kinase ULK1 is a target of multiple phosphorylation events.* Biochem J, 2011. **440**(2): p. 283-91.

130. Nazio, F., et al., *mTOR inhibits autophagy by controlling ULK1 ubiquitylation, self-association and function through AMBRA1 and TRAF6.* Nat Cell Biol, 2013. **15**(4): p. 406-16.
131. Russell, R.C., et al., *ULK1 induces autophagy by phosphorylating Beclin-1 and activating VPS34 lipid kinase.* Nat Cell Biol, 2013. **15**(7): p. 741-50.
132. Nazio, F. and F. Cecconi, *mTOR, AMBRA1, and autophagy: an intricate relationship.* Cell Cycle, 2013. **12**(16): p. 2524-5.
133. Mizushima, N., *The role of the Atg1/ULK1 complex in autophagy regulation.* Curr Opin Cell Biol, 2010. **22**(2): p. 132-9.
134. Matsunaga, K., et al., *Two Beclin 1-binding proteins, Atg14L and Rubicon, reciprocally regulate autophagy at different stages.* Nat Cell Biol, 2009. **11**(4): p. 385-96.
135. Hamasaki, M. and T. Yoshimori, *Where do they come from? Insights into autophagosome formation.* FEBS Lett, 2010. **584**(7): p. 1296-301.
136. Kabeya, Y., et al., *LC3, GABARAP and GATE16 localize to autophagosomal membrane depending on form-II formation.* J Cell Sci, 2004. **117**(Pt 13): p. 2805-12.
137. Fullgrabe, J., D.J. Klionsky, and B. Joseph, *The return of the nucleus: transcriptional and epigenetic control of autophagy.* Nat Rev Mol Cell Biol, 2014. **15**(1): p. 65-74.
138. Grumati, P., et al., *Physical exercise stimulates autophagy in normal skeletal muscles but is detrimental for collagen VI-deficient muscles.* Autophagy, 2011. **7**(12): p. 1415-23.
139. He, C., et al., *Exercise-induced BCL2-regulated autophagy is required for muscle glucose homeostasis.* Nature, 2012. **481**(7382): p. 511-5.
140. Sanchez, A.M., R.B. Candau, and H. Bernardi, *FoxO transcription factors: their roles in the maintenance of skeletal muscle homeostasis.* Cell Mol Life Sci, 2014. **71**(9): p. 1657-71.
141. Russell, R.C., H.X. Yuan, and K.L. Guan, *Autophagy regulation by nutrient signaling.* Cell Res, 2014. **24**(1): p. 42-57.
142. Mizushima, N. and B. Levine, *Autophagy in mammalian development and differentiation.* Nat Cell Biol, 2010. **12**(9): p. 823-30.
143. Kim, J. and K.L. Guan, *Regulation of the autophagy initiating kinase ULK1 by nutrients: roles of mTORC1 and AMPK.* Cell Cycle, 2011. **10**(9): p. 1337-8.
144. Shang, L. and X. Wang, *AMPK and mTOR coordinate the regulation of Ulk1 and mammalian autophagy initiation.* Autophagy, 2011. **7**(8): p. 924-6.
145. Alers, S., et al., *Role of AMPK-mTOR-Ulk1/2 in the regulation of autophagy: cross talk, shortcuts, and feedbacks.* Mol Cell Biol, 2012. **32**(1): p. 2-11.
146. Dunlop, E.A. and A.R. Tee, *The kinase triad, AMPK, mTORC1 and ULK1, maintains energy and nutrient homoeostasis.* Biochem Soc Trans, 2013. **41**(4): p. 939-43.
147. Otomo, C., et al., *Structure of the human ATG12~ATG5 conjugate required for LC3 lipidation in autophagy.* Nat Struct Mol Biol, 2013. **20**(1): p. 59-66.
148. Hanada, T., et al., *The Atg12-Atg5 conjugate has a novel E3-like activity for protein lipidation in autophagy.* J Biol Chem, 2007. **282**(52): p. 37298-302.
149. Sakoh-Nakatogawa, M., et al., *Atg12-Atg5 conjugate enhances E2 activity of Atg3 by rearranging its catalytic site.* Nat Struct Mol Biol, 2013. **20**(4): p. 433-9.
150. He, C. and D.J. Klionsky, *Regulation mechanisms and signaling pathways of autophagy.* Annu Rev Genet, 2009. **43**: p. 67-93.
151. Mizushima, N., *Autophagy: process and function.* Genes Dev, 2007. **21**(22): p. 2861-73.
152. Pyo, J.O., et al., *Overexpression of Atg5 in mice activates autophagy and extends lifespan.* Nat Commun, 2013. **4**: p. 2300.
153. Yang, L., et al., *Defective hepatic autophagy in obesity promotes ER stress and causes insulin resistance.* Cell Metab, 2010. **11**(6): p. 467-78.
154. Kim, K.H., et al., *Autophagy deficiency leads to protection from obesity and insulin resistance by inducing Fgf21 as a mitokine.* Nat Med, 2013. **19**(1): p. 83-92.

155. Kahn, S.E., M.E. Cooper, and S. Del Prato, *Pathophysiology and treatment of type 2 diabetes: perspectives on the past, present, and future.* Lancet, 2014. **383**(9922): p. 1068-83.
156. Liu, Y., et al., *Adiponectin corrects high-fat diet-induced disturbances in muscle metabolomic profile and whole-body glucose homeostasis.* Diabetes, 2013. **62**(3): p. 743-52.
157. Turer, A.T. and P.E. Scherer, *Adiponectin: mechanistic insights and clinical implications.* Diabetologia, 2012. **55**(9): p. 2319-26.
158. Sandri, M., *Autophagy in skeletal muscle.* FEBS Lett, 2010. **584**(7): p. 1411-6.
159. Huang, C., et al., *Sustained exposure of L6 myotubes to high glucose and insulin decreases insulin-stimulated GLUT4 translocation but upregulates GLUT4 activity.* Diabetes, 2002. **51**(7): p. 2090-8.
160. Tajmir, P., et al., *Acute and chronic leptin treatment mediate contrasting effects on signaling, glucose uptake, and GLUT4 translocation in L6-GLUT4myc myotubes.* J Cell Physiol, 2003. **197**(1): p. 122-30.
161. Schuiki, I., L. Zhang, and A. Volchuk, *Endoplasmic reticulum redox state is not perturbed by pharmacological or pathological endoplasmic reticulum stress in live pancreatic beta-cells.* PLoS One, 2012. **7**(11): p. e48626.
162. Revel, M. and Y. Groner, *Post-transcriptional and translational controls of gene expression in eukaryotes.* Annu Rev Biochem, 1978. **47**: p. 1079-126.
163. Day, D.A. and M.F. Tuite, *Post-transcriptional gene regulatory mechanisms in eukaryotes: an overview.* J Endocrinol, 1998. **157**(3): p. 361-71.
164. Mizushima, N., et al., *Dissection of autophagosome formation using Apg5-deficient mouse embryonic stem cells.* J Cell Biol, 2001. **152**(4): p. 657-68.
165. Gustafsson, A.B. and R.A. Gottlieb, *Recycle or die: the role of autophagy in cardioprotection.* J Mol Cell Cardiol, 2008. **44**(4): p. 654-61.
166. Hamacher-Brady, A., et al., *Response to myocardial ischemia/reperfusion injury involves Bnip3 and autophagy.* Cell Death Differ, 2007. **14**(1): p. 146-57.
167. Pyo, J.O., et al., *Essential roles of Atg5 and FADD in autophagic cell death: dissection of autophagic cell death into vacuole formation and cell death.* J Biol Chem, 2005. **280**(21): p. 20722-9.
168. McMillan, E.M. and J. Quadrilatero, *Autophagy is required and protects against apoptosis during myoblast differentiation.* Biochem J, 2014. **462**(2): p. 267-77.
169. Iovino, S., et al., *PED/PEA-15 induces autophagy and mediates TGF-beta1 effect on muscle cell differentiation.* Cell Death Differ, 2012. **19**(7): p. 1127-38.
170. Almeida, P.C., et al., *Cathepsin B activity regulation. Heparin-like glycosaminogylcans protect human cathepsin B from alkaline pH-induced inactivation.* J Biol Chem, 2001. **276**(2): p. 944-51.
171. Henriksen, E.J., M.K. Diamond-Stanic, and E.M. Marchionne, *Oxidative stress and the etiology of insulin resistance and type 2 diabetes.* Free Radic Biol Med, 2011. **51**(5): p. 993-9.
172. Tangvarasittichai, S., *Oxidative stress, insulin resistance, dyslipidemia and type 2 diabetes mellitus.* World J Diabetes, 2015. **6**(3): p. 456-80.
173. Evans, J.L., et al., *Are oxidative stress-activated signaling pathways mediators of insulin resistance and beta-cell dysfunction?* Diabetes, 2003. **52**(1): p. 1-8.
174. El Midaoui, A., et al., *Comparative effects of N-acetyl-L-cysteine and ramipril on arterial hypertension, insulin resistance, and oxidative stress in chronically glucose-fed rats.* Can J Physiol Pharmacol, 2008. **86**(11): p. 752-60.
175. Fulghesu, A.M., et al., *N-acetyl-cysteine treatment improves insulin sensitivity in women with polycystic ovary syndrome.* Fertil Steril, 2002. **77**(6): p. 1128-35.

176. Gonzalez, C.D., et al., *The emerging role of autophagy in the pathophysiology of diabetes mellitus.* Autophagy, 2011. **7**(1): p. 2-11.
177. Novoa, I., et al., *Feedback inhibition of the unfolded protein response by GADD34-mediated dephosphorylation of eIF2alpha.* J Cell Biol, 2001. **153**(5): p. 1011-22.
178. Boyce, M., et al., *A selective inhibitor of eIF2alpha dephosphorylation protects cells from ER stress.* Science, 2005. **307**(5711): p. 935-9.
179. Schewe, D.M. and J.A. Aguirre-Ghiso, *Inhibition of eIF2alpha dephosphorylation maximizes bortezomib efficiency and eliminates quiescent multiple myeloma cells surviving proteasome inhibitor therapy.* Cancer Res, 2009. **69**(4): p. 1545-52.
180. Kaneto, H., et al., *Oxidative stress and the JNK pathway are involved in the development of type 1 and type 2 diabetes.* Curr Mol Med, 2007. **7**(7): p. 674-86.

Appendix A: Supplementary Figures

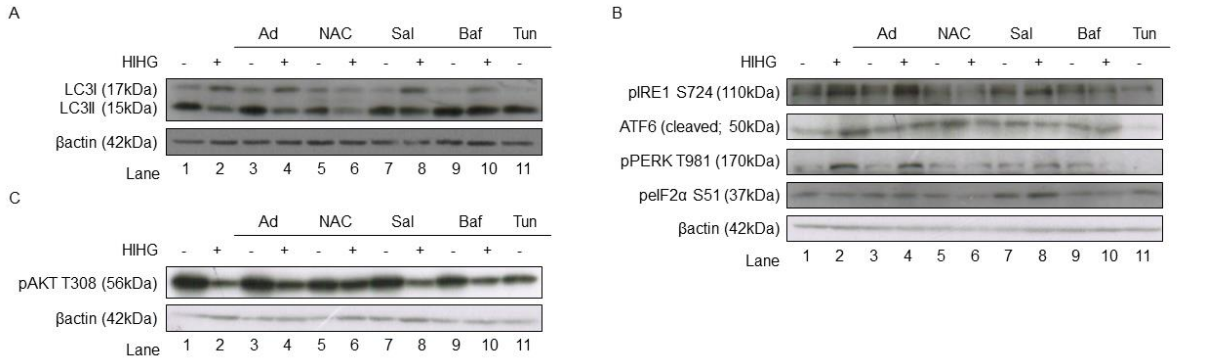

Supplementary Figure 1. Uncut blots showing the regulation by adiponectin, NAC, salubrinal, bafilomycin and tunicamycin of proteins involved in the UPR, insulin signaling and autophagy in control and HIHG condition in WT MT L6 cells. Representative blots previously shown in Figure 3.10 (B; lane 1-4), Figure 3.12 (A; lane 1-2, 9-10), Figure 3.13 (C; lane 1-2, 9-10), Figure 3.16 (B; lane 1-2, 7-8, 11), Figure 3.17 (A; lane 1-2, 7-8, 11), Figure 3.18 (C; lane 1-2, 7-8, 11), Figure 3.21 (C; lane 1-2, 5-6), Figure 3.22 (A; lane 1-2, 5-6) and Figure 3.24 (B; lane 1-2, 5-6).

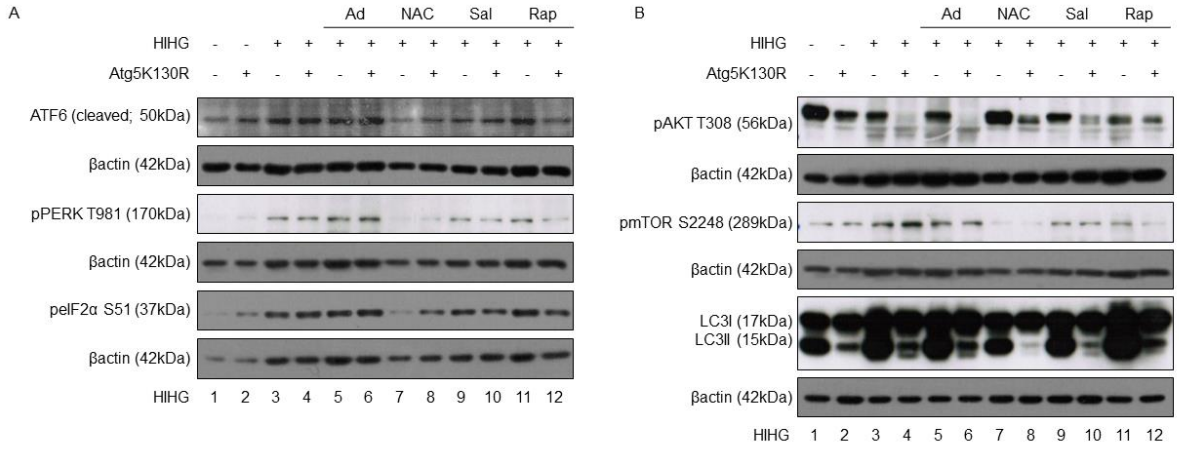

Supplementary Figure 2. Uncut blots showing the regulation by adiponectin, NAC, salubrinal, and rapamycin of proteins involved in the UPR, insulin signaling and autophagy in HIHG condition compared to control in EV and Atg5K MB L6 cells. Representative blots previously shown in Figure 3.9 (B; lane 1-6), Figure 3.11 (A; lane 1-6), Figure 3.15 (A and B; lane 3-4, 11-12), Figure 3.20 (A and B; lane 3-4, 9-10) and Figure 3.25 (A and B; lane 3-4, 7-8).

Appendix B: List of Contributions

The thesis was researched and written by Penny Ahlstrom (P.A.) who helped plan experiments and develop protocols; P.A. also performed the majority of the experimental work. P.A. worked with Suharto Chakma (S.C.) and while P.A. trained S.C. in cellular and molecular assays he contributed to some of the experimental work. An account of contributions by S.C. are listed as follows. Note that when no specification are detailed P.A. performed all the experimental work.

Chapter 3. Results

Figure 3.1 (A) S.C. re-ran samples for representative blots.

Figure 3.3 (A) S.C. prepared fluorescence microscopy slides, took some representative images and helped with quantification.

Figure 3.6 (C-E) S.C. prepared fluorescence microscopy slides for 4 hours HIHG treatment, took representative images and helped with quantification.

Figure 3.9 (A-F) S.C. developed beta-actin blots.

Figure 3.11 (A-H) S.C. developed beta-actin blots.

Figure 3.14 (A) S.C. prepared fluorescence microscopy slides, took some representative images and helped with quantification.

Figure 3.15 (A-G) S.C. developed beta-actin blots.

Figure 3.20 (A-G) S.C. developed beta-actin blots.

Figure 3.25 (A-G) S.C. developed beta-actin blots.

Appendix A: Supplementary Figures

Supplementary Figure 2. (A-B) S.C. developed beta-actin blots.